SMALL STRAIN DEFORMATION BEHAVIOR OF INTERSTITIAL-FREE (IF) STEELS

by

Mukul Prabhakar Renavikar

B.E (Metallurgy), College of Engineering, Pune, India, 1994

M.S (Materials Science), University of Pittsburgh, 1997

Submitted to the Graduate Faculty of

School of Engineering in partial fulfillment

of the requirements for the degree of

Doctor of Philosophy

University of Pittsburgh

2003

UNIVERSITY OF PITTSBURGH

SCHOOL OF ENGINEERING

This dissertation was presented

by

Mukul Prabhakar Renavikar

It was defended on

January 7, 2003

and approved by

Jean Blachere, Assistant Professor, Materials Science and Engineering

Dennis Haezebrouck, US Steel Corporation

Dipo Onipede, Assistant Professor, Mechanical Engineering

Jorg Wiezorek, Assistant Professor, Materials Science and Engineering

Peter Wray, Visiting Researcher

Calixto Isaac Garcia, Research Professor,

Dissertation Advisor: Anthony J. DeArdo, Professor, Materials Science and Engineering

ABSTRACT

SMALL STRAIN DEFORMATION BEHAVIOR OF INTERSTITIAL-FREE (IF) STEELS

Mukul Prabhakar Renavikar, PhD

University of Pittsburgh, 2003

Two types of small strain deformation behaviors of IF steels were studied. The role of solute phosphorus in affecting the small strain yielding behavior was investigated in two IF steels containing 20 ppm and 600 ppm bulk P levels. The role of crystallographic texture in affecting the small strain unloading or springback behavior was theoretically modeled to identify those textures which would impart minimum variability in springback of IF steel sheets.

The addition of solute P brings about solid solution strengthening, the magnitude of which was determined to be 2.38 MPa/0.01 wt % P. The segregation of solute P to ferrite grain boundaries brings about extensive grain boundary hardening (GBH), which results in a substantial increase in the Hall-Petch slope, k_y. Based upon the results from Auger Electron Spectroscopy (AES), tensile testing and hardness measurements, the increase in the Hall-Petch slope due to phosphorus segregation is quantified to be ~18.6 MPa.$\mu m^{1/2}$/at% P segregated. Grain boundary hardening is postulated to be caused by a combination of dislocation forest hardening and the pinning of these grain boundary dislocations by segregated solute P.

Additionally, the role of FeTiP and FeTiNbP precipitates in affecting the strength of IF steels has been studied in Ti-bearing and (Ti+Nb)-bearing IF steels. The presence of large

volume fractions of grain boundary phosphides results in a decrease in the strength due to scavenging of solute P at the grain boundaries.

Theoretical modeling proved that gamma-fiber texture components exhibit isotropic springback behavior in the plane of the sheet on account of their high in-plane elastic isotropy, whereas, alpha and epsilon fiber components exhibit highly anisotropic springback behavior in plane strain bending applications. FEM modeling in draw-bend test applications shows that sheet steels with high elastic moduli and low yield strengths along the axis of the draw-bend test specimen exhibit minimum springback. Thus, the presence of high volume fractions of gamma fiber components in IF steel sheets provides excellent deep drawability as well as isotropic in-plane springback behavior.

ACKNOWLEDGEMENTS

First and foremost, I would like to thank my advisors namely, Dr. A.J. DeArdo, Dr. C.I. Garcia and Peter Wray for their unstinting support and guidance in this research. The invaluable suggestions provided by the committee members are gratefully acknowledged.

I would like to extend my gratitude to Dr. Harry Meyer and Dr. Lidia Storojeva for extending help in performing some of the experimental work. The help extended by Dr. Mingjian Hua in the use of TEM and STEM is kindly acknowledged.

I would like to thank all my BAMPRI colleagues for their encouragement throughout my stay at the University of Pittsburgh. Thanks are also due to the staff and faculty members of the Department of Materials Science and Engineering for their constant support. I would like to sincerely thank Dr. Ken Goldman for being an excellent mentor.

The financial support provided by the BAMPRI-IF Steel Consortium is gratefully acknowledged.

I would like to thank my parents and all my family members for believing in my capabilities and constantly supporting me in this challenging endeavor. Finally, I would like to thank my wife, Aarati, for her love and patience and being with me through the most critical stages of this work.

Thank you all!

TABLE OF CONTENTS

LIST OF TABLES

LIST OF FIGURES

1.0 INTRODUCTION

The primary user of sheet steels is the automotive industry. Sheet steels have to satisfy a variety of requirements such as:

i) Good deep drawability and stretch formability.

ii) Sufficiently high levels of strength for improved dent resistance and vehicle weight reduction.

iii) High aesthetic quality especially the absence of unsightly stretcher strains.

iv) Good coatability and paintability required for excellent corrosion resistance.

v) Good weldability required for ease of fabrication.

Initially, low carbon aluminum killed (LCAK) steels were used to meet all the above requirements. However, these steels tended to have large amounts of carbon as well as nitrogen in solid solution and suffered from the phenomenon of strain aging that manifested itself in the formation of 'stretcher strains'. It has also been well established that high levels of interstitial elements such as C and N in solid solution resulted in a decrease in the deep drawability of the sheet steels. This decrease has been attributed to the degradation of crystallographic texture of the sheet steel[1-4] from the favorable 'cube on corner {111}' to the unfavorable 'rotated cube {100}' texture[5-10] as a result of high interstitial content. Additionally, high levels of C and N also have a detrimental effect on the strain hardening coefficient, 'n', of the sheet metal, which results in poor stretch formability[11, 12].

With considerable technological advances in vacuum degassing techniques, steel manufacturers were able to produce a new class of steels with C and N levels less than 25-30 ppm (0.0025 – 0.003 wt%) each. This class of steels is known as ultra-low carbon (ULC) steels or interstitial-free (IF) steels. In order to render these steels interstitial free, Ti and Nb, in

relatively small amounts (400 – 700 ppm Ti and 100 – 300 ppm Nb), are added to stabilize the residual carbon as carbo-sulphides such as (Ti, Nb)$_4C_2S_2$ and/or carbides such as TiC or NbC. These fully stabilized IF steels are characterized by high values of R-bar (the normal anisotropy of sheet metals) and high values of the strain hardening exponent (0.2-0.28) and hence are extremely suited for forming operations typically encountered in automotive applications[13]. IF steels are also amenable to continuous annealing processes thereby resulting in considerable time and energy savings.

The excellent formability of IF steels, though, comes at the expense of strength. IF steels exhibit lower values of yield strength (150-250 MPa) compared to traditional LCAK steels. With new CAFE (Corporate Average Fuel Economy) stipulations, extensive efforts have been launched to reduce the weight of automobiles in order to increase the fuel economy. Thus, auto manufacturers now face the need to use thinner sheet steels without significantly compromising the rigidity and stiffness of the automobile. The trend in the automotive steel industry is thus shifting towards using higher strength, thin gauge sheet steels. This has served as a challenge to the steel industry and extensive research has been undertaken to improve the strength of IF steels while maintaining their excellent formability. The steel industry has used conventional solid solution strengthening in conjunction with work hardening and bake hardening mechanisms to achieve higher strength levels in IF steels. An extremely cost effective and potent method of increasing the yield strength has been through the use of phosphorus as an alloying element. It has been shown that P imparts the highest increase in YS per unit wt. pct. added compared to other substitutional solutes in steel[14]. However, after many years of research, the role of P in bringing about strengthening in IF steels is still not completely understood. There are two schools of thought:

a) P strengthens IF steels by means of solid solution strengthening.

b) P segregates to the ferrite grain boundaries and hence brings about strengthening by grain boundary hardening.

The implications of the presence of grain boundary hardening due to P can be enormous. For the same bulk P content, the yield strength of IF steels can vary significantly, depending upon the degree of P segregation to ferrite grain boundaries. Thus, if grain boundary hardening exists, then the variability in yield strength can be controlled by controlling the amount of P segregation to grain boundaries. Yielding constitutes one type of 'small strain deformation behavior' during loading in IF steels. The principal focus of this research is to determine the role of phosphorus in affecting the yielding behavior of IF steels, especially via the grain boundary hardening mechanism.

Another type of 'small strain behavior' in IF steel sheets that warrants further investigation is the phenomenon of "Springback". Springback is defined as the elastic recovery of sheet metal in any forming operation after the forming load has been released. High strength IF steels obtained by increased levels of solid solution strengthening, work hardening and/or bake hardening, inherently show a larger variability in mechanical properties. This variability in properties has a deleterious effect on the springback behavior of sheet steels. Controlling the amount of and variability in springback, especially in high strength IF steels, is proving to be a major challenge to the auto industry. An important feature of the microstructure that affects the mechanical properties of IF steel sheets is the crystallographic texture of the sheet. The role of crystallographic texture in controlling the springback behavior of IF steels has not been investigated before. An equally important focus of this research is to determine whether crystallographic texture can affect the springback behavior of IF steels. In summary, the focus of

this work is to study the 'Small Strain Deformation Behavior' of IF steels comprised of the following:

a) Yielding behavior: To study the fundamental role of P in bringing about strengthening in IF steels.

b) Springback behavior: To investigate the role of crystallographic texture in controlling the amount and variability of springback.

The two types of small strain deformation behaviors in IF steel sheets investigated in this research have been schematically shown in Figure 1.1.

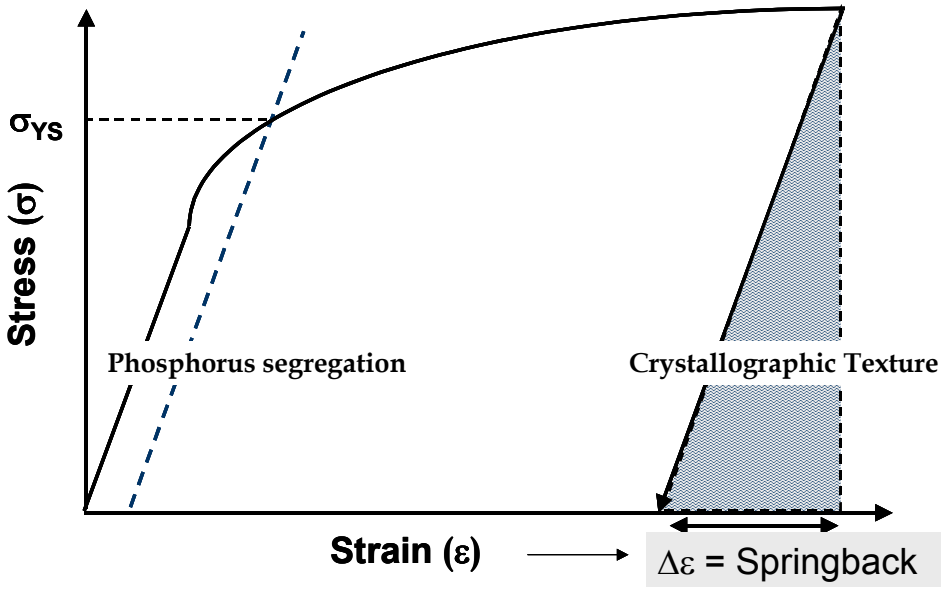

Figure 1.1 Schematic Illustration of Small Strain Deformation Behavior in IF Steels

2.0 BACKGROUND

Interstitial free steels are described as steels with C and N levels less than 25-30 ppm each, which are alloyed with Ti (400-700 ppm) and/or Nb (100-300 ppm). The addition of Ti and/or Nb renders these steels truly solute interstitial free by the formation of relatively coarse nitrides (TiN), carbosulfides $(Ti,Nb)_4C_2S_2$ and carbides (TiC/NbC). This process of stabilization of the interstitials solutes imparts excellent formability to IF steels, enabling them to be extensively used in automotive applications.

Based upon the chemistry, IF steels are typically classified into single stabilized (Ti-IF) and Nb-IF or as dual stabilized (Ti-Nb IF). In order to enhance the strength of IF steels without considerably compromising the formability, alloying elements such as P, B, Mn, and Si are also added. The effect of these alloying additions, especially that of P, on the strength of IF steels will be discussed in subsequent sections.

2.1 Commercial Processing of IF Steels

IF steel sheets undergo several thermomechanical (TMP) processing steps before being finally used in the automotive industry. The sequence of these processing steps is typically, as follows:

i) Slab reheating

ii) Hot rolling:

  a) Roughing

  b) Finishing

iii) Cooling and Coiling

iv) Cold rolling

v) Batch/Continuous annealing or Hot dip galvanizing (HDG)

vi) Temper rolling

vii) Electrogalvanizing

Each of the above processes affects the microstructure, texture evolution and precipitation and hence, in turn, affects the final properties such as strength and formability of IF steel sheets.

As mentioned earlier, IF steel sheets are mainly used in applications demanding excellent formability. Hence it is imperative to understand the effects of chemistry and processing variables on the formability of IF steel sheets. The following section discusses the formability aspects of IF steels.

2.2 Formability of IF Steels

IF steel sheets are subjected to a variety of forming operations and, hence, require excellent deep drawability and stretch formability. IF steels are typically characterized by high R-bar values (>2.0) and low ΔR (<+/- 0.1) as well as high n values (>0.25). In order to evaluate the deep drawability and stretch formability of sheet materials, certain parameters have been developed, which can be determined during a standard uniaxial tensile test [15].

2.2.1 Deep Drawability

The deep drawability of IF steel sheets is related to the R-value or the plastic strain ratio. It is defined as the ratio of the true width strain to the true thickness strain, in the uniform elongation region of a tensile test. The R-value frequently changes with the test direction in the sheet. This variation results in an undesirable phenomenon called 'earing' in a deep drawn cup. It is, therefore common to measure the average R-value or normal anisotropy, R-bar, and the planar anisotropy, ΔR [16, 17]. These values are calculated as follows:

$$\text{R-bar} = (R_0 + 2\,R_{45} + R_{90}) / 4 \qquad (2\text{-}1)$$

$$\Delta R = (R_0 - 2\,R_{45} + R_{90}) / 2 \qquad (2\text{-}2)$$

where subscripts stand for the angle between the tensile specimen axis and the rolling direction of the sheet.

A combination of high R-bar value and low ΔR provides excellent deep drawability [9, 18]. It has been shown that the R-bar value is strongly governed by the chemistry and TMP of IF steel sheets. The TMP affects the crystallographic texture as well as the final microstructure. It has been well established that crystallographic texture controls the deep drawability of IF steels as shown in Figure 2.1. As can be seen from the figure, a high intensity of the {111} ("cube on corner") texture as opposed to {001} ("cube on face") texture, is favorable for achieving high R-bar values. The composition of IF steels also has a strong influence on the R-bar values. Hutchinson[4] has shown that lowering the levels of C and N in solid solution increases the R-bar values. See Figure 2.2. The value of R-bar also depends upon the microstructure especially the ferrite grain size developed during and after processing[18, 19]. It has been observed that a fine grain size after hot rolling (prior to cold rolling) is suitable for high R-bar values.

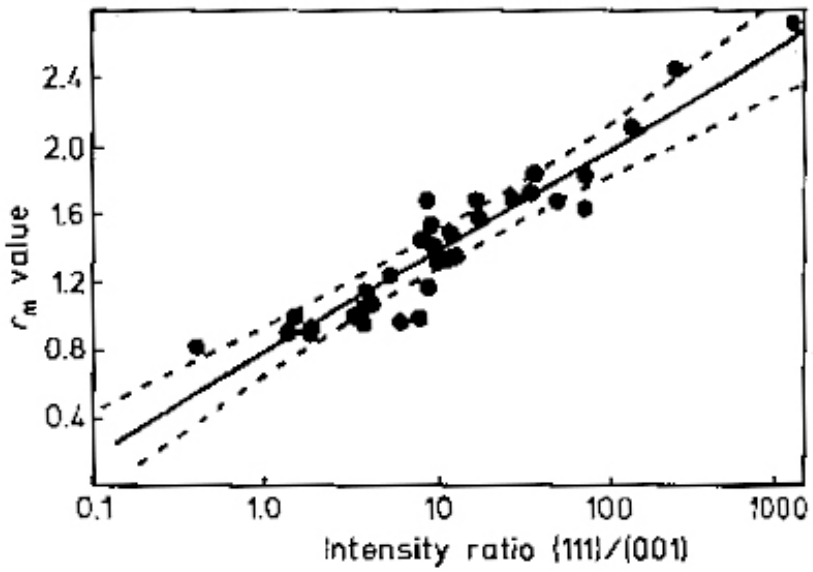

Figure 2.1 Influence of Crystallographic Texture on R-bar Values[9]

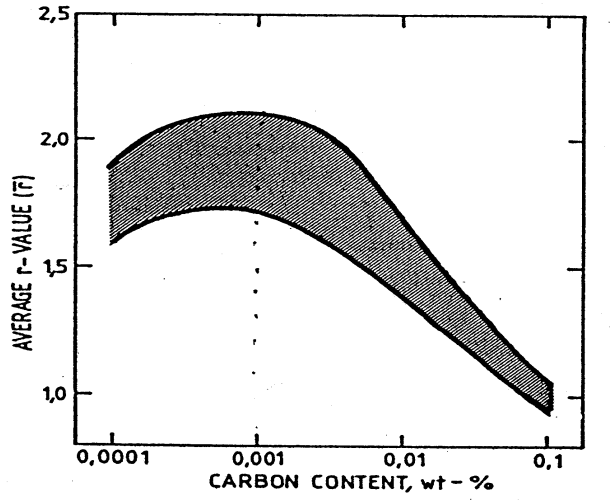

Figure 2.2 Variation of R value with Carbon Content in Steels[4]

On the other hand, a large recrystallized ferrite grain size yields high R-bar values as given by the following equation:

$$R = A + B \log d \qquad (2\text{-}3)$$

where A and B are constants and d is the recrystallized ferrite grain size.

A considerable amount of research[20-26] has been performed to study the effect of processing variables on the deep drawability of IF steels. To summarize the salient results, low slab reheating temperatures, coarse austenite grain size prior to roughing, heavy deformations in the roughing pass, finishing just above the Ar_3 (in pancaked austenite), high coiling temperatures (> 700°C), heavy cold reductions (>80%) and high annealing temperatures (along with high heating rates during annealing), produce high intensities of the {111}// to ND recrystallization texture, thereby maximizing the deep drawability of the IF steel sheets.

2.2.2 Stretch Formability

The stretch formability of IF steel sheets is quantified by the strain hardening exponent, 'n', and it is a measure of the ability of the steels to distribute the applied strain evenly. In metals with high 'n' values, the flow stress increases rapidly with strain. This tends to distribute further strain to regions of lower strain and flow stress. In the region up to uniform elongation, 'n' is defined as:

$$n = (\varepsilon/\sigma)\,(d\sigma / d\varepsilon) \qquad (2\text{-}4)$$

or $$n = \varepsilon_u \qquad (2\text{-}5)$$

where, σ = true stress ε = true strain

$d\sigma/d\varepsilon$= work hardening rate ε_u = uniform strain in tensile test

The 'n' value depends upon the composition and microstructure of the steel as shown by Pickering[27, 28]. In effect, sheet metals with high values of 'n' exhibit excellent stretch formability.

Processing variables influence the distribution of solutes, the amount, size and distribution of precipitates, the ferrite grain size and hence, the mean ferrite free path, of IF steels. The effect of grain size on 'n' value is shown in Figure 2.3[29] and predicted by the following equation:

$$n = A_1 / (A_2 + d^{-1/2}) \quad (2\text{-}6)$$

where, A_1 and A_2 are constants.

Thus, steels rendered free of interstitials such as C and N and having large annealed grain sizes will exhibit excellent formability. This "interstitial-free" condition adversely affects the strength of IF steels. It is thus also important to understand the strengthening mechanisms that are operative in IF steels and identify those mechanisms which can impart sufficient strength without compromising the formability. A description of the various microstructural features that affect the yield strength of IF steels is given in the following sections.

2.3 Strength of IF Steels

As mentioned in the previous section, the high formability of IF steels comes at the expense of strength. IF steels show considerably lower values of yield strength compared to HSLA, dual phase, multi phase and TRIP steels. The steel industry has used several approaches to improve the strength of IF steels including solid solution strengthening, work hardening

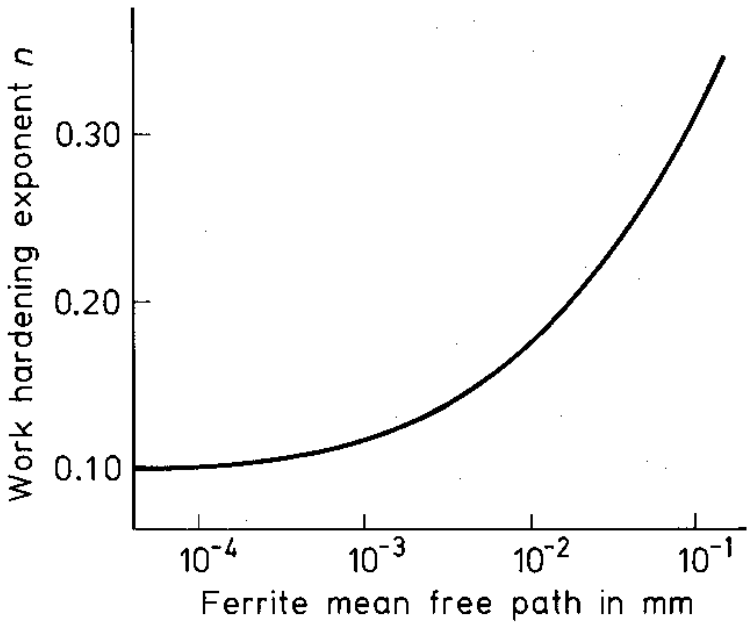

Figure 2.3 Influence of Ferrite Free Path on 'n' Value[29]

hardening. The following is a review of the strengthening mechanisms that govern the yield strength of IF steels.

Mechanistically, yielding in polycrystalline metals occurs by the activation of five independent slip systems. In order to maintain plastic compatibility at the grain boundaries, geometrically necessary dislocations (GNDs') are introduced in the vicinity of the grain boundaries as shown in Figure 2.4 [30]. Strength of metals essentially arises from the resistance faced by these GNDs' during their activity. Essentially, all obstacles that hinder the motion of GNDs' bring about an increase in the yield strength. Depending upon the nature of these obstacles, the yield strength of metals and that of steels in particular, is usually expressed in the form of an expanded Hall-Petch equation:

$$\sigma_y = \sigma_{PN} + \sigma_{SS} + \sigma_D + \sigma_{pptn.} + \sigma_{text} + \sigma_{GSS} \quad (2\text{-}7)$$

σ_y: yield strength

σ_{PN}: lattice friction stress

σ_{SS}: solid solution strengthening

σ_D: dislocation strengthening

$\sigma_{pptn.}$: precipitation hardening

σ_{text}: texture hardening

σ_{GSS} : grain size strengthening

The mechanisms involved in each of the above contributions are discussed in the next few sections with particular attention being focused upon solid solution strengthening, grain size strengthening and texture hardening since these mechanisms can considerably affect the yield strength of IF steels.

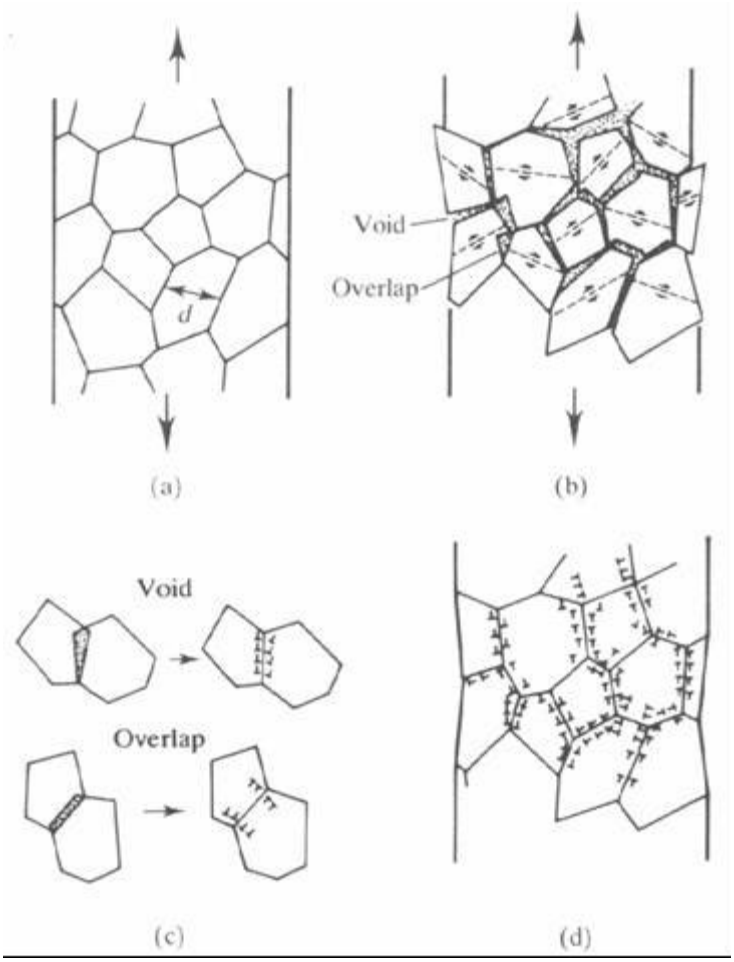

Figure 2.4 GNDs' Introduced at the Grain Boundaries to Maintain Plastic Compatibility[30]

2.3.1 Peierls-Nabarro or Lattice Friction Stress

This is termed the lattice friction stress and measures the inherent resistance of the lattice to dislocation motion. In steels, and generally in all BCC metals, σ_{PN} is strongly temperature dependent [31].

2.3.2 Solid Solution Strengthening

The introduction of both substitutional and interstitial solutes in iron causes an increase in the yield strength[27, 32] as shown in Figure 2.5 and Figure 2.6. Typical substitutional solutes added to IF steels are P, Mn, Si, Ti and Nb. These solutes replace the Fe atoms in the Fe crystal structure, thus causing a symmetrical distortion in the lattice. The increase in the yield strength of iron due to substitutional solutes is found to be proportional to the square root of the solute concentration[27]. In dilute solutions, as in the case of IF steels, the dependence on concentration is found to be linear. A striking feature in Figures 2.5 and 2.6 is the strengthening contribution of P, which is a substitutional solute. P increases the yield strength to a much greater extent than any of the other substitutional solutes.

The interstitial solutes, on the other hand, such as C and N, occupy octahedral interstices in the Fe crystal structure[33], thereby causing asymmetrical or tetragonal lattice distortions with an accompanying strengthening effect, which is 10-100 times that of substitutional solutes. In IF steels, C and N are almost completely stabilized as precipitates, namely, TiN, TiC, NbC, $Ti_4C_2S_2$, and hence, the contribution to strength due to the presence of C and N in solid solution

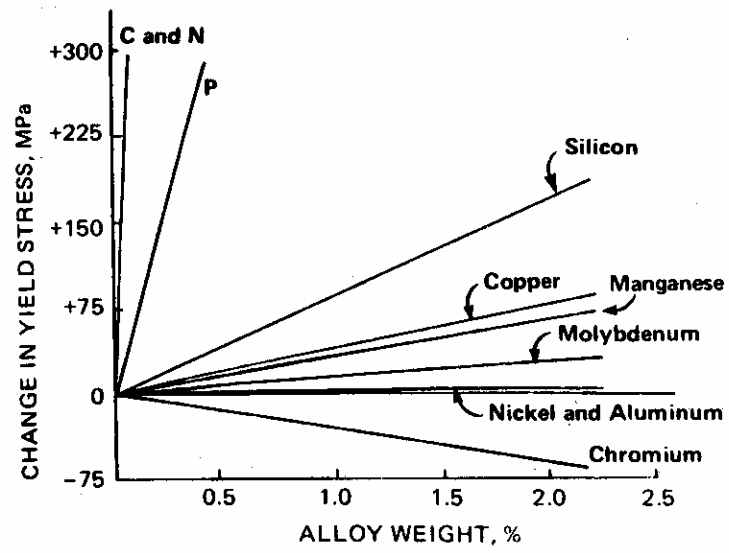

Figure 2.5 Solid Solution Strengthening of Iron[27]

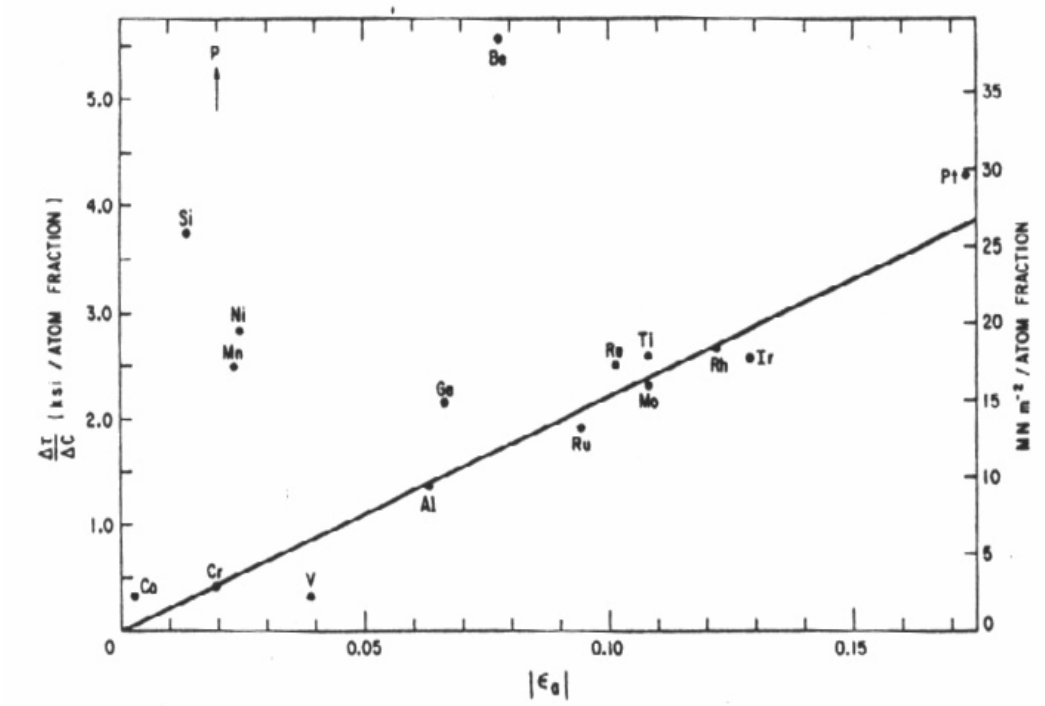

Figure 2.6 Solid Solution Strengthening in Iron Alloys[32]

is non existent. B, which is an interstitial solute, is also added to IF steels and also can bring about substantial solid solution strengthening.

There are various mechanisms by which solid solution strengthening occurs. The following is a list of the several mechanisms involved in solid solution strengthening:

a) Atomic misfit between solute and solvent, known as the size effect.

b) Differences in elastic modulus of solvent and solute, known as the modulus effect.

c) Differences in the electro negativities of solvent and solute atoms, known as the electronegativity effect.

d) Suzuki or chemical effect.

All the above theories have been extensively reviewed[30, 32, 34] and a summary is shown in Table 2.1.

2.3.3 Dislocation Strengthening

Both edge and screw dislocations in a lattice create a strain field in a finite region surrounding them. The mutual interaction between strain fields of adjacent dislocations results in strengthening of the lattice and this increment is given as [35]:

$$\Delta\sigma_D = \alpha G b \rho^{1/2} \tag{2-8}$$

where, G = shear modulus; ρ = dislocation density

b = Burger's vector; α = constant depending upon crystal structure

Table 2.1 Solid Solution Strengthening Mechanisms[32]

Expression of Strengthening	Meaning of Symbols
$\tau = G\,\epsilon_a^2 c$	τ = yield stress in shear
$\Delta\tau = 2G\,\epsilon_a c$	$\Delta\tau$ = solid solution component of yield stress in shear
	G = shear modulus
$\Delta\tau = G/700(\lvert\alpha\epsilon_a - \epsilon_G'\rvert)^{3/2} c^{1/2}$	c = concentration of solute, atom fraction
	a = lattice constant of α Fe, 2.86×10^{-10}m
	ϵ_a = size misfit parameter = $1/a\ da/dc$
$d(\Delta\tau/G)/dc = 0.04\,(\epsilon_\mu' + 1.5\,\epsilon_a)^2$	$\epsilon_G' = \epsilon_G/(1 + \lvert\epsilon_G/2\rvert)$
	ϵ_G = modulus misfit parameter = $1/G\ dG/dc$
$\Delta\tau = ZG(\lvert\epsilon_G'\rvert + \alpha\lvert\epsilon_a\rvert)^{4/3} c^{2/3}$	E = $0.12\,(\epsilon_\mu' + 1.52\,\epsilon_a)$ electron volts
	k = Boltzmann's constant
$\tau \cong \alpha E^2 c/kT\mathbf{b}^3$	$\mathbf{b}$ = Burgers vector (Fe = 2.48×10^{-10}m)
	Sf = size factor = $d_a - d_b/d_a \times 10^2$
	d = closest approach of atoms
	a = solvent
	b = solute
$\Delta\tau/\Delta c = (\mathrm{Sf} + \Sigma\,En)^m$	En = electronegativity
	$\Sigma\,En$ = sum of electronegativities of solvent and solute
	$\epsilon_\mu' = \epsilon_G + A\,\epsilon_a/1 - ½\,(\epsilon_G + A\,\epsilon_a)$
	T = temperature (Kelvin)
	A, Z, α, m } constants

2.3.4 Precipitation Hardening

Precipitates offer resistance to dislocation motion by either the Friedel (shearing of precipitates by dislocations) or by the Orowan (bypassing of precipitates by dislocations) mechanism. This resistance manifests itself in an increase in strength, and is strongly governed by the size, spatial distribution and volume fraction of the precipitates[36-39]. It is to be noted that IF steels contain very small amounts of alloying elements. Various types of precipitates reported in IF steels are TiN, TiS, $Ti_4C_2S_2$, TiC, NbC and FeTiP.

The volume fraction of these precipitates is observed to be extremely low (~ 10^{-4} - 10^{-5}). Additionally, these precipitates are relatively coarse (10 – 400 nm). The increment in precipitation hardening due to these precipitates is of the order of 1–5 MPa and therefore, is insignificant in IF steels.

2.3.5 Texture Hardening

The texture of sheet metals is denoted by {hkl}<uvw>, where {hkl} are the crystallographic planes parallel to the rolling plane and <uvw> are the crystallographic directions parallel to the rolling direction of the sheet. As mentioned in Section 2.2.1, texture is known to strongly influence the deep drawability of sheet steels. In fact, presence of texture introduces strong anisotropy in the yield strength of the sheet (both planar and normal). This anisotropy of yield strength strongly affects the deep drawability of the sheet as is explained in this section.

For excellent deep drawability, sheet steels with high values of R-bar are desired. R_θ, the plastic strain ratio as determined from a tensile test, is defined as:

$$R_\theta = \varepsilon_w / \varepsilon_t \tag{2-9}$$

where, ε_w = true strain in the width of the tensile specimen.

ε_t = true strain in the thickness of the tensile specimen.

Hence, in order to attain high R_θ values, thickness strains, ε_t, should be restricted to a minimum. This can be achieved by having a sheet steel with a relatively high yield strength in the thickness direction compared to the yield strength in the rolling and transverse directions. This anisotropy of yield strength can be effectively utilized to improve the deep drawability of the sheet. For such anisotropic materials, the Von Mises Yield Criterion (VMYC), for principal axes of orthotropic symmetry, can be written as[40]:

$$F(\sigma_2 - \sigma_3)^2 + G(\sigma_3 - \sigma_1)^2 + H(\sigma_1 - \sigma_2)^2 = 1 \tag{2-10}$$

where, F,G,H are constants defining the degree of anisotropy.

For plane stress situations, typically encountered in sheet metal forming, Eqn. 2-10, with proper substitutions, can be expressed as:

$$\sigma_1^2 + \sigma_2^2 - [2R/(1+R)]\sigma_1 \sigma_2 = Y^2 \tag{2-11}$$

where, R = Plastic strain ratio = $\varepsilon_w / \varepsilon_t = 2(Z/Y)^2 - 1$ (2-12)

Y = Yield strength of metal in transverse direction (TD).

Z = Yield strength of metal in thickness or normal direction (ND).

It is seen from Eqn. 2-12, that as the through thickness strength, Z, increases, the R-value also increases.

Figure 2.7[41] represents Eqn. 2-11 plotted in the σ_x - σ_y space. It can be seen that as the value of R increases, the yield locus in the first and third quadrant expands. This expansion

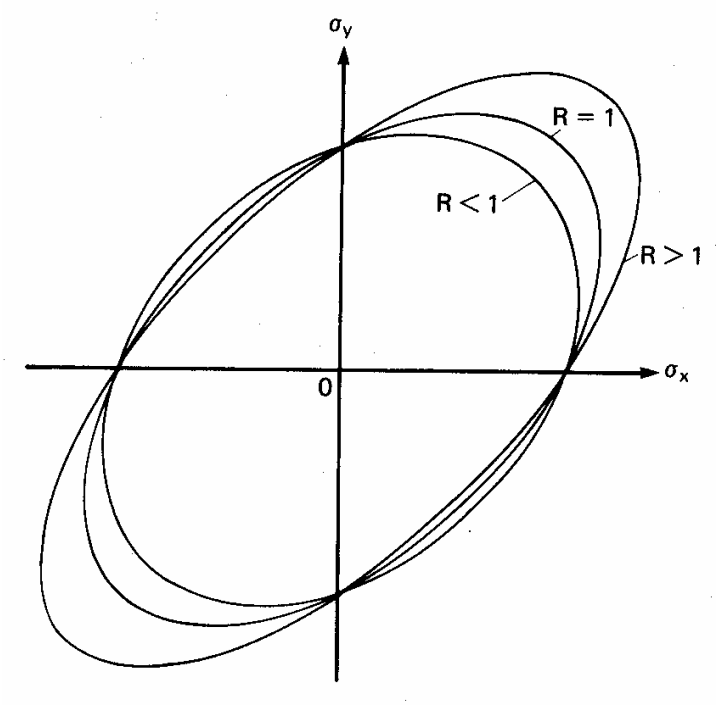

Figure 2.7 Dependence of the Von Mises Yield Locus on the R Value[41]

of the yield locus implies an increased resistance to plastic deformation of the sheet steel when it is subjected to stress states in the first (I) and third (III) quadrants. The stress state in the wall of the deep drawn sheet is that of biaxial tension ($\sigma_1,\sigma_2 > 0$) and lies in the first quadrant. Thus, a high value of Z (through thickness yield strength) will reduce plastic strains in the thickness direction, thereby reducing failures due to excessive through thickness thinning.

In sheet steels, it is observed that the {111}<uvw> (cube on corner) type of texture shows relatively high yield strength in the thickness direction compared to the {001}<uvw> (cube on face) type of texture. Hence, {111}<uvw> textures are associated with higher R-values. Thus, it is seen that certain crystallographic textures introduce strong anisotropy of the yield strength in the sheet steel. This phenomenon is called texture strengthening and affects not only the strength of the sheet steel but also the formability. Other researchers, namely, Kozasu[42] and Barlat[43] have also studied the influence of texture on yield strength of sheet metals. The results obtained by these researchers are shown in Figure 2.8 (a) and (b).

From Kozasu's data, it can be seen that the crystallographic texture can have a significant effect on the yield strength of sheet steels. For example, the (111)<112> texture is seen to be approximately 35 percent stronger than the (001)<110> texture, when compared in the rolling direction ($\theta = 0$). In summary, crystallographic texture can significantly affect the yield strength of IF steels.

2.3.6 Grain Size Strengthening

The quantitative relationship between yield strength and grain size in metals was first described by Hall[44], based upon experimental observations in steels, and by Petch[45],

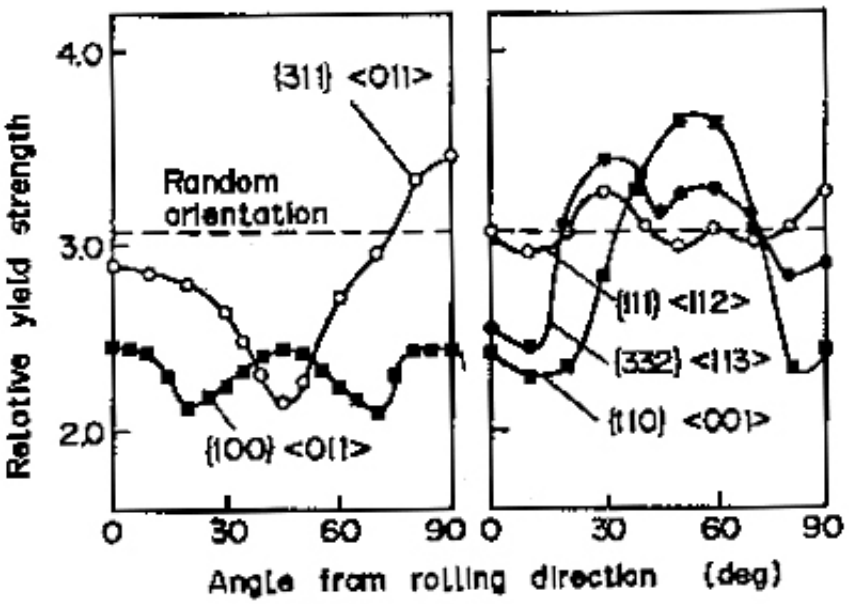

Figure 2.8 (a) Variation of Yield Strength with Crystallographic Texture[42]

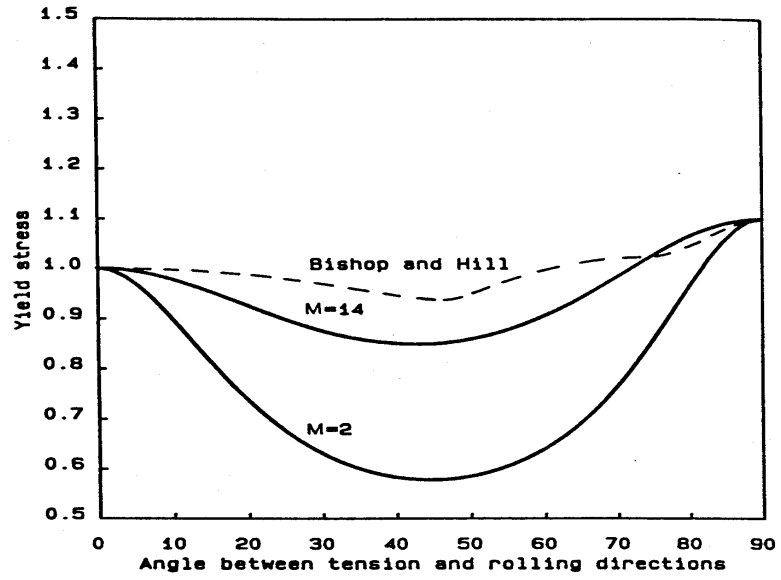

Figure 2.8 (b) Variation of Yield Strength in the Plane of the Sheet[43]

based upon both experimental observations and theoretical considerations. This relationship between yield strength and grain size is known as the Hall-Petch equation and is given as:

$$\sigma_y = \sigma_i + k_y d^{-1/2} \tag{2-13}$$

where, σ_y = yield strength; σ_i = friction stress;

d = mean grain size; k_y = the Hall-Petch slope or coefficient.

In principle, the H-P coefficient, k_y, depends on the nature of slip propagation from the yielded grain to the unyielded grain. It should be recognized that slip will only be transmitted across the boundary of a yielded grain, if the applied stress is sufficient to nucleate the slip event and propagate it across the unyielded grain. The local stress necessary to propagate slip may be determined by any of the following processes:

i) Unpinning of existing dislocations in the unyielded grain.

ii) Creation of dislocations in the unyielded grain.

iii) Donation of dislocations from the grain boundary or creation of new dislocations at the boundary.

The H-P equation formulates in a general way the resistance of grain boundaries to the spread of slip bands. Several theories have been proposed[(46-48)] to explain the microscopic mechanisms contributing to grain size strengthening and understanding the physical meaning of k_y. Some of these theories are described below[(47)].

A) Hall-Petch theory:

The basic idea in this theory is that a dislocation pile-up can "burst" through a grain boundary due to stress concentrations at the head of the pile-up. If τ_a is the shear stress applied on the slip plane, τ_i is the friction stress, d is the grain diameter, then according to Eshelby's analysis, the Hall-Petch equation can be rewritten as:

$$\tau_a = \tau_i + (2Gb/\alpha\pi)\, d^{-1/2} \tag{2-14}$$

where, G = shear Modulus; b= Burger's vector

α = constant = 1 for screw dislocations.

= (1-ν) for edge dislocations, ν = Poisson's ratio

Thus the value of k_y, for shear stresses in Eqn. 2-14 is given as:

$$k_y = 2Gb/\alpha\pi \tag{2-15}$$

B) Cottrell's Theory:

Cottrell used a somewhat similar approach; however, he recognized that it is virtually impossible for dislocations to "burst" through boundaries as reported by Tjerkstra[49]. Instead, he assumed that the stress concentration produced by a pile-up in one grain activated a dislocation source in the adjacent grain. The stress concentration is dependent upon the mean grain size, d, and the distance, 'r', of the dislocation source in the adjacent grain from the grain boundary. The stress concentration, at the head of the pile-up, is proportional to $(d/4r)^{1/2}$. See Figure 2.9[48]. With this assumption, the Hall-Petch equation (2-14) can be rewritten as:

$$\sigma_o = \sigma_i + \left(9\tau_c r^{1/2}\right) d^{-1/2} \tag{2-16}$$

where, τ_c is the critical shear stress required to activate the new source in the adjacent grain.

C) Armstrong's theory:

Armstrong et al.[50] presented the following explanation for the H-P equation based upon Taylor's theory for the deformation of a polycrystal by applying a tensile stress, σ. According to Armstrong's postulation, the H-P equation can be written as:

$$\sigma_y = m\tau_o + (m^2\tau^* r^{1/2}) d^{-1/2} \tag{2-17}$$

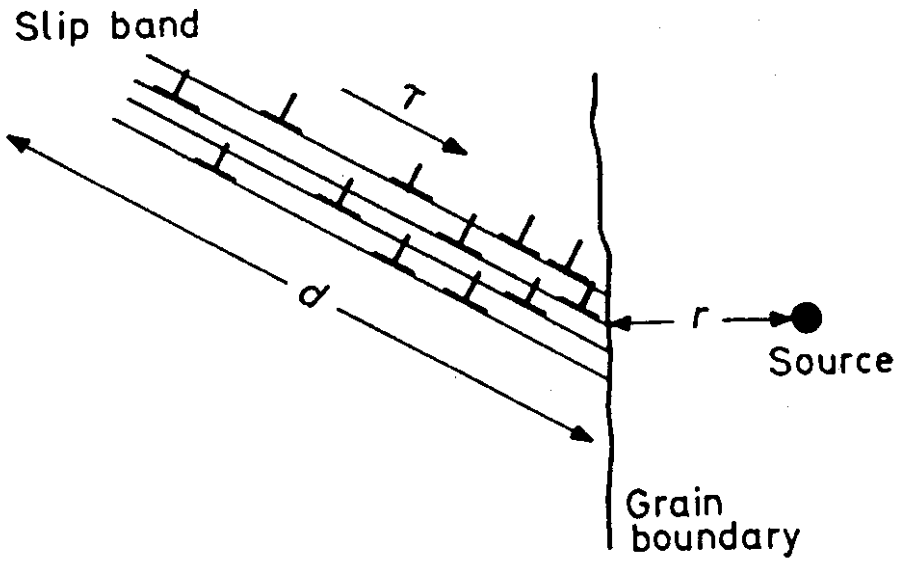

Figure 2.9 Grain Boundary Pile-up Model for k_y[49]

where, m = orientation factor related to the number of available slip systems; = 2.2 - 3.1 for cubic materials.

τ^* = critical shear stress developed at a distance r from the slip band.

Thus factors which increase the values of m, τ^* or r should increase the value of k_y. m is determined by the number of available slip systems and hence is higher for c.p.h materials and in the range of 2.2-3.1 for cubic materials. Strong solute pinning will increase the value of τ^*. Strongly ordered alloys, in which cross slip is more difficult will also have a higher value of m and consequently show higher k_y values.

D) Conrad's Theory:

Also known as the work hardening theory[51], this theory starts from the assumption that the small-grain-sized specimens have a higher dislocation density than the large-grain-sized specimens at a given value of plastic strain. With these assumptions and the appropriate substitutions, the Hall-Petch equation, as per this theory, is rewritten as:

$$\tau_a = \tau_i + \alpha' G b^{1/2} \gamma^{1/2} d^{-1/2} \qquad (2\text{-}18)$$

where, γ is the shear strain.

E) Li's Theory:

The most important objection to the dislocation pile-up mechanism was the lack of direct observation of dislocation pile-ups. Hence, Li proposed an alternative theory not based on pile-ups. Li[52, 53] considered that the grain boundary is a source of dislocations. According to Li, irregularities at grain boundaries (steps or ledges) generated dislocations, "pumping" them into the grains. These dislocations form a forest in regions close to the boundary. The yield stress, according to Li, is the stress required to move dislocations through these forests. Brandon[54] and Murr[55], showed that grain boundaries in several metals and alloys namely, Ni, Cu, Ir, Al, Ta,

Mo and 304 stainless steel could actually emit dislocations after a small level of cold reduction is applied. Murr[55] concluded that dislocations emitted from grain boundaries could be mistaken for grain boundary pile-ups. He also concluded that grain boundary ledges are a prominent source of dislocations during the onset of yielding in metals and alloys. Worthington and Smith[56] also observed the emission of slip bands from grain boundaries in 3% Si-iron. Price[57] and Hirth[58, 59] proposed a specific mechanism for screw dislocation generation from grain boundaries.

In many metals and alloys, the flow stress is related to the dislocation density (ρ) by the relationship:

$$\tau_a = \tau_i + \alpha G b \rho^{1/2} \tag{2-19}$$

It is also known that the dislocation density, ρ , is inversely proportional to the grain size, d. Substituting this relationship, the following equation is obtained:

$$\tau_a = \tau_i + \alpha' G b d^{-1/2} \tag{2-20}$$

The value of k_y, in Eqn 2-13, is given as:

$$k_y = \alpha G b (8m/\pi)^{1/2} \tag{2-21}$$

where, m = ledge density in the grain boundary, α = constant depending upon the stacking fault energy and usually has a value of 0.4.

Consequently, the stress required to penetrate the grain boundary is essentially identical to the stress necessary to initiate plastic deformation by generating dislocations from grain boundary ledges to form a forest array near the interface. The average dislocation density in the forest is given as:

$$\rho = (8mB_L / \pi d) \tag{2-22}$$

where B_L is the burger's vector of the grain boundary ledge.

Based upon Li's theory, Hutchinson and Pascoe[60] rationalized the observations they made in copper-based solid solutions and derived the following equation for k_y:

$$k_y = 3\mu bm / 2\rho^{1/2} \tag{2-22a}$$

where, ρ = total density of dislocations donated by the grain boundaries and that present in the lattice.

Thus, k_y would tend to: a) decrease with increasing density of mobile dislocations in the lattice b) increase on release of further dislocations from the boundaries and c) increase with increasing value of m, resulting from the multiplication of dislocations originating in the boundary.

2.3.6.1 <u>Grain Boundary Ledges.</u> The presence of grain boundary dislocations (GBDs') is responsible for the formation of grain boundary ledges. Grain boundary dislocations are incorporated in grain boundaries when the orientation relationships between the two grains deviate from ideal coincidence orientations. The agglomeration of these GBDs' can lead to the formation of large steps or ledges in the boundary. The process of formation of grain boundary ledges is shown schematically in Figure 2.10[61].

The number of GBDs' governs the size of the grain boundary ledges coalescing or agglomerating within the interface to form a particular ledge.

As a result, the effective Burger's vector of a grain boundary ledge can be represented as:

$$B_L = 2nb\sin(\theta/2) \tag{2-23}$$

where n is an integer representing the number of glide dislocations of Burger's vector b, or more generally:

$$B_L = mb \tag{2-24}$$

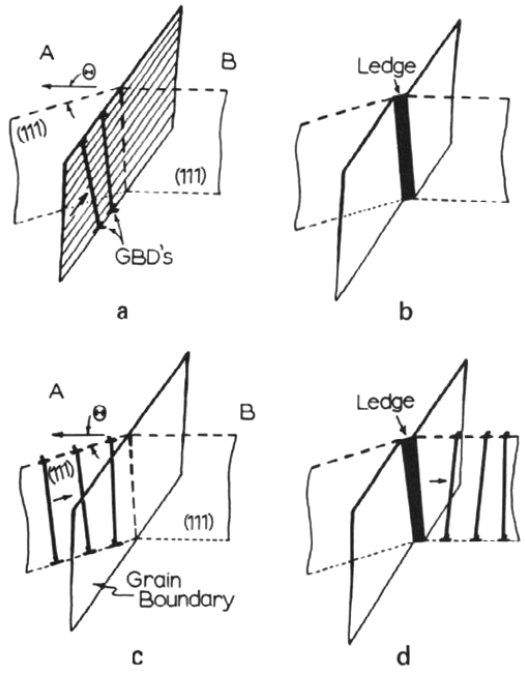

Figure 2.10 Formation of Grain Boundary Ledges[61]

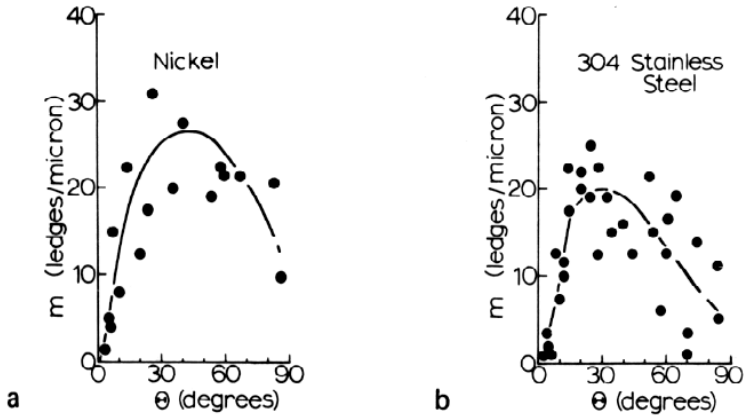

Figure 2.11 Dependence of Ledge Density (m) on Grain Boundary Misorientation [55]

where m is the number of GBDs' composing the ledge.

It has been observed that the free energy of a ledge is a strong function of the grain boundary misorientation and is small for high angle boundaries [53, 55, 62]. As a result, ledges are readily formed in high angle grain boundaries. Some experimental observations have been shown in Figure 2.11[55]. An important feature of grain boundary ledges is that they are highly effective sources of dislocations. This phenomenon has been shown schematically in Figure 2.12[63]. Some experimental observations of this phenomenon are shown in Figure 2.13[61]. Hornbogen[64, 65] has also observed the formation of dislocations loops from both high and low angle grain boundaries in a Fe-3.17 at pct. P alloy. This process of dislocation emission from the boundaries is shown in Figure 2.14[64]**.** Based on the measurement of Lüders strain in phosphorus, tin and silicon-added low carbon sheet steels, Hu[66] has shown that the segregation of solutes to ferrite grain boundaries results in an increased density of grain boundary dislocations emitted from grain boundary ledges.

It is thus seen that the segregation of solutes to grain boundaries can affect the yielding behavior of metals and alloys by affecting the ledge density at the grain boundaries. Additionally, segregation of solutes can also bring about the phenomenon of "Grain Boundary Hardening". These effects are discussed in the next section.

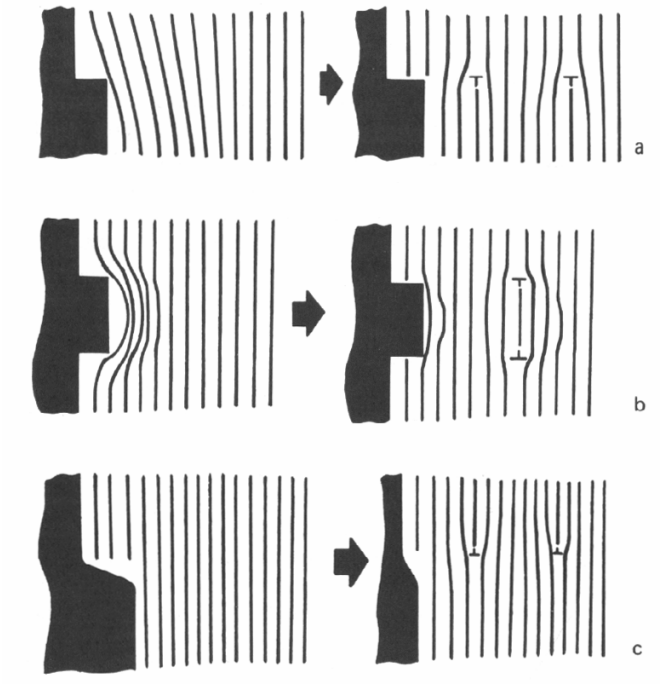

Figure 2.12 Schematic of Grain Boundary Ledges Acting as Dislocation Sources[63]

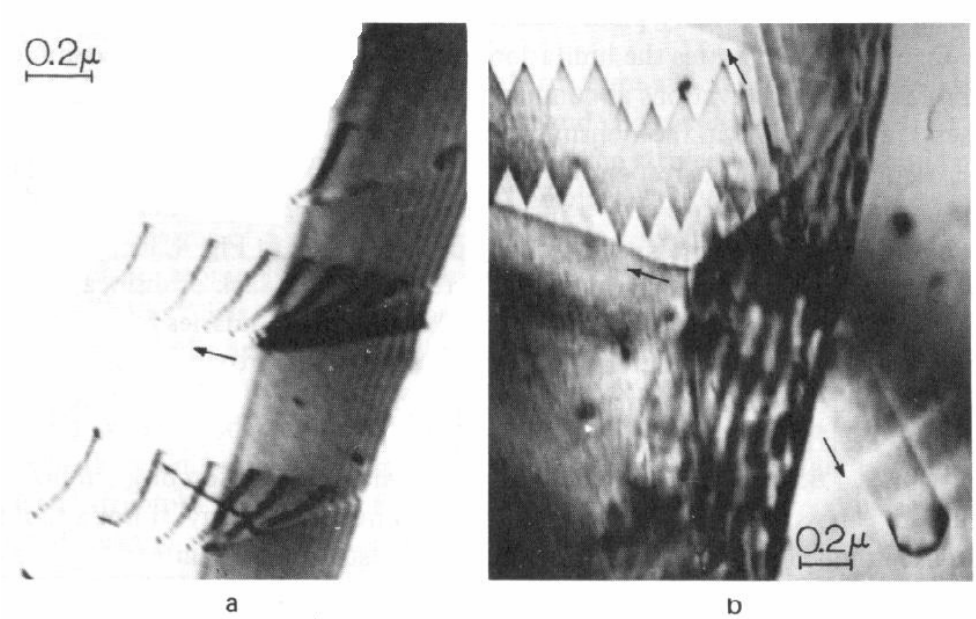

Figure 2.13 Evidence of Dislocation Emission from Grain Boundary Ledges in: [61]

a) 304 Stainless Steel b) Aluminum

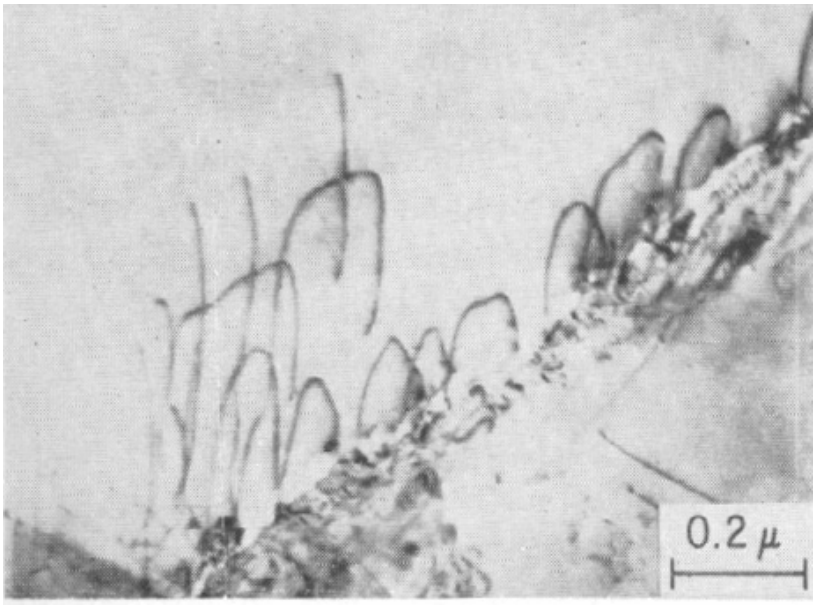

Figure 2.14 Dislocations Emitted at Grain Boundaries in Fe-3.17 at% P Alloy after 1% Deformation[64]

2.3.6.2 Segregation of Solute Elements to the Grain Boundaries. Wilson[67, 68] showed that on quenching low carbon steels from 700°C and aging at 90°C for different times, the k_y value increased from the as-quenched value of approximately 10 MPa $mm^{1/2}$ to the saturation value of approximately 22 MPa $mm^{1/2}$ in aged samples. See Figure 2.15[67]. Wilson concluded that the segregation of solutes, namely carbon, to ferrite grain boundaries modified the stress required to nucleate/activate mobile dislocations from grain boundaries, thereby causing an increase in the value of k_y. Cottrell[69] also has shown that the value of k_y in low carbon steels can be strongly influenced by the rate of cooling after high temperature holding. This is shown in Figure 2.16[69]. Other researchers, namely, Morrison and Leslie[70] have also observed a similar behavior for steels containing Ni and Si and so have Mintz et al.[71] for C in low carbon steels. Mintz[72-74] and Turner[75] have also shown that the additions of Si and Mn to steels result in a decrease in the k_y value, which is due to the suppression of nitrogen segregation to ferrite grain boundaries.

2.3.6.3 Solute Segregation and Grain Boundary Hardening. Solute segregation not only affects the value of k_y, but also affects the grain boundary microhardness in the vicinity of the grain boundaries. Floreen and Westbroook[76] observed this effect in Ni-S alloys. These researchers measured the microhardness of Ni-S alloys and found that when S is segregated to the Ni grain boundaries, the hardness in the immediate vicinity of the grain boundary is approximately 50% higher than in the matrix. This phenomenon has been termed as "Grain Boundary Hardening". Seybolt and Westbrook[77] observed similar effects in NiGa intermetallic where oxygen at grain boundaries caused grain boundary hardening. Braunovic[78-80] et al. have

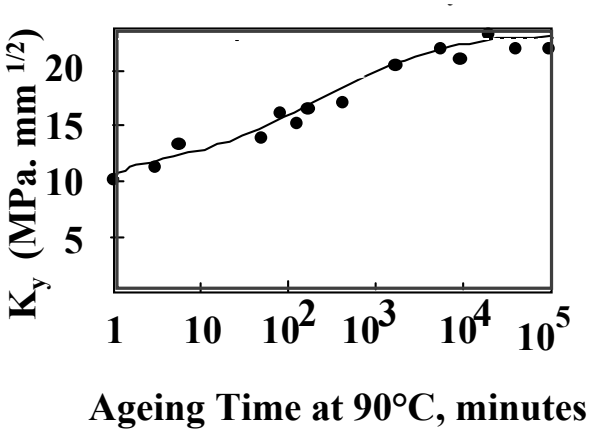

Figure 2.15 Dependence of k_y on the Segregation of C to Grain Boundaries[67]

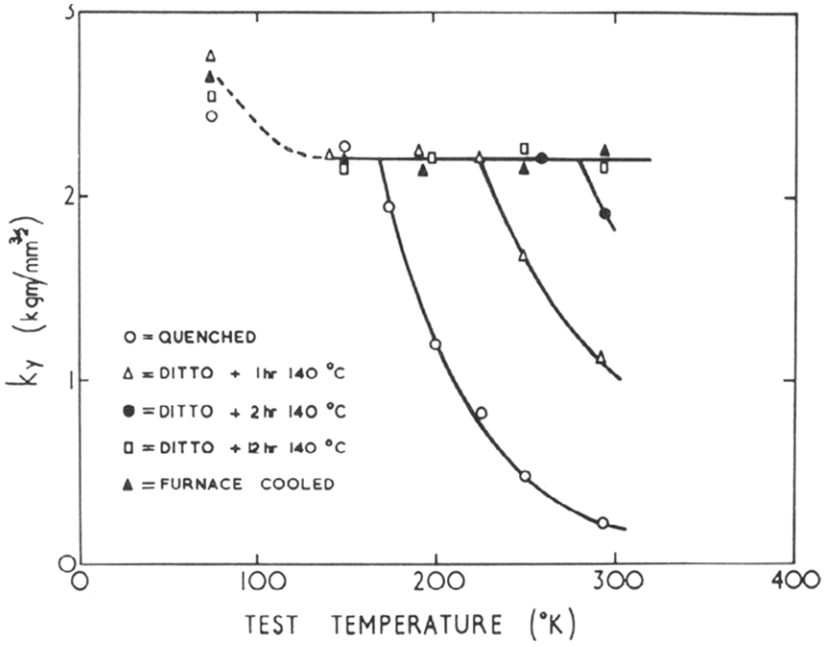

Figure 2.16 Dependence of k_y on Rate of Cooling in Low Carbon Steels[69]

done extensive studies in iron with the addition of solutes such as W, Sn, Si, Cr, P and S**.** By employing a load of 3 g in a microhardness test, Braunovic observed that the addition of certain solutes such as Sn, P, S, W resulted in a much higher grain boundary microhardness compared to the grain center or matrix hardness. This is shown in Figure 2.17[(81)] for Fe alloyed with W. It was postulated that the segregation of solutes to ferrite grain boundaries resulted in an increase in the grain boundary hardness. Similar studies were conducted by Aust et al.[(82)] in Sn, Pb and Zn alloys. Aust observed that certain solutes brought about grain boundary hardening whereas others resulted in grain boundary softening. This result was rationalized based upon the vacancy-solute binding energy, E_{VI}. For solutes having positive E_{VI} values in the solvent, grain boundary hardening is observed, whereas solutes having negative E_{VI} values show grain boundary softening. The grain boundary hardening for solutes having positive E_{VI} values is also related to the thermodynamic stability of the solute clusters at the grain boundary. Thus it was seen that solutes which exhibit positive deviations from ideality and positive values of E_{VI} result in grain boundary hardening, whereas those exhibiting negative deviations from ideality and negative values of E_{VI} show grain boundary softening. For phosphorus in iron, the value of E_{VI} is 0.36, which is highly positive. Hence, phosphorus bears the potential to bring about grain boundary hardening in iron.

Floreen and Westbrook[(76)] proposed that segregation of solutes to the grain boundaries reduces the grain boundary energy, thereby increasing the ledge density in the grain boundaries and hence, as predicted by Li in Eqn. 2-20, increasing the value of k_y. They also suggested that the increased ledge density would increase the number of dislocations emitted from the grain boundaries and additional hardening could occur because of S atoms pinning these grain

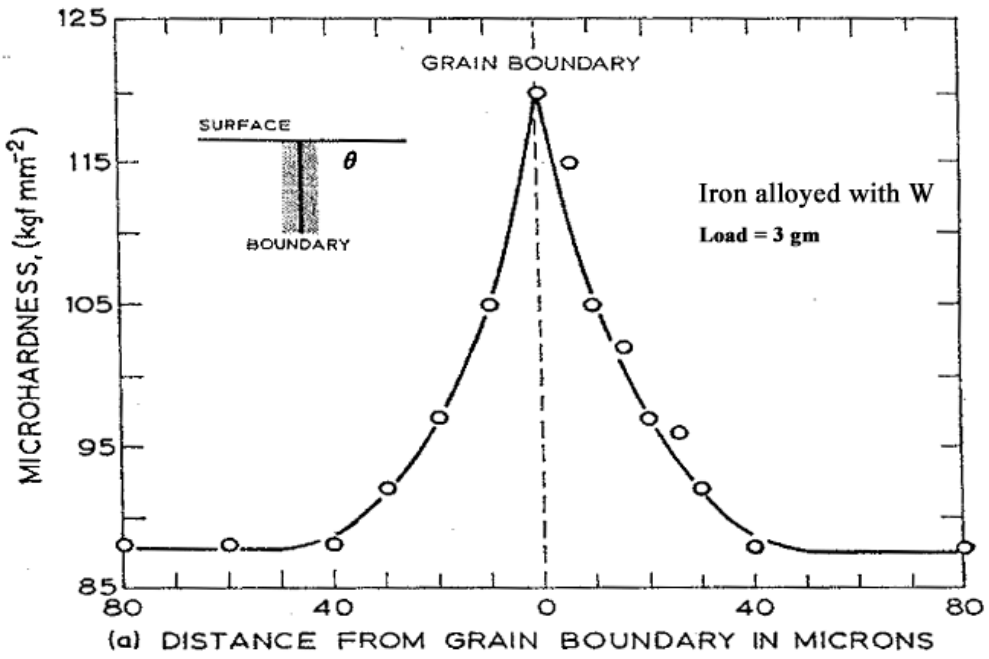

Figure 2.17 Grain Boundary Hardening in Fe-W Alloy[78]

boundary dislocations. By measuring the grain boundary and grain interior hardness of iron alloys with solute Sn, Braunovic has also shown that the ledge density, m, at the ferrite grain boundaries is strongly influenced by the tin content. This variation has been shown in Figure 2.18[83].

One of the objectives of this research is to understand the role of P in determining the strength of IF steels. The following section describes, briefly, the various effects of P observed in IF steels as reported earlier by a number of researchers.

2.4 The Role of Phosphorus in IF Steels

The addition of phosphorus is known to affect several mechanical properties of IF steels. The complexity of the various effects arises primarily from the relative distribution of phosphorus at different locations in the IF steels. Phosphorus shows limited solubility in ferrite. Phosphorus atoms can reside in the ferrite matrix, can strongly segregate to external surfaces as well as to ferrite grain boundaries and can also form precipitates either at the grain boundaries or in the ferrite matrix, as shown schematically in Figure 2.19.

The relative distribution of P between these locations is strongly influenced by the thermo-mechanical processing of IF steels and also on the presence of alloying additions such as Ti and/or Nb and interstitial elements such as C and B. An excellent review of the various effects of P in steels has been given by Bloom et al[84] .

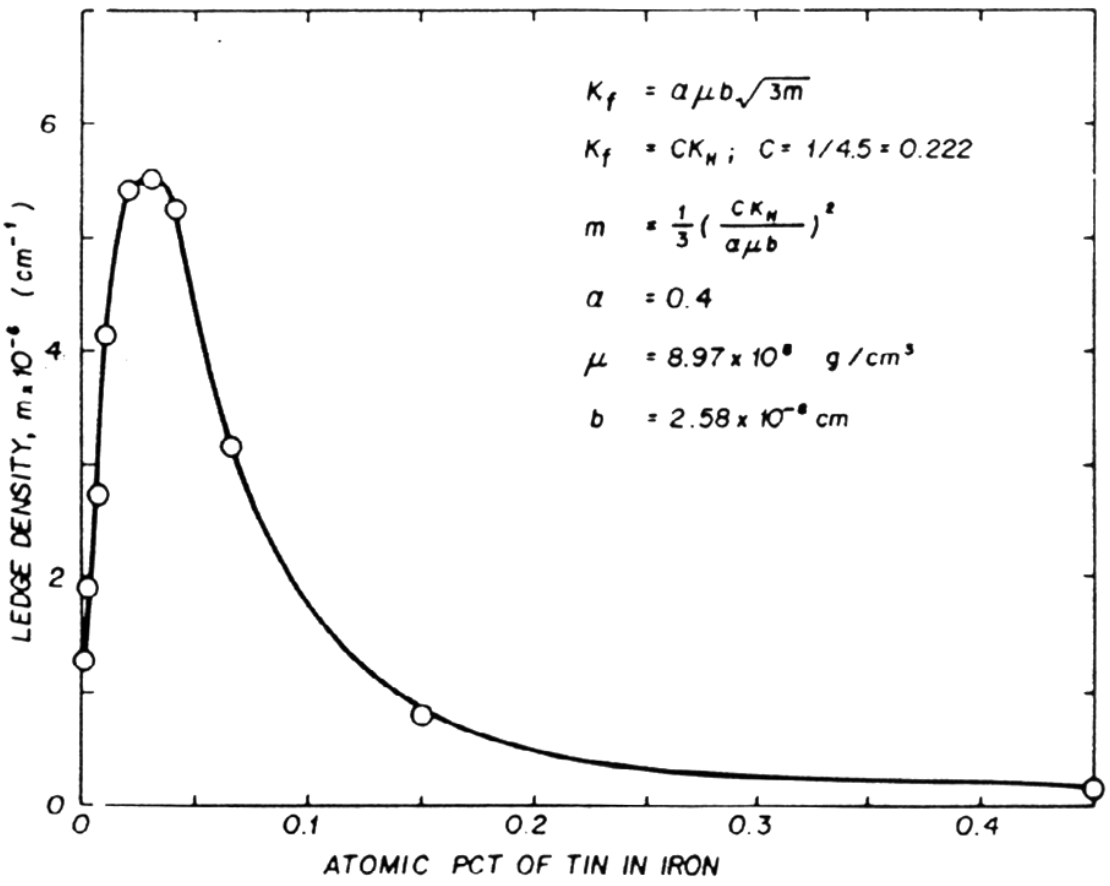

Figure 2.18 Effect of Sn Segregation on Grain Boundary Ledge Density in Iron[83]

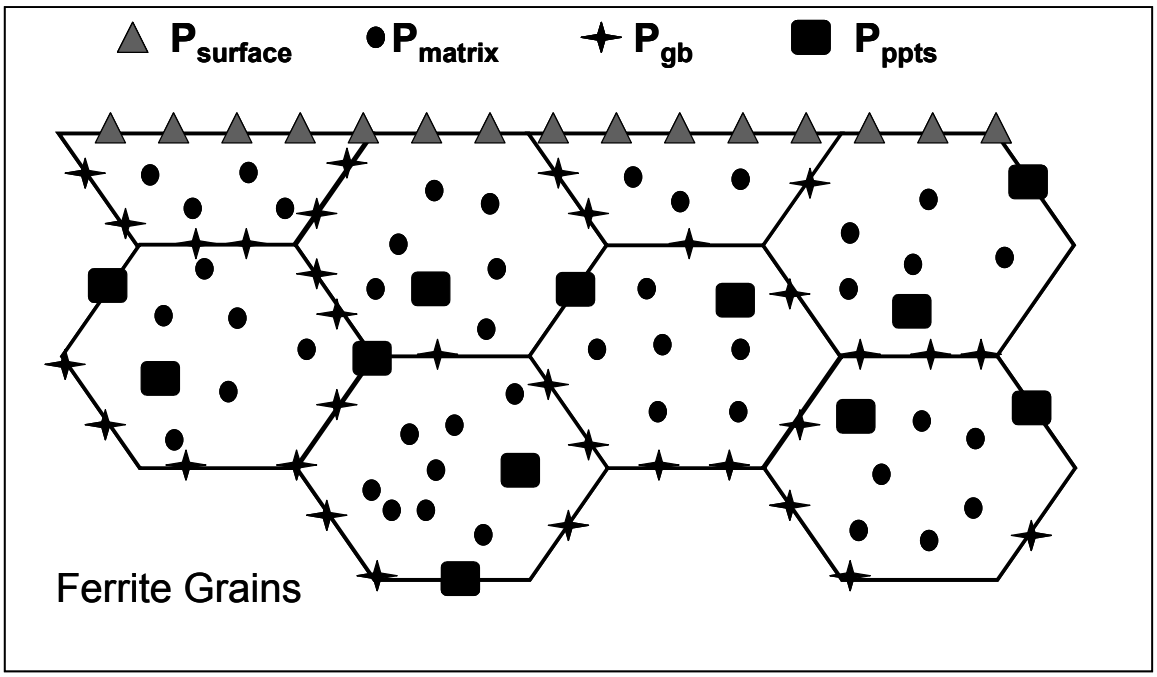

Figure 2.19 Schematic Illustration of Possible Locations of P in Ferrite Grains

2.4.1 Effect on Yield Strength

Phosphorus is known to be the most efficient substitutional solute in steels. Several researchers have investigated the role of P as a strengthener of steels. Phosphorus is a substitutional solute in iron which brings about a contraction in the lattice parameter of iron. Substitutional solutes in Fe are seen to typically bring about solid solution strengthening via atomic misfit, modulus strengthening and difference in electronegativity between the solute and solvent atoms. The atomic misfit parameter (ε_a) for P in Fe is -0.014, the modulus misfit parameter (ε_G) is 0.928 and the difference in electronegativities (ΔE_n) of P and Fe is 0.23. As shown in Figures 2.5 and 2.6, P brings about strengthening far greater in proportion than that predicted by its atomic misfit parameter in Fe. This anomaly also could not be accounted for by the combined effect of atomic misfit, modulus misfit and electro-negativity differences between P and Fe.

Solid solution strengthening is usually expressed as:

$$\Delta YS_{SSS} = k_s \text{ (wt\% Solute)} \qquad (2\text{-}25)$$

Several studies have been performed to evaluate the value of k_s for the addition of P in steels. These results have been summarized in the Table 2.2. It can be seen from the table that there is a huge variation in the reported values of k_s for P in steels. There are several factors responsible for this variation. Some of the important factors are the interaction of different solutes such as Ti, Nb, C, Mn, B with P, the precipitation of P bearing precipitates such as FeTiP, Fe(Ti,Nb)P during processing and the grain refinement caused by the addition of P. It is known that the addition of P brings about grain refinement in steels.

Table 2.2 Values of Solid Solution Strengthening Coefficients Reported for P in Fe

Reference	k_s (MPa/0.01 wt% P)	Steel Composition
Leslie[32]	2.84	0.1wt% C, 0.16 wt% Ti
Spitzig et al[85, 86]	5	0.1 C, 1 Mn
Spitzig[87]	4.83	0.005 C, 0.03 Mn
Matsuoka et al[88]	5.55	0.04 C, 0.3 Mn
Engl et al[89]	8	0.003 C, 0.3 Mn, 0.04 Ti
Ushioda et al[1]	7.5	0.0025 C, 0.042 Ti
Pickering et al[27]	6.2	NA
Hopkins et al[90]	4.6	0.003 C, 0.002 Mn
Gupta et al[20]	6.9	0.005 C, 0.04 Nb
Nilsson et al[91]	15.5	Ti-ULC steel
Pradhan et al[92]	6.22	0.01 C, 0.06 Al
Tokunaga et al[93]	8.7	0.005 C, 0.04 Nb, 0.03 Al
Pradhan et al[94]	12.5	Ti- IF steel
Bleck et al[95]	12.5	Ti- IF steel
Irie et al[96]	7.4	Nb-IF steel

Some researchers have accounted for the grain refinement and recalculated the values for true solid solution coefficient, k_s, for P in steels. For example, Ushioda recalculated the value to

be 6 MPa/0.01wt% P and Engl recalculated it to be 3.5 MPa/0.01wt% P after corresponding grain size corrections. The above table highlights the following issues:

1) Conventional solid solution strengthening mechanisms cannot account for all the strengthening seen due to P in steels.

2) Chemistry and processing plays an important role in determining the final strengthening that can be obtained by the addition of P to steels.

3) In addition to solid solution strengthening, there might a possibility of another mechanism being in operation when P additions are made to steel. It was stated earlier that segregation of solutes to grain boundaries can bring about the phenomenon of grain boundary hardening. P is known to a strong segregant in IF steels. Work done by Braunovic[78] and Spitzig[87] has shown that the addition of P to steels not only can increase the grain boundary microhardness but also the value of the H-P slope, k_y. Spitzig reported that the value of k_y increases initially with increasing bulk P content and then decreases after a certain level of bulk P is reached. The results from Spitzig's work have been shown in Figure 2.20. The role of P in bringing about GBH has thus been suggested but not substantially investigated.

2.4.2 Phosphorus-bearing Precipitates and the Strength of IF Steels

In addition to being in the matrix and segregating to grain boundaries, P can also be precipitated in IF steels in the form of FeTiP, either in the matrix or at ferrite grain boundaries. A

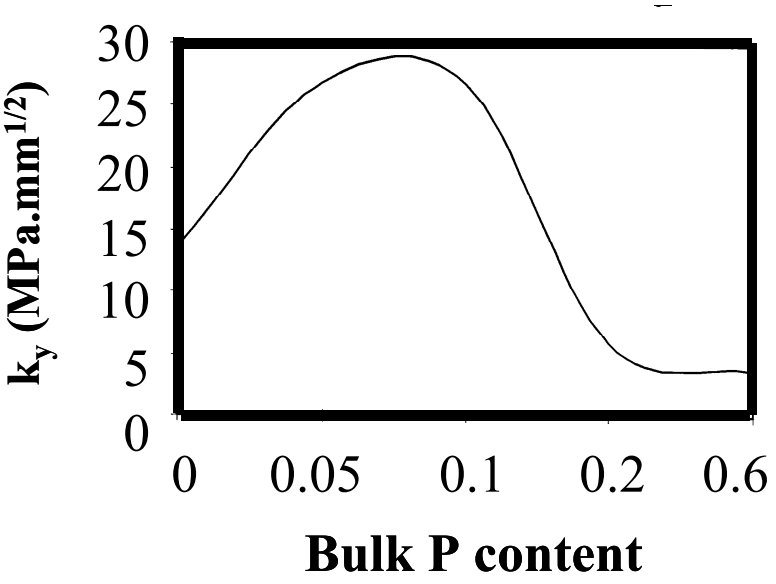

Figure 2.20 Effect of Bulk P Content on k_y Value in ULC Steel[87]

considerable amount of interest has been generated concerning the precipitation of FeTiP particles during the processing of IF steels, since this has implications for both the strength and formability of these steels [89, 97-109]. FeTiP precipitates have been observed both at the grain boundaries and in the ferrite matrix. The structure of FeTiP precipitates has been studied by Gupta et al[110]. FeTiP has an orthorhombic crystal structure with 4 atoms of Fe, Ti and P each in the unit cell and a density of 6 g/cc. It is generally believed that the precipitation of FeTiP is deleterious to the strength since it locks up solute P and hence reduces the amount of P available to bring about solid solution strengthening. This has been shown by Engl et al[89]. Engl showed that the absence of FeTiP in low Ti-IF steels (0.04 wt% Ti, 0.044 wt% P) resulted in a k_s value of 8 MPa /0.01 wt% P in this steel. On the other hand, in a high Ti-IF steel (0.079 wt% Ti, 0.044 wt% P), the presence of FeTiP reduces the value of k_s in the range of 2.8 - 4.2 MPa /0.01 wt% P. Thus the precipitation of FeTiP results in a loss of strengthening in IF steels.

The precipitation of FeTiP also affects the formability of IF steels by affecting the texture development during recrystallization. The presence of FeTiP precipitates has been shown to be both useful and harmful for the formation of the beneficial {111}<uvw> texture. The formation of coarse FeTiP precipitates in the hot band processing of high Ti, high P IF steels is found to be beneficial in subsequent cold rolling and annealing, since these precipitates act as nucleation sites for {111}<uvw> oriented grains.

On the other hand, if FeTiP precipitates form during annealing prior to the onset of the recrystallization of ferrite, then the growth of {111}<uvw> oriented grains tends to be retarded. It has also been postulated that the formation of FeTiP consumes all excess Ti in the IF steel, thus leaving solute C in the ferrite matrix. The presence of solute C results in the degradation of the {111}<uvw> recrystallization texture, thus negatively affecting the formability of IF steels.

Thus, the FeTiP precipitates can be both beneficial and harmful for preferred texture development, and thereby, to the formability of IF steels.

The occurrence of FeTiP ppts in the hot band is mainly dependent upon the chemistry of the IF steel. High bulk values of Ti and/or P that would exceed the solubility product of FeTiP coupled with high coiling temperatures, results in FeTiP precipitation in the hot band. During annealing after cold rolling, prolonged exposure in the temperature range of 700-800 C will result in the precipitation of FeTiP in the matrix provided the solubility product can be exceeded. This has important implications in the annealing of IF steels. Thus, batch annealing cycles are more prone to FeTiP precipitation compared to the continuous annealing process. It has also been shown that in P bearing Nb-IF steels, FeNbP precipitates can be precipitated[111]. FeNbP precipitation might bring about similar effects as FeTiP in Nb-stabilized IF steels.

2.4.3 Segregation of Phosphorus in IF Steels

As mentioned earlier, the segregation of P to ferrite grain boundaries in steels can affect the grain boundary microhardness as well as the Hall-Petch slope, k_y, and, as a result the overall strength of steels. It is therefore, imperative to understand the thermodynamic basis and the kinetics of P segregation in steels. There are several factors which govern the segregation of solutes, P in particular, to ferrite grain boundaries. The following is a brief review of the mechanisms of solute segregation in steels.

There are two types of segregation behavior that need to be taken into account. These are: a) Equilibrium segregation and b) Non-equilibrium segregation.

2.4.3.1 <u>Equilibrium Segregation.</u> The driving force for equilibrium segregation is derived from the elastic strain energy of the solute in the matrix, valency effects, electronegativity effects and the solid solubility of the solute in the matrix. Since grain boundaries are regions of atomic mismatch, solute atoms tend to minimize the overall energy of the system by segregating to such distorted regions in the microstructure. The solute concentration at grain boundaries is usually expressed in the form of the Langmuir-McLean equation as[112-114]:

$$\frac{X_b}{X_{bo} - X_b} = \frac{X_c}{1 - X_c} \exp\left(-\Delta G / RT\right) \tag{2-26}$$

where, X_b = grain boundary composition of solute

X_{bo} = saturation value of X_b

X_c = bulk solute concentration

ΔG = free energy of solute segregation

R = gas constant; T = absolute temperature

X_{bo} is generally of the order of a monolayer of segregated atoms, where one monolayer contains a^{-2} solute atoms per unit area, where a^3 is the atomic volume of the segregant. In the Langmuir-McLean equation, the free energy of segregation is derived only from the elastic misfit energy between the solute and solvent atoms. This shortcoming of the Langmuir-McLean formalism was accounted for by the truncated BET theory, wherein the solid solubility of the solute atoms in the matrix was also included in the driving force for segregation. The truncated BET equation for equilibrium segregation thus gives the following:

$$\frac{X_b}{X_{bo} - X_b} = \frac{X_c}{X_{co}} \exp\left(-\Delta G_1 / RT\right) \tag{2-27}$$

where, X_{co} = solute molar fraction at the solubility limit

$$X_{co} = \exp\left(-\Delta G_s / RT\right) \tag{2-28}$$

ΔG_s = free energy of the solution

Substituting for X_{co} in the above equation gives:

$$\frac{X_b}{X_{bo} - X_b} = X_c \exp\left(-\Delta G / RT\right) \tag{2-29}$$

where, $\Delta G = \Delta G_1 - \Delta G_s$ (2-30)

For P segregation to ferrite grain boundaries in IF steels, the value of ΔG has been determined to be:

$$\Delta G = -34300 - 21.5\ T\ (J/mole)^{(115)} \tag{2-31}$$

Thus it is seen from the Langmuir-McLean equation that the segregation of P to ferrite grain boundaries will be increased if the bulk concentration of P, X_c, is increased or as the temperature of segregation is decreased.

For low solute levels, the truncated BET equation can be written as:

$$\frac{X_b}{X_{bo}} \frac{1}{X_c} = \exp\left(-\Delta G_1 / RT\right) / X_{co} \tag{2-32}$$

or,
$$\beta_b = \exp\left(-\Delta G_1 / RT\right) / X_{co} \tag{2-33}$$

where, β_b = enrichment ratio of the solute

It is seen that β_b is inversely proportional to the solid solubility of the solute in the solvent. The solid solubility of P in Fe is low and of the order of $\sim 10^{-2}$ because of the large elastic misfit of P in Fe as well as the large electronegativity difference between P and Fe atoms. As a result, P acts as a strong grain boundary segregant in iron and its alloys showing grain boundary enrichment ratios of the order of 10^3. Several researchers have characterized the

equilibrium segregation behavior of P in iron and its alloys[115-133]. A representative plot of effect of bulk P concentration and segregation temperature on the extent of P segregation in iron alloys has been shown in Figure 2.21 [134].

The segregation of P in steels is affected by the presence of other impurity elements and alloying additions. Thus, in IF steels, the presence of C, Ti, Nb, B can significantly alter the extent of P segregation. It is known that the competitive segregation occurs between P and C as well as P and B in IF steels. Thus, P competes with C and B for grain boundary sites due to the repulsive interaction between the atoms and hence the segregation of P is significantly reduced by the presence of solute C and B in IF steels. The role of Ti and Nb in affecting P segregation can be very complex due to the following factors:

a) Ti and Nb are strong carbide formers.
b) Ti and Nb also have strong affinity for P

Nb also segregates to ferrite grain boundaries and participates in competitive segregation with P at grain boundaries. Thus, if Ti and Nb mainly scavenge C from the matrix, then the segregation of P to grain boundaries will be higher because of lack of P-C competitive segregation. On the other hand, if Ti and Nb are present in excessive amounts in the matrix, they can reduce the activity of P in the matrix, thereby increasing its solubility, thus reducing the level of P segregation. Niobium, by itself can compete with P at grain boundaries and can reduce the amount of P segregation. Thus the amount and extent of P segregation in IF steels is governed by complex interactions of P with the alloying additions.

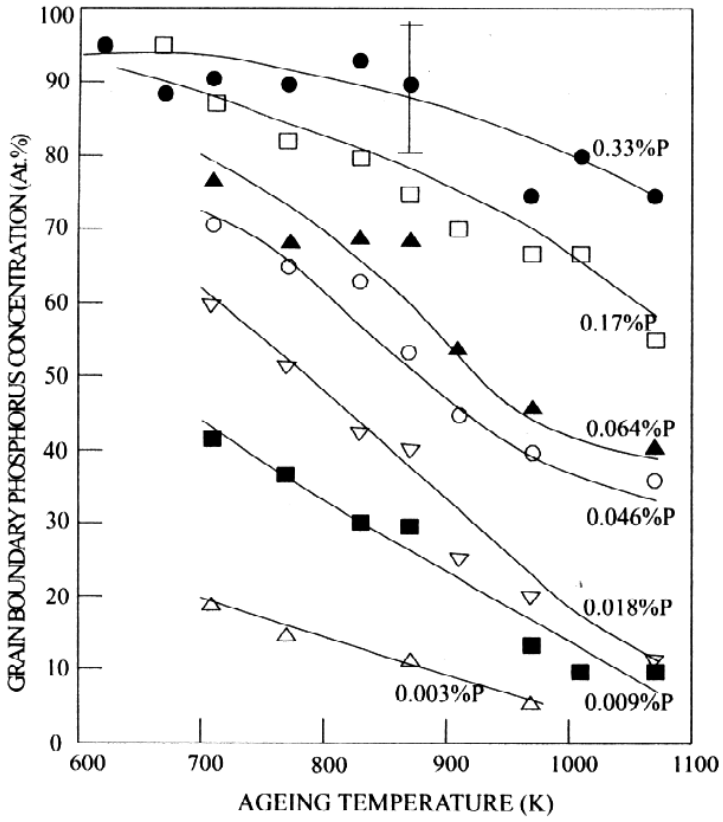

Figure 2.21 Variation in P Segregation to Grain Boundaries for Different Fe-P Alloys[134]

2.4.3.2 Kinetics of Equilibrium Segregation. Although it is important to know the maximum extent of P segregation that can occur in IF steels of a certain bulk P concentration at a certain temperature, it is equally important to know the rate at which this equilibrium concentration will be achieved. This has important implications in the processing of P-bearing IF steels since the thermal path will determine the level of P segregation actually achieved in the IF steel. The approach to equilibrium is dealt with in this section.

McLean dealt with this problem and provided the following equation by applying Fick's laws of diffusion to equilibrium solute segregation:

$$\frac{C_{gbt} - C_{gb0}}{C_{gb\infty} - C_{gb0}} = 1 - \exp^{4Dt/\alpha_2^2 d^2} \left(1 - erf\left\{2\sqrt{(Dt)} / \alpha_2 d\right\}\right) \qquad (2\text{-}34)$$

where, C_{gbt} = grain boundary concentration at time t

C_{gb0} = initial grain boundary concentration

$C_{gb\infty}$ = equilibrium grain boundary concentration attained after infinite time at temperature

D = diffusion coefficient at temperature

t = time

d = thickness of the grain boundary

α_2 = ratio $C_{gb\infty} / C_1$

C_1 = bulk solute concentration

Two useful times can be obtained from this equation.

a) Time for 50% segregation at a given temperature (t^s_{50}):

$$t^s_{50} = 0.591 \alpha_2^2 d^2 / 4D \qquad (2\text{-}35)$$

b) Time for 90% segregation at a given temperature (t^s_{90}):

$$t_{90}^{s} = 30.8 \alpha_2^2 d^2 / 4D \tag{2-36}$$

The diffusion coefficients for P in iron have been reported by several researchers [127, 128].

2.4.3.3 Non-Equilibrium Segregation of Solutes. The mechanism of NES relies on the formation of excess quantities of vacancy-solute complexes. At any given temperature, solutes, vacancies and their complexes are in equilibrium with each other. When the material is quickly cooled from a higher temperature (T_o) to a lower temperature (T_i), the excess vacancies are quenched in. These vacancies tend to diffuse to the grain boundaries which act as sinks for the excess vacancies. If the solute has a high binding energy with the vacancies, excess solute-vacancy complexes are formed. These complexes diffuse towards the grain boundaries, where they dissociate thus annihilating the excess vacancies. The excess solute associated with these complexes thus segregates to the grain boundaries. This mechanism of segregation aided by the diffusion of excess vacancies is termed as "Non-equilibrium segregation". Several researchers[135-141] have studied the thermodynamics and kinetics of NES. The maximum concentration of non-equilibrium grain boundary segregation, C_b^m, induced during quenching from a temperature, T_o, to a lower temperature, T_i and holding at T_i, is given by the following equation:

$$C_b^m(T_i) = C_g \left(E_b / E_f^v \right) \exp\left(\frac{E_b - E_f^v}{kT_o} - \frac{E_b - E_f^v}{kT_i} \right) \tag{2-37}$$

where, C_g = bulk concentration of solute

E_f^v = the energy of vacancy formation

E_b = vacancy-solute binding energy

k = Boltzmann constant

The kinetics of NES is given by the following equation:

$$\frac{C_b(t) - C_b^m(T_o)}{C_b^m(T_i) - C_b^m(T_o)} = 1 - \exp^{4D_c t / \alpha_j^2 d_n^2} (1 - erf\{2\sqrt{(D_c t)} / \alpha_j d_n\}) \quad (2\text{-}38)$$

where, D_c = diffusion coefficient of complex in the matrix

t = holding time at temperature T_i

d_n = width of the concentrated layer of impurities

$$\alpha_j = C_b^m(T_i) / C_g \quad (2\text{-}39)$$

The following values of the different parameters have been reported for P in Fe [142]

E_f^v = 1.6 eV and E_b = 0.36 eV

Both mechanisms of segregation simultaneously occur for P in iron alloys. It should be noted that the kinetics of the overall segregation of solutes are considerably accelerated due to the NES mechanism.

2.4.3.4 <u>Role of Grain Boundary Misorientation on Phosphorus Segregation.</u> In the previous sections, the thermodynamics of grain boundary segregation were discussed. These models do not take into account the fact that not all grain boundaries are created equal. In essence the role of grain boundary structure and misorientation on the amount of solute segregation is not reflected in the segregation models discussed previously. Several researchers[143-150] have addressed this issue of grain boundary misorientation and solute segregation. Suzuki et al performed one of the earlier studies on the segregation of solute phosphorus to ferrite grain boundaries. They concluded that the degree of P segregation does depend on the crystallographic orientation of the boundary plane. The results obtained by these researchers have been shown in

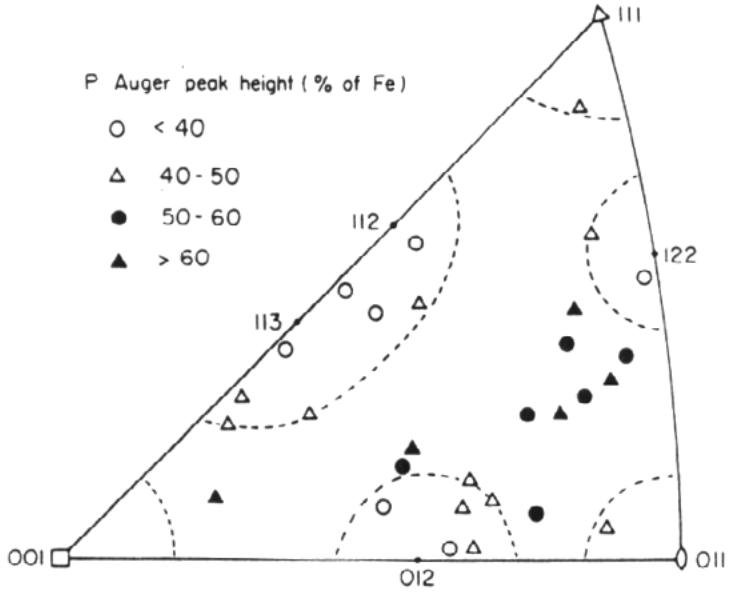

Figure 2.22 Variation of P Segregation with Orientation of Grain Boundary Planes[144]

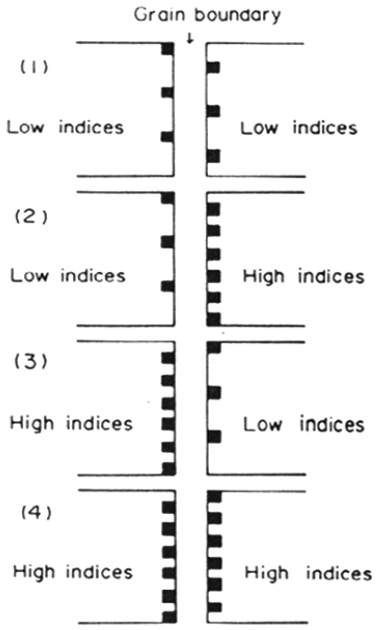

Figure 2.23 Schematic Showing P Segregation Predominant on Grain Boundary Planes of High Indices than on those with Low Indices. Dark Marks Denote P Segregation[144]

Table 2.3 Segregation Enthalpy and Entropy, of Si, P, C for Individual [100] Tilt Grain Boundaries[143]

Grain boundary	ΔH^{o}_{Si}	ΔS^{o}_{Si}	$\Delta H_P{}^{o}$	$\Delta S_P{}^{o}$	$\Delta H_C{}^{o}$	$\Delta S_C{}^{o}$
{016}	−16000	−15	−31000	17	−49000	1
{015}	−12000	−9	−16000	38	−43000	7
{014}	−14000	−9	−35000	19	−50000	2
{013}	−8500	−3	−13000	45.2	−40000	12
{0*kl*}	−17000	−13	−37000	18	−51000	6
{0 7 15}	−12000	−3	−31000	25	−45000	6
{012}	−4100	0.2	−10900	42.5	−35000	12
{059}	−12000	−5	−34000	20	−48000	4
{058}	−16000	−11	−37000	16	−53000	−1
(018)/(047)	−10000	−8	−32000	19	−50000	3
(001)/(034)	−9000	−9	−25000	29	−44000	6
(017)/(011)	−6100	−2.2	−14500	39.3	−36000	14
(0 3 11)/(097)	−11000	−5	−32000	21	−48000	3
(001)/(011)	−6000	2	−19000	38	−39000	11
(001)/(012)	−10200	−5.3	−26000	28	−47000	4
(001)/(013)	−7000	−2	−19000	35	−38000	13
(001)/(015)	−8000	−3	−22000	32	−41000	10
(011)/(015)	−7000	−2	−18000	37	−40000	9
(011)/(013)	−6000	−1	−17000	37	−36000	14
(011)/(012)	−6000	−2	−16800	36.1	−34000	16

Figures 2.22[144] and 2.23[144]. It is seen that the high index grain boundary planes show higher levels of P segregation compared to low index planes. These researchers have also shown that on account of the different grain boundary structural units, the density of segregation sites is different at each grain boundary. These different structural units have been shown in Figure 2.24[144]. The different structural units give rise to different grain boundary energies. As a result, the segregation energy of solutes to different grain boundaries would be different.

The segregation energy is given as:

$$\Delta G_I^o = \Delta H_I^o - T\Delta S_I^o \tag{2.40}$$

where; ΔG_I^o = the free energy of segregation

ΔH_I^o = the enthalpy of segregation

ΔS_I^o = the entropy of segregation

The values of the segregation enthalpy and entropy for any element at any grain boundary can be calculated from the properties of bulk solid solubility data and the linear relationship between segregation enthalpy and entropy. Using this data, Lejcek calculated the segregation enthalpy and entropy for several grain boundaries and these results are shown in Table 2.3[143]. It is evident from the table that, depending upon the crystallography of the boundary planes, the segregation free energy is different. This difference results in a difference in the degree of solute segregation at the grain boundaries. The results from Lejcek et al.[143] have been shown in Figure 2.25**.** Thus it is seen that grain boundary misorientation results in a significant anisotropy in P segregation in iron.

Work done by Boyle et al.[151] brings about an interesting point about the nature of ferrite grain boundaries and its influence on P segregation. These researchers have reported that the amount of P segregated to the ferrite grain boundaries depends upon the degree of misorientation

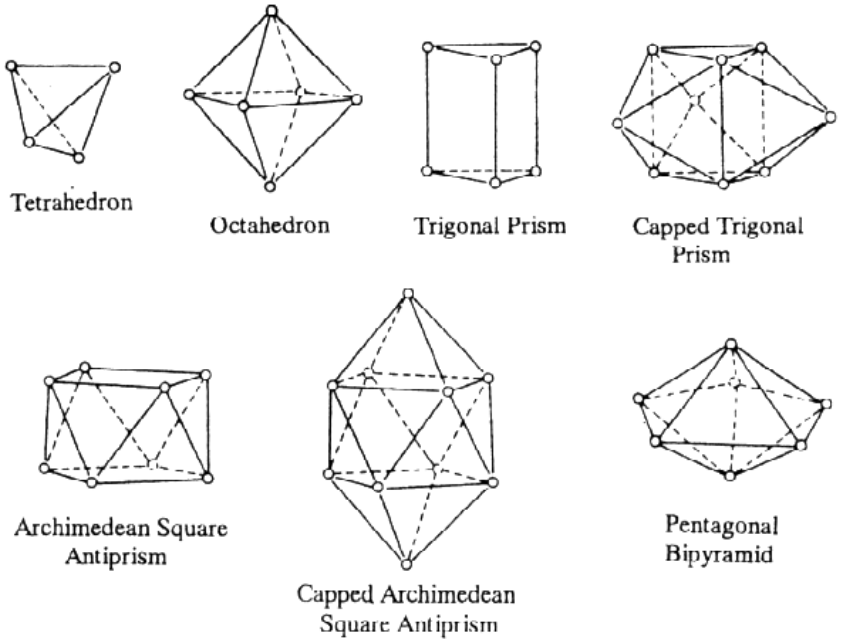

Figure 2.24 Compact Polyhedra Found at Grain Boundaries[144]

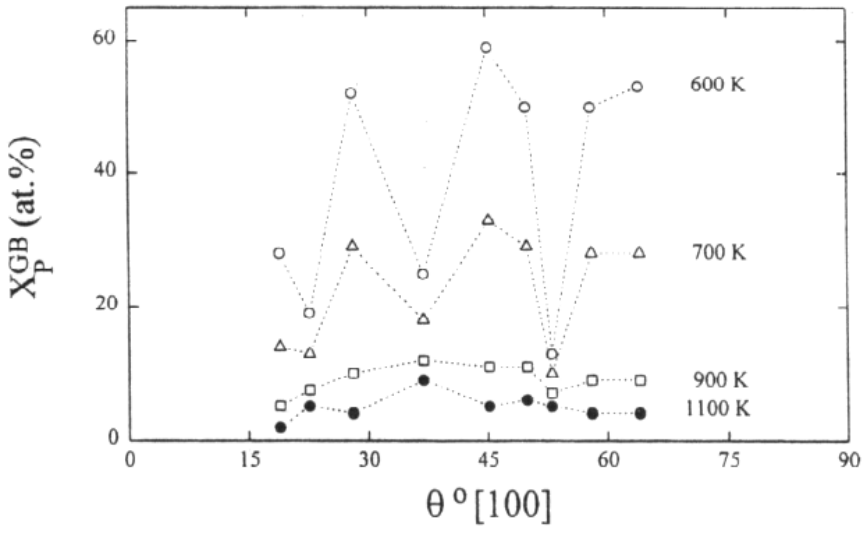

Figure 2.25 Calculated P Segregation Compositions at Ferrite Grain Boundaries for Symmetrical Tilt Grain Boundaries[143]

Similar behavior has been reported earlier in a Pb-Sn system by Aust and Rutter[152], during their study of the recrystallization behavior of Pb. Keast and Williams[153] have also observed this dependence of solute segregation on grain boundary misorientation in the Cu-Bi system. A recent review by Wray[154] also has addressed this issue. Since the value of the Hall-Petch slope, k_y, could vary with the amount of P segregated to the ferrite grain boundaries, it is critical to know the nature of the ferrite grain boundaries and the possible variation of the amount of P segregated because of different misorientations across the ferrite boundaries.

2.4.4 Effect of P segregation on Cold-Work Embrittlement (CWE)

It has been observed that the addition of P to IF steels causes the phenomenon of CWE[94, 155-158], which produces brittle fracture during the deep drawing of sheet steels. As mentioned previously, P has a strong tendency to segregate to ferrite grain boundaries and this segregation is believed to be the cause of CWE.

Several theories have been proposed to explain the thermodynamics of grain boundary segregation of solutes to interfaces, which take into account the elastic misfit, valence and limited solubility of the solute in the matrix. Additionally, the role of solutes, segregated to grain boundaries, in strengthening or weakening of bonds at the interface has also been well documented[159-162]. All of the above theories predict that P has a strong tendency to segregate to ferrite grain boundaries, more so in IF steels, and this segregation can result in the weakening of the bonds thereby causing brittle intergranular fracture. It is, hence, imperative to understand at what stage, during the processing, P segregates to ferrite grain boundaries. Work done by Rege[85] has shown that segregation of P to ferrite grain boundaries occurs during coiling of the steels in

hot band processing. Phosphorus segregation can also occur during the annealing treatment, more so during batch annealing, as has been shown by Boyle et al.[86]

2.5 Phenomenon of Springback in Steel Sheets

An equally important small strain deformation behavior that has been focused upon in this research is the phenomenon of springback. Springback is defined as the elastic recovery of the sheet metal that occurs after a forming operation is completed. It is a formidable problem in a wide range of sheet metal forming operations including deep drawing and stretch forming. The phenomenon of springback is schematically illustrated in Figure 2.26 for a typical plane-strain bending application. The amount of springback, S, for a non-strain-hardening sheet metal, can be calculated from the following equation[100]:

$$S = 1/r - 1/r' = \left(3\sigma_{ys}\right)/\left(tE'\right) \tag{2-41}$$

where, r = radius of curvature of the sheet with the forming load applied

r' = radius of curvature of the sheet after the forming load is released

σ_{ys} = yield strength of the sheet

t = thickness of the sheet

E' = Plane strain elastic modulus = $E/(1-\nu^2)$

E = Young's modulus; ν = Poisson's ratio

The major issues in sheet metal forming are:

a) To minimize the amount of springback, S.

b) To minimize the variability in springback, ΔS.

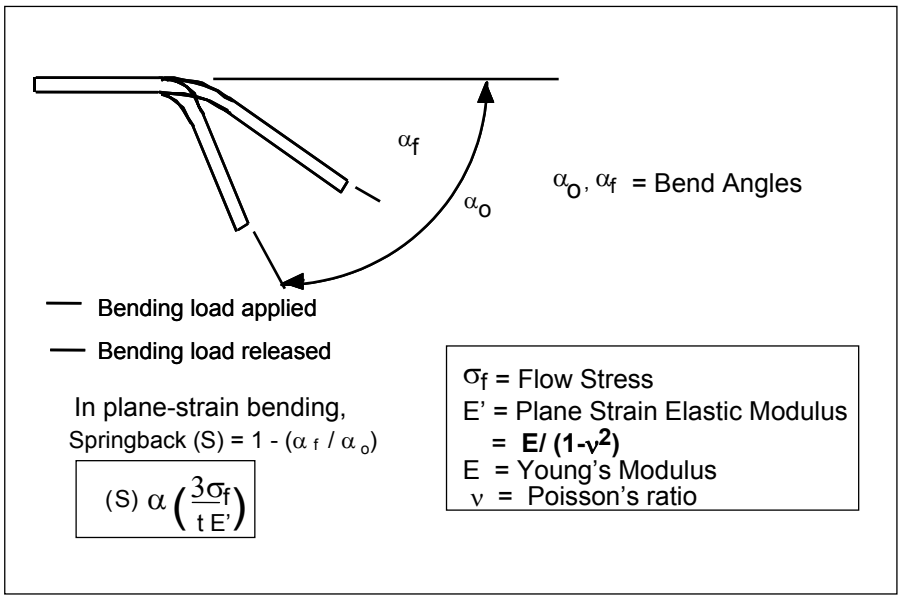

Figure 2.26 Schematic Illustration of Springback in Plane Strain Bending

In this work, the variability of springback implies the in-plane variability in the sheet of the IF steel. It can be seen from Eqn. 2-41 that the variability of springback, ΔS, can be minimized by reducing:

a) the variability in the yield strength ($\Delta\sigma_{ys}$)

b) the variability in plane strain elastic modulus ($\Delta E'$).

The focus of the current work is to theoretically model the role of crystallographic texture in determining the variability of the yield strength and elastic modulus in the plane of the sheet and hence, in controlling the in-plane variability in springback, (ΔS).

2.5.1 Crystallographic Texture and its Effect on Yield Strength

As shown earlier in Figure 2.8 (a), for a given ideal crystallographic texture of the sheet metal, the yield strength can sometimes vary considerably in different directions with respect to the rolling direction (RD) of the sheet. Additionally, this variability of yield strength is different for different textures, the variability being the least for the {111}<112> texture and the most for the {110}<001> (Goss) texture. Thus, it can be seen that crystallographic texture can significantly affect the variability of the yield strength.

2.5.2 Crystallographic Texture and its Effect on Plane Strain Elastic Modulus

The plane strain elastic modulus E', is defined as:

$$E' = E/\left(1-\nu^2\right) \tag{2-42}$$

Both E and ν vary with crystallographic direction <uvw> in the plane of the sheet. This variation is mathematically given as[163]:

$$E = 1/\left[S_{11} - \left(2S_{11} - S_{12} - S_{44}\right)\Sigma\right] \tag{2-43}$$

$$\nu = \left[S_{12} + \tfrac{1}{2}\left(2S_{11} - S_{12} - S_{44}\right)\right]/\left[S_{11} - \left(2S_{11} - S_{12} - S_{44}\right)\Sigma\right] \tag{2-44}$$

where, $\Sigma = l^2m^2 + m^2n^2 + n^2l^2$

l, m, n are direction cosines of <uvw>

S_{11}, S_{12}, S_{44} are the compliance coefficients of the crystal [164].

Therefore, for a given ideal crystallographic texture {hkl}<uvw>, the value of E' will also change in the plane of the sheet as a function of the angle (θ) from the rolling direction of the sheet.

Thus, theoretically, each direction in the sheet metal can have a unique yield strength and plane strain elastic modulus. This concept has been illustrated in Figure 2.27. Due to the cubic symmetry of iron and the orthorhombic symmetry of the sheet, it is sufficient to represent the data of YS and E' variation in only one quadrant of the plane of the sheet [$\theta = 0^o$ (RD) to $\theta = 90^o$ (TD)].

In summary, each crystallographic texture will have its own variation of yield strength and E' in the plane of the sheet and hence a unique variation in springback, as predicted by Eqn. 2-41. The texture which shows minimum variability in springback is of huge technological importance. The following section reviews some of the work that has been done by other researchers in studying the springback behavior in sheet metals.

The problem of springback and its control has been approached in two ways:

a) Simulation of springback behavior by finite element modeling (FEM): The focus of this approach is to use FEM to simulate springback behavior in a variety of springback tests. One such test is shown in Figure 2.28[165]. While performing the simulations, these researchers looked at the effect of a variety of process and material property variables on the springback parameters such as angles θ_1, θ_2 and radius of curvature, ρ, as defined in Figure 2.29[165]. The following is a brief list of variables that are taken into account:

Process variables:

i) Radius of the punch ii) Bend radii of the sheet.

iii) Coefficient of friction (lubrication) iv) Blankholder force

v) Rate and profile of applying the blankholder force

Material property variables:

vi) Elastic modulus vii) Poisson's ratio

viii) Yield strength ix) Strain hardening exponent

x) Strength coefficient

The combined effect of all the above variables is quite complex and has been summarized by Zhang and Lee[166]. Some predictions have also been shown in the work done by Schmoeckel and Beth[167] as well as Du et al.[168].

b) Experimental determination of springback parameters: In addition to FEM simulations, some researchers have experimentally determined the springback parameters using laboratory test equipment[169-171]. As was described in the previous sections, crystallographic texture affects the isotropy of elastic and plastic properties in the plane of the sheet. It is, thus, important to

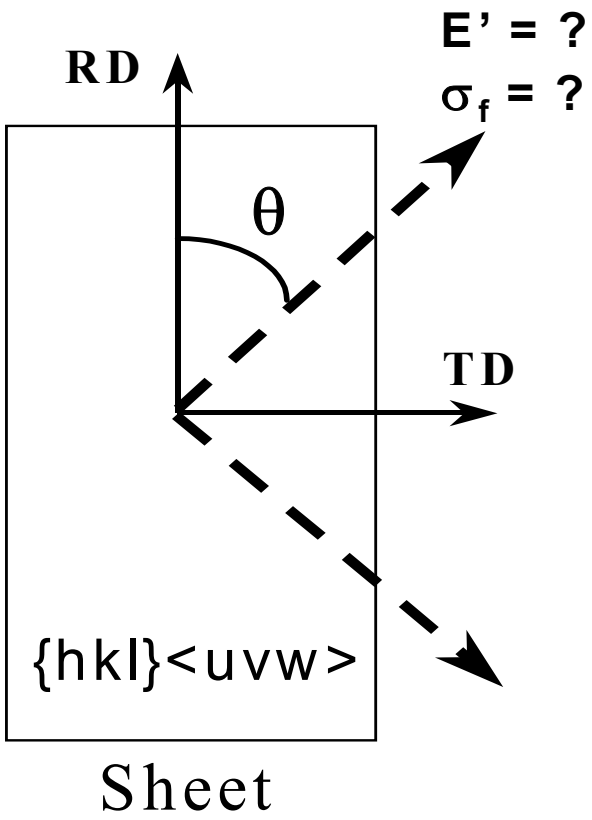

Figure 2.27 The In-plane Variation of Yield Strength and E' with Angle in the Plane of the Sheet for a Certain {hkl}<uvw> Crystallographic Texture

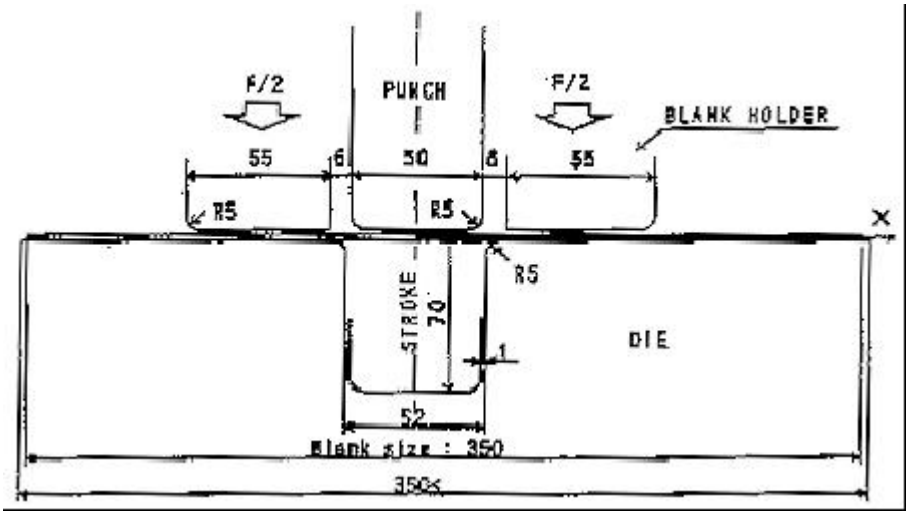

Figure 2.28 Schematic Draw-bend Test Modeled Using FEM[165]

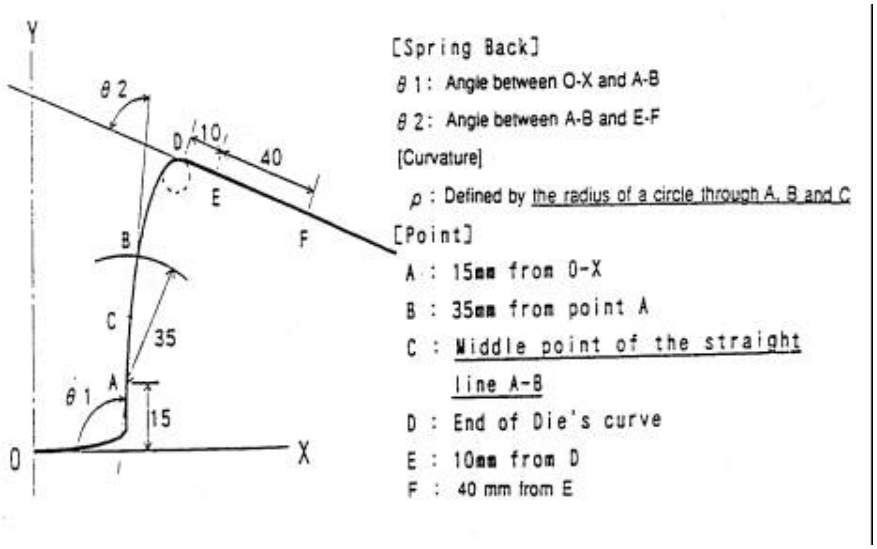

Figure 2.29 Springback Parameters Obtained from Simulation[165]

understand some of the basic concepts involved in describing the texture of sheet steels. The following is a brief review of these concepts.

2.6 Description of Crystallographic Texture in Sheet Metals

Crystallographic texture refers to the preferred orientation of the constituent crystal grains in a polycrystalline material. It denotes the statistical tendency of the grains in a specimen to be oriented in a particular way. The presence of texture can impart strong anisotropic properties to metals and alloys and this anisotropy forms the basis of a number of technological applications of these materials[172]. The crystallographic texture is described either as a macrotexture or microtexture. In describing the macrotexture, the grains in a polycrystal are regarded as constituting a single statistical population without regard to the spatial location of any particular grain or its relation to its neighbors. The microtexture, on the other hand, involves determining the orientation of each grain of the population and determining the nature and degree of its misorientation with respect to its immediate neighbors.

The macrotexture of sheet metals is characterized by a crystallographic plane (hkl) that is parallel to the rolling plane (RP) of the sheet and a crystallographic direction [uvw] parallel to the rolling direction of the sheet and lying in the plane of the sheet. The texture is denoted as (hkl)[uvw]. Macrotexture is determined by employing X-ray or neutron diffraction and these techniques are referred to as bulk measurement techniques. There are two ways of determining and graphically depicting such a texture. In the first, the intensity of diffraction from one particular family of lattice planes in the polycrystal is measured as a function of direction in space and the results are collected in the form of a pole figure which refers exclusively to that family of planes. The alternative is to record many such pole figures for different

crystallographic planes and combine them by a process of pole figure inversion to produce an Orientation Distribution Function (ODF), which gives fuller information about the nature of the texture than a single pole figure can. This technique is referred to as 3-D texture analysis. In general, an ODF function, f(g), is the volume fraction of crystallites, dV, having a common crystallographic orientation, g, with respect to a chosen sample coordinate system as expressed in the following equation[24]:

$$f(g)\, dg = dV(g)/V \tag{2-44}$$

The sample coordinate system, K_s, is usually defined in terms of convenient sample direction namely rolling, transverse and normal direction in the sheet. In order to specify grain in this material, a crystal coordinate system, K_c, has to be defined. The orientation of a grain is then defined by the rotation, g, that matches the sample coordinate system, K_s, to the crystal coordinate system, K_c. See Figure 2.30[24].

The rotation parameters to represent f(g) are usually the Euler angles (ϕ_1, ϕ, ϕ_2) which are shown in Figure 2.30. Each individual grain is characterized by three Euler angles ϕ_1, ϕ, and ϕ_2, which can be used to determine which (hkl) plane in that crystal is parallel to the rolling plane of the sheet and which [uvw] direction is parallel to the rolling direction. In measuring the macrotexture by X-ray diffraction, diffracted intensities are measured simultaneously for a large number of grains. The data thus obtained is processed and plotted in the form of Orientation Distribution Functions (ODFs') and can be represented in a 3-D Euler space defined by three orthogonal axes namely ϕ_1, ϕ, ϕ_2. See Figure 2.31[173]. It is to be noted that each combination of ϕ_1, ϕ, ϕ_2 represents a particular crystallographic orientation (hkl)[uvw] of the grain or grains. The data obtained from the ODF analysis can be used to determine what volume fraction of the grains in the sample are of a particular orientation (hkl)[uvw].

From the standpoint of IF sheet steels, the $\phi_2 = 45^o$ section of the Euler space is technologically the most important and this section is shown in Figure 2.32. The figure shows the following three important fibers:

a) α-fiber ($\phi_1 = 0$), where all the orientations have the [110] direction parallel to the rolling direction.

b) γ-fiber, $\phi_1 = 0^o$ to $\phi_1 = 90^o$, where all the orientations have (111) plane in the rolling plane of the sheet.

c) The ε-fiber ($\phi_1 = 90^o$), where all the orientations have [110] directions parallel to the transverse direction of the sheet.

It has been established that the γ-fiber orientations are most ideally suited for excellent deep-drawability of the sheet steels, whereas the presence of α-fiber components imparts poor deep drawability.

The description of microtexture involves the determination of the orientation of each grain of the population and the nature and degree of its misorientation with respect to its immediate neighbors[174]. Crystallographic orientations of individual grains are obtained from Kikuchi patterns in reflection (SEM) or in transmission (TEM). Use of Electron Backscattering Diffraction (EBSD) in the SEM has become an established method for determining microtexture. In this method, the electron beam is carefully positioned in an individual grain and the resulting Kikuchi patterns are recorded. Using automated measurement techniques, the electron beam can be systematically scanned over a designated area on the sample, collecting Kikuchi patterns from individual grains. With built-in computer software, the Kikuchi patterns are indexed to identify the various 'poles' or intersections of different {hkl} planes in a particular grain. This indexing is performed for all the grains that are scanned. After the indexing is completed, the orientation of

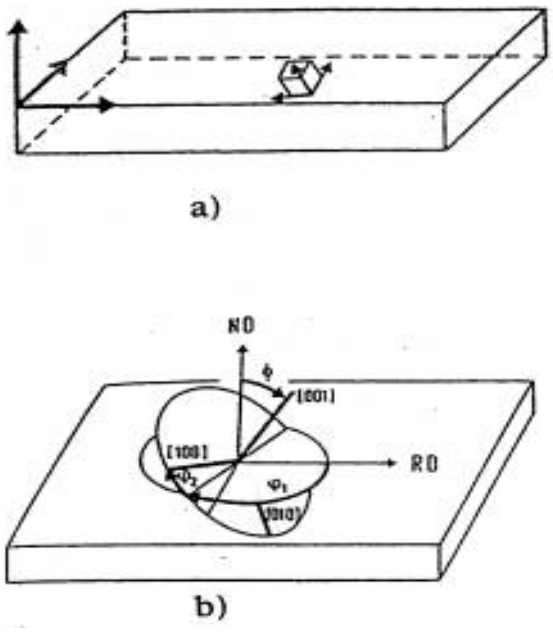

Figure 2.30 Rotation of Sample Coordinate System into the Crystal Coordinate System [24]

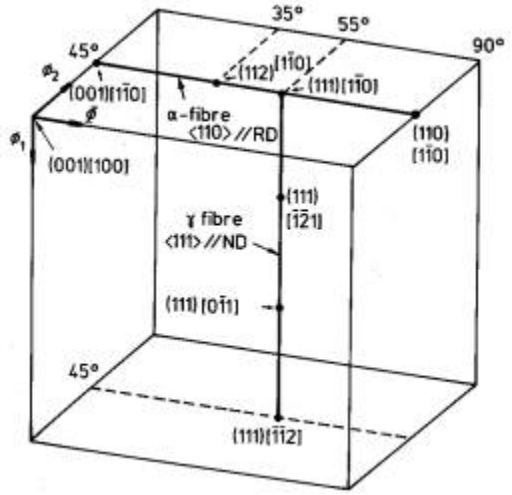

Figure 2.31 Illustration of the 3-D Euler Space[173]

$\Phi_2 = 45^0$ section of Euler Space

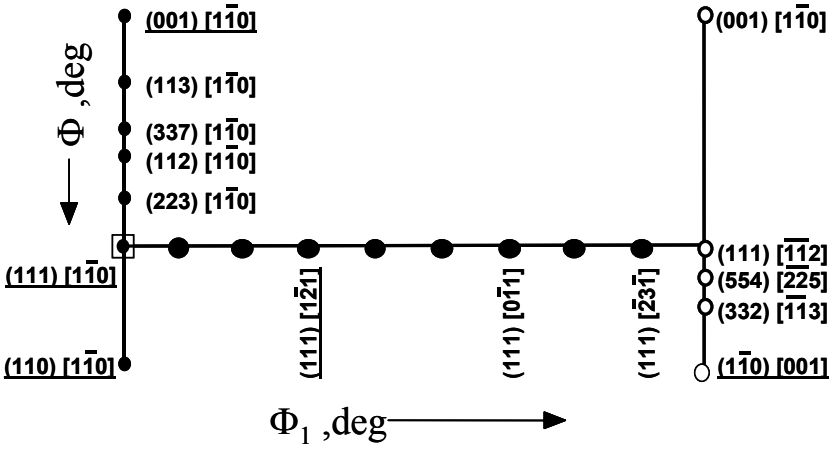

Figure 2.32 phi2 = 45° Section of Euler Space Showing:

a) Alpha Fiber (Vertical Line at phi1 = 0°)

b) Gamma Fiber (Horizontal Line from phi1 = 0° to phi1= 90°)

c) Epsilon Fiber (Vertical Line at phi1 = 90°)

each grain with respect to that of the specimen is determined. This procedure, when repeated for a sufficiently large number of grains, gives a statistical distribution of the orientations in the specimen. This technique enables the determination of "micro" as well as "macro" texture of the specimen. There are several advantages of using the SEM-EBSD technique over the conventional X-ray diffraction method, some of which are listed below:

a) allows orientation mapping of individual grains in the sample.

b) can generate pole figures, inverse pole figures and ODFs' as in X-ray diffraction.

c) allows grain boundary mapping and determination of misorientation between neighboring grains.

d) can determine grain size distribution in the sample as well as Taylor factors of individual grains, which are useful in predicting the mechanical properties of the sheet.

It is seen that the SEM-EBSD technique can be used as a powerful tool in characterizing textures and microstructures in metals and alloys.

3.0 STATEMENT OF OBJECTIVES

There are two main objectives of this research.

Objective 1: To study the complex role of phosphorus in affecting the small strain yielding behavior of IF steels.

The following issues will be addressed in this objective:

a) Does the addition of phosphorus to IF steels bring about primarily solid solution strengthening?

b) Does the segregation of phosphorus to ferrite grain boundaries bring about grain boundary hardening?

c) How does the presence of phosphide precipitates affect the yield strength of IF steels?

Objective 2: To study the role of crystallographic texture in controlling the small strain elastic recovery i.e. springback behavior of IF steel sheets.

The following issues will be addressed in this objective:

a) Does crystallographic texture significantly affect the elastic anisotropy of IF steel sheets?

b) How does this elastic anisotropy affect the in-plane variability of springback in IF steels?

c) Are there certain technologically important crystallographic textures that impart minimum variability of in-plane springback to IF steel sheets?

4.0 EXPERIMENTAL APPROACH

The following is description of the experimental approach employed in each of the objectives.

4.1 Experimental Approach: Objective 1

Hypothesis: Segregation of P to ferrite grain boundaries brings about localized grain boundary hardening with a corresponding increase in the value of Hall-Petch slope, k_y. The addition of solute P to IF steels can bring about both grain boundary hardening and conventional solid solution strengthening. The hypothesis has been schematically illustrated in Figures 4.1 (a) and (b).

1) Selection of steels: Two Ti stabilized IF steels were selected for this study. One was denoted as **Base-IF** steel with **390 ppm Ti and 20 ppm P** and the second one was denoted as **Phos-IF** steel with **390 ppm Ti and 600 ppm P**. These steels were supplied by Ispat-Inland Steel. The composition of these steels is listed in Table 4.1.

Table 4.1 Chemical Composition of IF Steels

(Amounts in ppm)

Label	**C**	**N**	**S**	**Mn**	**Ti**	**Nb**	**P**
Base	20	43	80	2000	390	0	**20**
P	13	43	70	2000	390	0	**600**

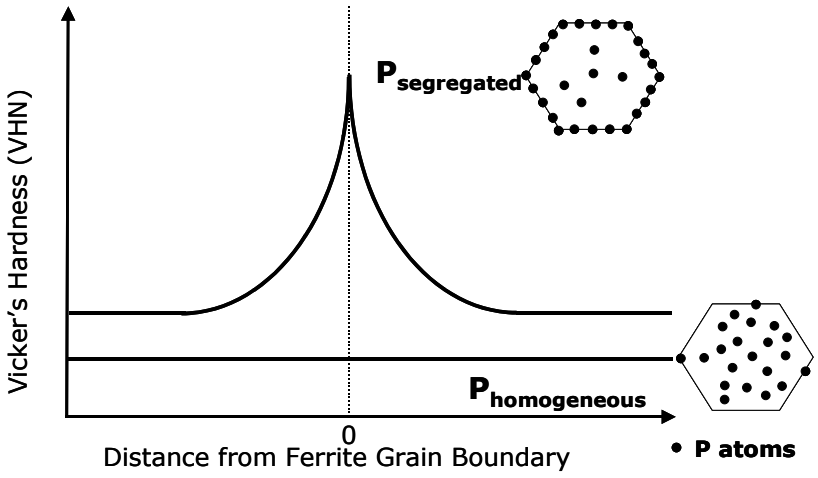

Figure 4.1 (a) Schematic Illustration of P Bringing About Grain Boundary Hardening

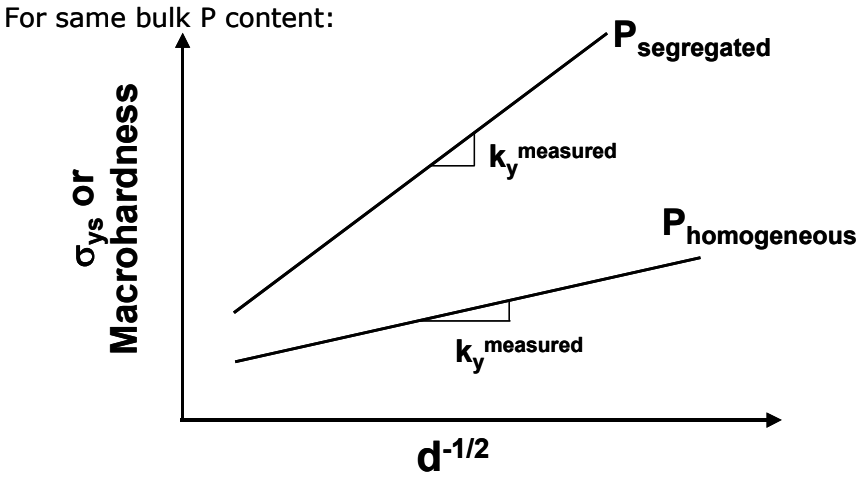

Figure 4.1 (b) Schematic Illustration of the Effect of P Segregation on Hall-Petch Slope, k_y

2) Hot rolling schedule: Both the steels were subjected to identical hot rolling schedules as shown in Figure 4.2. It should be noted that these IF steels were not subjected to conventional coiling treatment after hot rolling. The purpose of the 5 minute holding time at 850^{o}C was to allow complete stabilization of solute C as $Ti_4C_2S_2$. Additionally, it was expected that this heat treatment would preclude substantial segregation of P to ferrite grain boundaries, especially in the Phos-IF steel.

3) Cold rolling and annealing schedule: The hot rolling schedule was followed by cold rolling and annealing (CRA). The purpose of the CRA schedule was to develop three distinctly different ferrite grain sizes in both the Base-IF and Phos-IF steel. Use of varying levels of cold reduction, annealing temperatures and times was made to achieve the different ferrite grain sizes. The reason for developing three ferrite grain sizes was to determine the change in the Hall-Petch slope k_y, with and without P segregation to ferrite grain boundaries.

4) Phosphorus segregation heat treatments: In order to verify the hypothesis, it was necessary to develop two distinct locations of P in the IF steels in each of the grain sizes. These locations are:

a) Phosphorus predominantly locked up in the ferrite matrix to cause solid solution strengthening, denoted as $P_{homogeneous}$.

b) Phosphorus heavily segregated to ferrite grain boundaries bringing about grain boundary hardening, denoted as $P_{segregated}$.

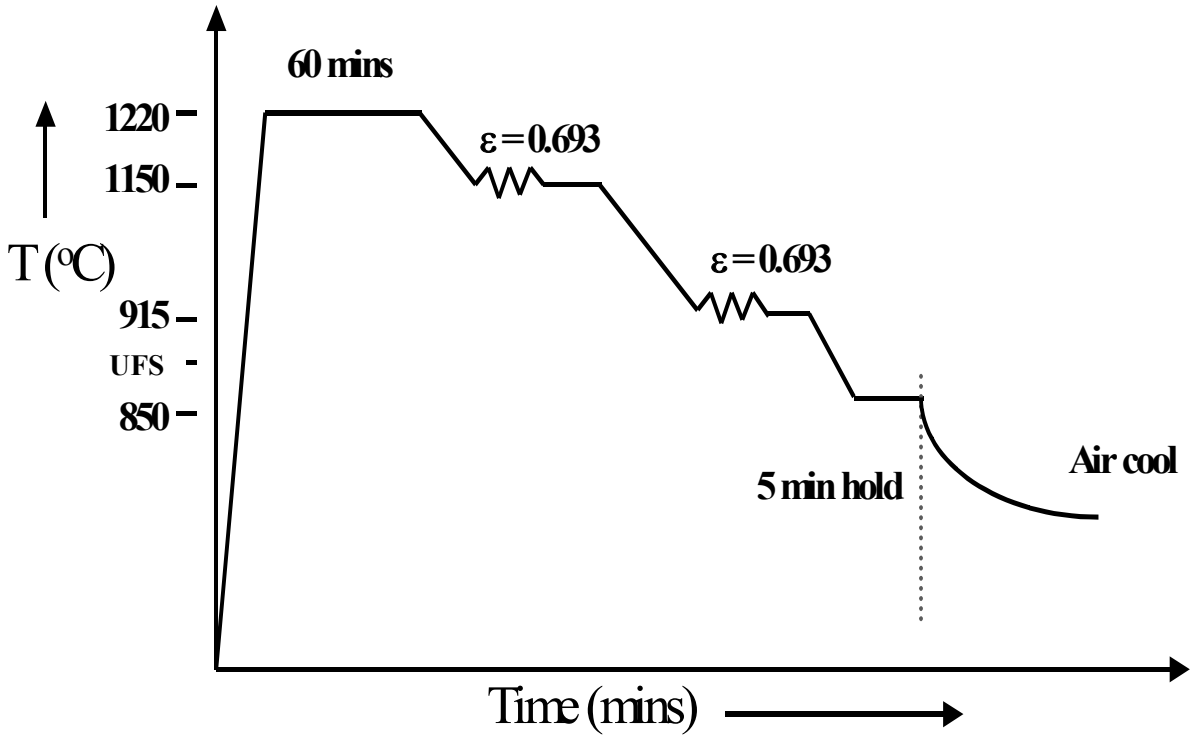

Figure 4.2 Hot Rolling Schedule

In order to perform the necessary heat treatments to achieve the above two conditions, diffusion modeling of P segregation to ferrite grain boundaries was performed. As mentioned in section 2.4.3.2, the Langmuir-McLean equation (Eqn. 2-26) was used to predict the thermodynamics of P segregation. Eqn. 2-34 was used to predict the kinetics of P segregation to ferrite grain boundaries for the bulk P levels of 20 ppm and 600 ppm in the two IF steels. Based upon the results of this diffusion modeling, appropriate time- temperature regimes were chosen to achieve the two conditions of P location. These segregation heat treatments were employed in each grain size after cold rolling and annealing. The two locations of solute P that were developed in each grain size have been shown schematically in Figure 4.3. Thus, with all the above processing schedules, the following is the matrix of test conditions.

Table 4.2 Matrix of Conditions to be Analyzed

Processing / Steel	Fine Grain Size		Medium Grain Size		Large Grain Size	
	P_{homog}	P_{segreg}	P_{homog}	P_{segreg}	P_{homog}	P_{segreg}
Base-IF 20 ppm P	X	X	X	X	X	X
Phos-IF 600 ppm P	X	X	X	X	X	X

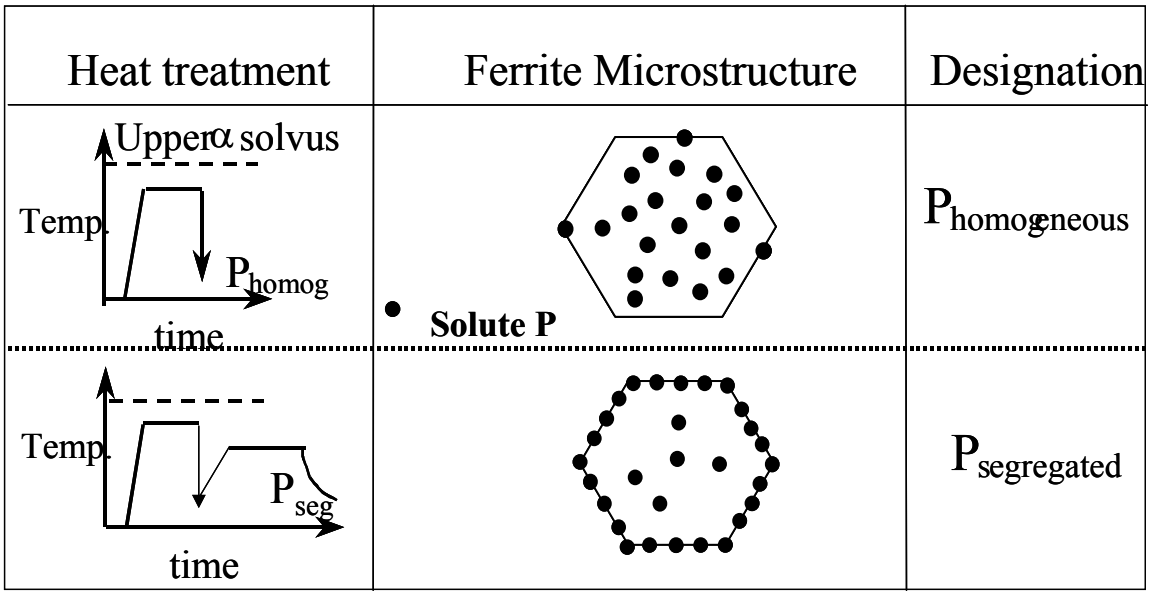

Figure 4.3 Schematic Representation of Two P Locations to be Developed in Each Grain Size

4.1.1 Concerns During Development of Ferrite Grain Sizes

The following were some of the concerns:

a) Stability of grain sizes during P segregation heat treatments: The grain sizes developed during the cold rolling and annealing schedules should remain stable during subsequent P segregation heat treatments. Hence, grain sizes were measured after each processing schedule namely, hot rolling, cold rolling and annealing, $P_{homogeneous}$ heat treatment and $P_{segregation}$ heat treatment.

b) Measurement of grain size, 'd':

The Hall-Petch equation predicts a $d^{-1/2}$ dependence on the yield strength. Hence, it is important to define a measure of grain size, 'd'. Some researchers[63-65] have used the mean linear intercept, l-bar, to describe the grain size and others have used some of the other various measures of grain size such as the equivalent grain diameter. It has been shown by Gladman[66] that the value of k_y can vary by as much as 23% depending upon the method used to measure the grain size. Hence, attention must be paid to the method of grain size measurement when comparing the Hall-Petch slope values. In this work, the linear intercept method[(175)] has been used to measure the grain size, d, since this measure is directly related to the grain boundary area per unit volume, S_v as per the equation:

$$S_v = 2/d \tag{4-1}$$

c) Texture hardening modification to the Hall-Petch slope, k_y:

In earlier determinations of the Hall-Petch slope, k_y, a wide range of grain sizes, from 5 μm to values exceeding 500 μm, was employed. In order to achieve this wide range of ferrite grain sizes, steels were subjected to widely different processing steps, such as varying levels of

cold reductions, temperatures and times of annealing. Changing the processing variables can result in the development of different crystallographic textures in the steel. Consequently, the texture of an extremely fine-grain-sized sample (5 μm) could be vastly different from that of the extremely large-grain-sized sample (500 μm). As described earlier in Section 2.3.5, texture can significantly affect the strength of sheet steels. Thus, in principle, the texture hardening contribution to the yield strength in each grain size would be different. In essence, the H-P slope, k_y, can be affected not only by the segregation of P but also by the different texture hardening contributions. Therefore, in order to isolate the effect on k_y due to P segregation, texture hardening correction has to be applied to the measured value of k_y, $k_y^{measured}$. This corrected value of k_y, is termed as $k_y^{corrected}$.

In this work, varying levels of cold reductions, (20-90%), have been used to achieve the required ferrite grain sizes in each IF steel. Subsequent annealing could lead to widely different recrystallization textures in each grain size. Since the presence of strong crystallographic texture can result in texture strengthening or softening, this contribution of texture to the yield strength has to be accounted for in each grain size.

$$\sigma_{text} = f(\text{grain size}) \qquad (4\text{-}2)$$

Thus it is important to determine the value of k_y corrected for texture hardening ,$k_y^{corrected}$, from the measured value of k_y, $k_y^{measured}$. This concept of texture hardening correction to $k_y^{measured}$ is illustrated in Figure 4.4.

In order to determine the texture hardening correction to $k_y^{measured}$, the following procedure was followed:

a) The texture hardening contribution to the yield strength of each ideal crystallographic

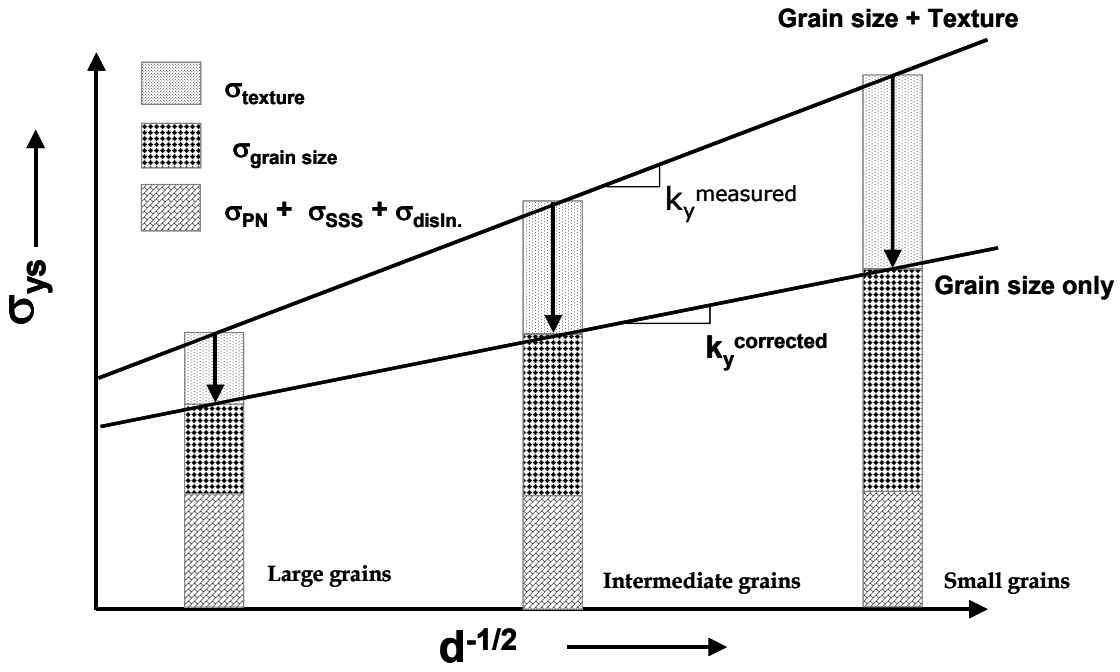

Figure 4.4 Schematic Illustration of Texture Hardening Correction to Measured Value of k_y

texture, theoretically, using the Bishop-Hill modeling approach[176, 177] for textured IF sheet steels. This calculation was done for each such {hkl}<uvw> texture in the rolling direction of the sheet.

b) The crystallographic texture in each grain size after the $P_{homogeneous}$ and $P_{segregated}$ condition was measured using the EBSD technique. The use of this technique gave the relative volume fractions of each texture component along the alpha, gamma and epsilon fibers for the two IF steels. Combining results from part (a) and (b) and using the law of mixtures, the texture hardening contribution to the yield strength in each grain size was determined. The results are shown in later sections.

5) Microhardness and macrohardness measurements: In addition to measuring the effect of P segregation on the measured value of k_y, it was also necessary to determine the effect of P segregation on the local grain boundary microhardness of ferrite grains. Microhardness measurements were performed using a load of 10g in the Vicker's hardness test. Samples were carefully mechanically polished, electropolished and etched with 2% Nital prior to making the indentations. Indentations were made in the center of the grains, away from any grain boundary effects, to determine the grain center (GC) or matrix microhardness. Indentations were also carefully made directly on the grain boundaries to determine the effect of P segregation. These indentations are shown in Figure 4.5. The resulting microhardness values were called grain boundary (GB) microhardness values. By measuring the grain center and grain boundary microhardness, it was also possible to determine the relative magnitudes of solid solution strengthening and grain boundary hardening due to P at ferrite grain boundaries. Additionally, macrohardness measurements using a 500 g load were also performed to evaluate the effect of P segregation on bulk properties.

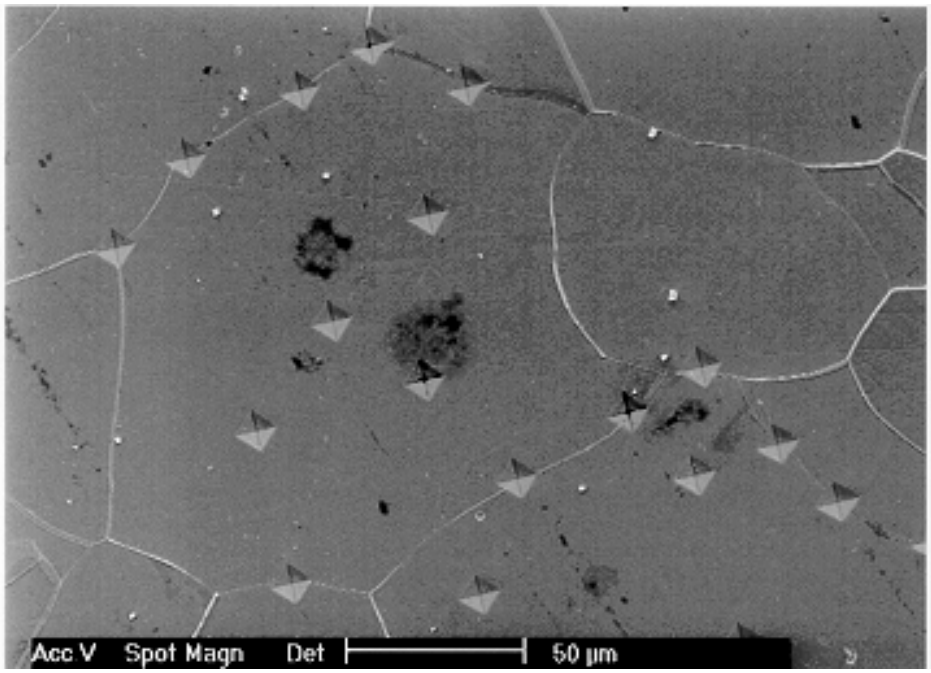

Figure 4.5 Grain Center and Grain Boundary Microhardness Indentations Using a 10 g Load

6) Tensile tests: Tensile tests were performed to determine the effects of P segregation on the bulk yield strength of both IF steels. Tensile tests were performed in the rolling direction, (RD), using sheet specimens of standard dimensions at a strain rate of 10^{-3}/s. It can be seen from Table 4.2 that there were 12 conditions to be tested. Two samples in each condition were tested to determine the tensile properties.

In addition to the processing schedules employed and the determination of mechanical properties, the experimental approach involved the use of several analytical tools to determine various microstructural features developed during processing. These are presented below.

7) Determination of crystallographic texture: The SEM-EBSD technique was used to determine the texture of the two IF steels in the homogeneous and segregated P condition.

8) Evolution of precipitation: SEM and TEM techniques were employed to observe and determine the nature of precipitation, especially that of phosphides.

9) Quantification of P segregation to ferrite grain boundaries: Auger Electron Spectroscopy (AES), courtesy of Dr. Harry Meyer at ORNL, TN , was employed to quantify the amount of P segregated to ferrite grain boundaries.

10) Determination of the amount of solute carbon in the matrix throughout the different stages of processing: Internal friction tests were performed on sheet samples at the I.P. Bardeen Institute in Moscow, Russia, courtesy of Dr. Lidia Storojeva. These tests were performed to determine the amount of solute carbon present in the matrix after different stages of processing. It was necessary to determine the status of the solute carbon, since it is well known that solute C takes part in competitive segregation with P at the ferrite grain boundaries.

The various characterization techniques employed in this work have been summarized and shown in Table 4.3.

Table 4.3 Summary of Characterization Techniques Used in This Research

Technique	Purpose
Electron Back Scattered Diffraction (EBSD)	Crystallographic Texture Grain Boundary Character
Scanning Electron Microscopy (SEM) Transmission Electron Microscopy (TEM) Scanning Transmission Electron Microscopy (STEM) Auger Electron Spectroscopy (AES) Atom Probe Field Ion Microscopy	Identification of precipitates Quantification of P segregation Presence of Ti-P clusters
Micro and Macrohardness	Determination of SSS and GBH
Tensile Tests	Determination of k_y
Charpy Impact Tests	Determination of P segregation
Internal Friction	Determination of solute carbon

4.2 Experimental Approach: Objective 2

Hypothesis: Crystallographic texture can significantly affect the in-plane variability of springback in IF sheet steels by affecting the elastic and plastic anisotropy in the plane of the sheet. As mentioned previously, the focus of this objective is to theoretically model the role of crystallographic texture in determining the variability of the yield strength and elastic modulus in the plane of the sheet and, hence, in controlling the in-plane variability in springback, (ΔS).

In this work, two types of theoretical modeling have been performed.

4.2.1 Plane Strain Bending Applications

In plane strain bending applications, springback is given as:

$$\text{Springback (S)} = (3\,\sigma_y) / (t\,E') \qquad (4\text{-}3)$$

where, σ_y = yield strength of the material; t = thickness of the sheet

E'= Plane strain elastic modulus = $E/(1-\nu^2)$

E = Young's modulus; ν = Poisson's ratio.

The aim is to minimize the in-plane variability of springback, ΔS, after sheet metal forming. In order to minimize ΔS, it is necessary to minimize the variability in the yield strength, $\Delta\sigma_y$, and the variability in plane strain elastic modulus, $\Delta E'$.

4.2.1.1 <u>Procedure for Theoretical Modeling in Plane Strain Bending Applications.</u> To predict the influence of each crystallographic texture on the springback behavior, it is assumed that the IF steel sheet is characterized by a unique, ideal crystallographic texture (hkl)[uvw]. With this assumption, the approach for modeling is as follows:

1) Select several ideal crystallographic textures (hkl)[uvw] from the $\phi_2 = 45^o$ section of the Euler space as shown previously in Figure 2.32.
2) For a certain (hkl)[uvw] texture, determine the crystallographic directions, $[u_1v_1w_1]$, at various angles, θ, with respect to the rolling direction (RD) in the plane of the sheet, using vector analysis.

3) For each crystallographic direction, meaning at a certain angle, θ, with respect to the rolling direction (RD), calculate E and ν using Equations 2-43 and 2-44 along with published values of the compliance coefficients. Hence, calculate E' in each direction using Equation 2-42.
4) From the calculated values of E', calculate the springback, S, in each direction using Equation 4-3 for a typical range of yield strengths found in IF steels.
5) For a certain sheet thickness having a certain nominal yield strength in the RD, a certain initial radius of bend (r_o), and a certain initial bend angle (α_o), calculate the springback, S, in each direction $[u_1v_1w_1]$ in terms of angular change, $(\alpha_o - \alpha_f)$.
6) Map the variability of E' and S in the form of polar plots of E' vs. θ and of S vs. θ for each texture (hkl)[uvw].
7) Calculate the following parameters for each texture:

$$E'_{bar} = (E'_o + 2E'_{45} + E'_{90})/ 4 \quad (4\text{-}4)$$

$$\Delta E' = (E'_o - 2E'_{45} + E'_{90})/ 2 \quad (4\text{-}5)$$

$$S_{bar} = (S_o + 2S_{45} + S_{90})/ 4 \quad (4\text{-}6)$$

$$\Delta S = (S_o - 2S_{45} + S_{90})/ 2 \quad (4\text{-}7)$$

The approach for theoretical modeling performed has been summarized in Figure 4.6.

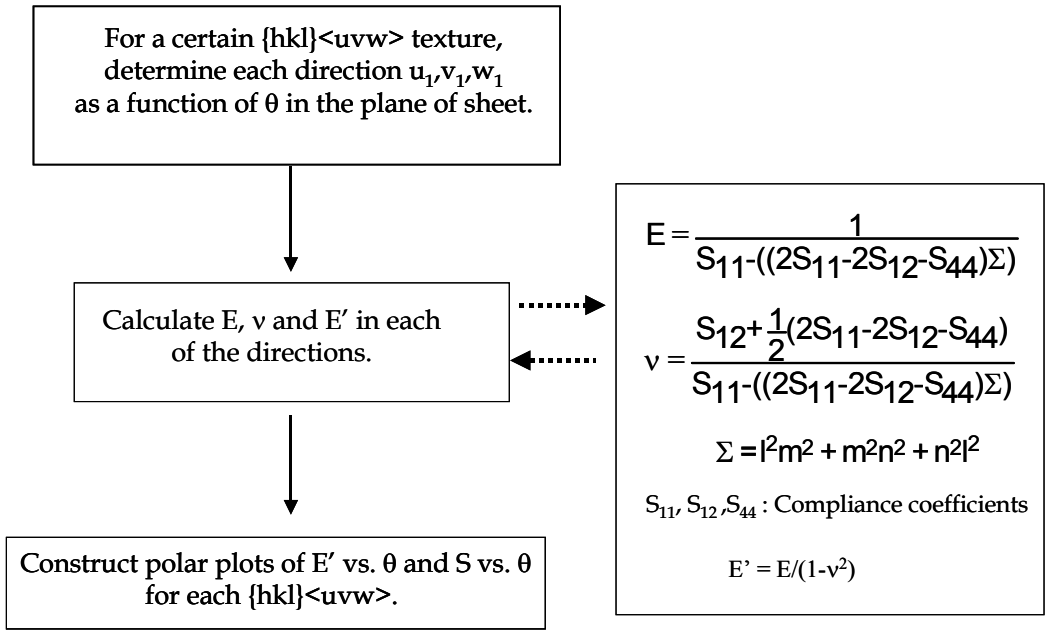

Figure 4.6 Summary of Theoretical Modeling Approach in Plane Strain Bending Application

4.2.2 Finite Element Modeling (FEM) in Draw-bend Applications

Finite element modeling was performed by Carlos Gomes and Dr. Dipo Onipede of the Mechanical Engineering department at the University of Pittsburgh, using the data of variability of E' and σ_y in the plane of the sheet. A draw-bend test, as shown previously in Figure 2.28, was simulated using the LS-DYNA FEM package to predict springback parameters (angles θ_1, θ_2 and radius of curvature, ρ) for certain values of the plane strain elastic modulus and yield strengths in IF steels. The test parameters used during the simulation are shown in Table 4.4.

Table 4.4 Test Parameters Used During Simulation of the Draw-bend Test Using LS-DYNA

Test parameter	Value
Width of the punch	50 mm
Stroke of the punch	70 mm
Bottom radius of punch	5 mm
Clearance between punch and die wall	1 mm
Punch speed	2.11 m/s (max)
Time to finish the stroke	50 ms
Blank holder force	600 kg
Coefficient of friction	0.1
Thickness of sheet	0.78 mm
Length of sheet	300 mm
Width of sheet	39 mm

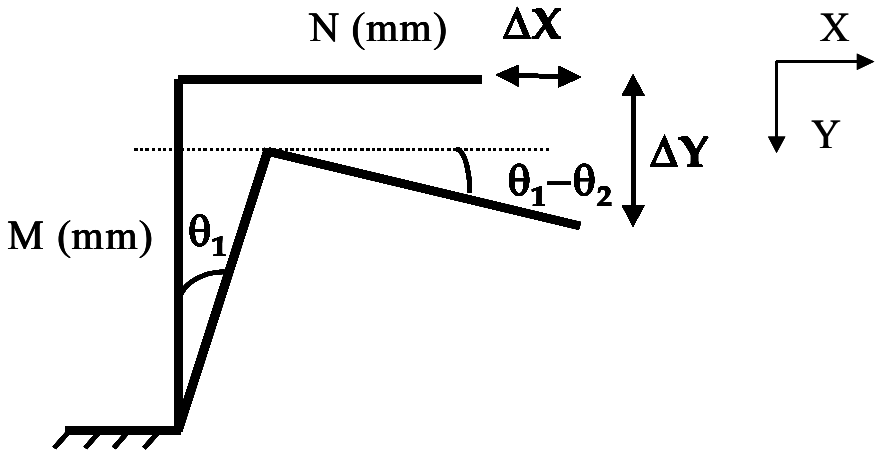

Minimum Springback implies minimum ΔX and ΔY

$$\Delta X = M\sin(\theta 1 - 90) - N[1 - \cos(\theta 1 - \theta 2)$$

$$\Delta Y = N\sin(\theta 1 - \theta 2) + M[1 - \cos(\theta 1 - 90)]$$

Figure 4.7 Relation of Degree of Springback and the Welding Gap in a Draw-bend Test

The parameters shown in the above table were chosen based upon the established procedure for Draw-bend test used in the sheet steel industry.

The springback parameters thus obtained after simulation, can be used to calculate the displacement of the end point of the strip in terms of ΔX and ΔY as shown in Figure 4.7**.** The magnitudes of these displacements represent the amount of springback and in practical terms could represent a welding gap between two sheet components that are welded during end fabrication. The concept of this welding gap (ΔX, ΔY)and its relation to the degree of springback is shown in Figure 4.7.

5.0 RESULTS

5.1 Objective 1: Phosphorus and Yield Strength of IF Steels

5.1.1 Hot Band Microstructure

The microstructure after the hot rolling schedule was characterized to determine the grain size and precipitation behavior. The results for both the steels, Base-IF and Phos-IF steel, are shown in Table 5.1. The mean linear intercept method has been employed to evaluate the grain size, d.

Table 5.1 Microstructural Features After Hot Rolling

Steel	Grain Size (μm)	Microstructure
Base-IF	39	No FeTiP or TiC ppts. seen. TiN, TiS, $Ti_4C_2S_2$ (H) observed. 80% of TiS ppts were transformed to H
Phos-IF	25	No FeTiP or TiC ppts. seen. TiN, TiS, $Ti_4C_2S_2$ (H) observed. 52% of TiS ppts were transformed to H

5.1.2 Cold Rolling and Annealing Schedules

Hot rolling was followed by a variety of cold rolling and annealing schedules to develop three different ferrite grain sizes. The schedules performed and the resulting grain sizes are

shown in Table 5.2. The cold rolling and annealing was performed at the University of Pittsburgh, LTV Steel and US Steel. It can be seen that for a given cold rolling and annealing schedule, the ferrite grain size in the Phos-IF steel is finer than that in the Base-IF steel. It should be noted that the final annealing temperature used for developing the small and intermediate grain sizes in both the steels is 750 ^{o}C, whereas that used for the large grain size is 850 ^{o}C.

Table 5.2 Cold Rolling and Annealing Schedules Performed

Cold rolling and annealing schedule	Grain size attained after annealing μm, ($\mu m^{-1/2}$)
Hot Rolling (HR) + 90% CR + 750^{o}C / 30 mins	Base-IF: 20 (0.22) Phos-IF:15 (0.26)
HR + 75% CR + 850^{o}C / 30 mins + 25% CR + 750^{o}C / 30 mins	Base-IF: 53 (0.14) Phos-IF: 39 (0.16)
HR + 75% CR + 850^{o}C / 30 mins + 20% CR + 850^{o}C / 30 mins	Base-IF: 103 (0.10) Phos-IF: 63 (0.13)

5.1.3 Segregation Heat Treatments to Control Location of P

In order to develop the two locations of phosphorus in each grain size, the appropriate temperature-time schedules had to be chosen. In order to facilitate this step, modeling of the equilibrium thermodynamics and kinetics of P diffusion to ferrite grain boundaries was performed. The results from the modeling are shown in Tables 5.3 and 5.4.

Table 5.3 Diffusion Modeling Results for Equilibrium Segregation of P in Base-IF Steel

Base-IF Steel	Bulk P content = 20 ppm = 0.003 at %		
Segregation Temp. (°C)	1 monolayer segregation Atomic % P at GB	0.5 monolayer Atomic % P at GB	0.33 monolayer Atomic % P at GB
500	5.35	2.67	1.77
550	4.31	2.15	1.42
600	3.55	1.78	1.17
650	2.99	1.49	0.99
700	2.55	1.28	0.84
750	2.22	1.11	0.73
800	1.95	0.97	0.64
850	1.73	0.87	0.57
875	1.64	0.82	0.54

Table 5.4 Diffusion Modeling Results for Equilibrium Segregation of P in Phos-IF Steel

Phos-IF Steel	Bulk P content = 600 ppm = 0.1 at %		
Segregation Temp. (°C)	1 monolayer segregation Atomic % P at GB	0.5 monolayer Atomic % P at GB	0.33 monolayer Atomic % P at GB
500	62.9	31.5	20.8
550	57.5	28.7	19.0
600	52.5	26.2	17.3
650	48.0	24.0	15.8
700	44.0	22.0	14.5
750	40.5	20.2	13.4
800	37.3	18.7	12.3
850	34.6	17.3	11.4
875	33.3	16.7	11.0

The diffusion modeling results are based upon the Langmuir-McLean equation (Eqn 2-26). The results show the dependence of the degree of equilibrium segregation of P on the temperature of segregation. It can be seen from the tables that, at any given temperature, the degree of P segregation in the Phos-IF steel is much higher compared to the Base-IF steel due to the higher bulk P content. The results of the diffusion modeling are plotted in Figure 5.1. It is seen that lower the temperature of segregation, higher is the P segregation that can be achieved under equilibrium segregation conditions. Previous studies of P segregation in steels have shown

that, typically, ~0.33 monolayer of coverage is achieved for P segregation to ferrite grain boundaries.

It should be noted that calculated values of P segregation are the maximum levels of equilibrium segregation that can be attained at a given segregation temperature. In addition to calculating the maximum levels of P segregation, the fraction of bulk P needed to achieve a certain equilibrium segregation was calculated for a certain bulk P content and a certain grain size. The results of this calculation are shown in Table 5.5 for the Phos-IF steel with 600 ppm bulk P content and for the smallest grain size of 15 μm achieved in this steel.

Table 5.5 Calculation of Saturation Levels of P Segregation vs. Segregation Temperature

Segregation Temperature °C	Bulk P content = 600 ppm Grain Size = 15μm Sv = 0.133/μm Fraction of Bulk P needed to saturate GB (%)	Assuming 1 monolayer segregation P needed to saturate GB (ppm)
500	1.90	11.4
550	1.73	10.4
600	1.58	9.5
650	1.45	8.7
700	1.33	8.0
750	1.22	7.3
800	1.13	6.8
850	1.04	6.3
875	1.01	6.0

It is seen that even for 1 monolayer segregation, < 2% of the bulk P is needed to saturate the ferrite grain boundaries at the 500 °C segregation temperature. This implies that even after 1 monolayer saturation, ~ 98% of P remains in the ferrite matrix. Table 5.5 shows that even for 1 monolayer segregation, ~ 12 ppm solute P is needed to saturate the grain boundary surface area in the smallest grain size. Although the Base-IF steel contains 20 ppm P, it is not possible to saturate the grain boundaries in the Base-IF steel because of the lack of sufficient driving force for P atoms to segregate to the grain boundaries. Using the results of the diffusion modeling as a

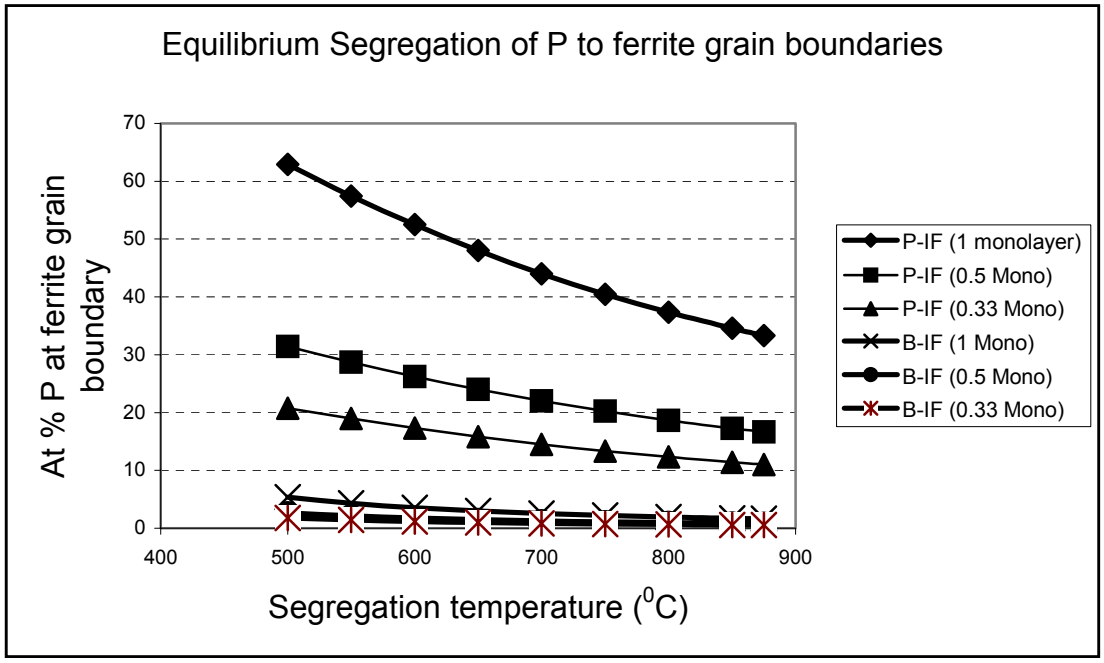

Figure 5.1 Results of Diffusion Modeling of Equilibrium Segregation of P to Ferrite Grain Boundaries in Base-IF and Phos-IF Steels

guideline, appropriate heat treatments were chosen to generate the two desired locations of P in both the IF steels. In order to achieve the condition of negligible P at the ferrite grain boundaries or alternately, to get a homogeneous distribution of P, it was necessary to choose as high a homogenizing temperature as possible without causing any grain coarsening in both the IF steels. For the same reason, the time at temperature had to be chosen so as to avoid grain coarsening, yet be sufficient enough to achieve the necessary homogenization. Based upon the above constraints, the following homogenizing heat treatment was chosen:

Homogeneous heat treatment: CRA + 850 ^{o}C / 5mins + Water Quench (WQ)

Holding time at 850 ^{o}C was curtailed to 5 mins in order to prevent any grain coarsening during this hold. The water quenching was done to ensure that no P segregation occurred during subsequent cooling. These conditions have been denoted as "Homogenized" or "Homogeneous" in both the Base-IF and the Phos-IF steel.

In order to heavily segregate the P to ferrite grain boundaries, the following heat treatment was chosen.

Segregation heat treatment: CRA + 850 ^{o}C / 5mins + Water Quench (WQ) +

550 ^{o}C / 24 hrs + Air cool

This condition has been denoted as "Segregated" in both the Base-IF and the Phos-IF steel. The long isothermal hold at 550 ^{o}C ensured that sufficient time was available for P to diffuse to the ferrite grain boundaries, without causing any grain coarsening. This processing schedule is shown schematically in Figure 5.2.

The grain sizes were measured after the as-annealed, homogenized and the segregated condition. It was observed that the grain sizes remained constant throughout the different stages

HR: Hot Rolled, CR: Cold Rolling, GSA: Grain size annealed,
Homog: Homogeneous P distribution, Seg: P heavily segregated to GB

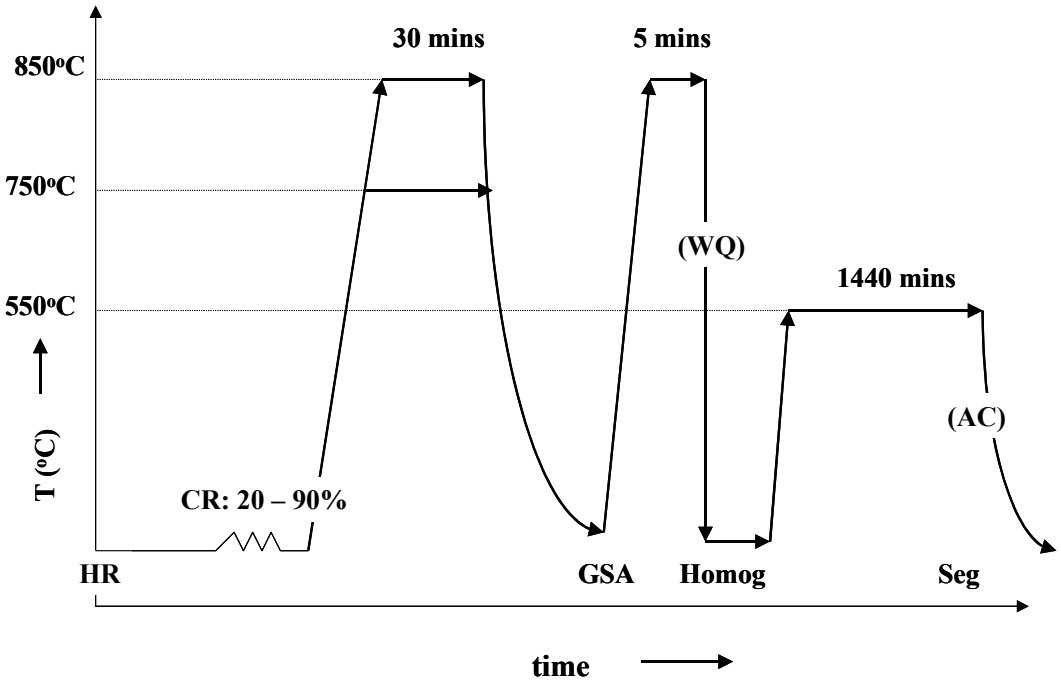

Figure 5.2 Schematic Illustration of Processing Schedule Followed

of processing. For example: In the 90% CR + 750^{o}C/30 mins annealing schedule, the average grain size in the Base-IF steel after the as annealed, homogenized and segregated condition were measured to be 20.2, 21.6 and 19.7 μm respectively, whereas those in the Phos-IF steel were measured to be 15.1, 15.6 and 14.6 μm respectively.

5.1.4 Microstructural Characterization

After the heat treatments for controlling the location of solute P were completed, it was necessary to determine:

a) Whether the segregation heat treatments resulted in the predicted amount of P at the ferrite grain boundaries?
b) Whether the segregation heat treatments resulted in the precipitation of FeTiPs at the ferrite grain boundaries and/or in the ferrite matrix?
c) What types of precipitates other than FeTiP occurred in these IF steels at different stages of the processing?
d) What is the status of solute C through the various stages of processing?

5.1.4.1 <u>Determination of Solute P at Grain Boundaries.</u> The amount of P at the ferrite grain boundaries was determined qualitatively by performing Charpy V-notch impact tests after performing the segregation heat treatments. The rationale was that the segregation of P to ferrite grain boundaries would result in extensive intergranular fracture whereas the absence of P at ferrite grain boundaries would result in transgranular or cleavage fracture. In order to quantify

the amount of P at the grain boundaries, Auger Electron Spectroscopy (AES) of certain critical samples was performed by Dr. Harry Meyer at Oakridge National Labs.

5.1.4.1.1 Results from Charpy Impact Tests. Charpy impact tests were performed for the conditions shown in Table 5.6 and the resulting fracture surfaces observed using the SEM. Some representative fracture surfaces have been shown in Figure 5.3.

Table 5.6 Conditions Tested Using Charpy Impact Tests

Steel	Processing Condition
Base-IF	Hot Rolled (HR) + Homogenized
	Hot Rolled (HR) + Homogenized + Segregated
Phos-IF	Hot Rolled (HR) + Homogenized
	Hot Rolled (HR) + Homogenized + Segregated

It is seen that profuse intergranular fracture is predominantly observed only in the Phos-IF steel segregated condition whereas in the Base-IF homogenized, Base-IF segregated as well as the Phos-IF homogenized condition, cleavage or transgranular fracture is seen. This observation is a qualitative proof that P segregation had occurred to grain boundaries in the Phos-IF steel during the isothermal hold at 550^{o}C.

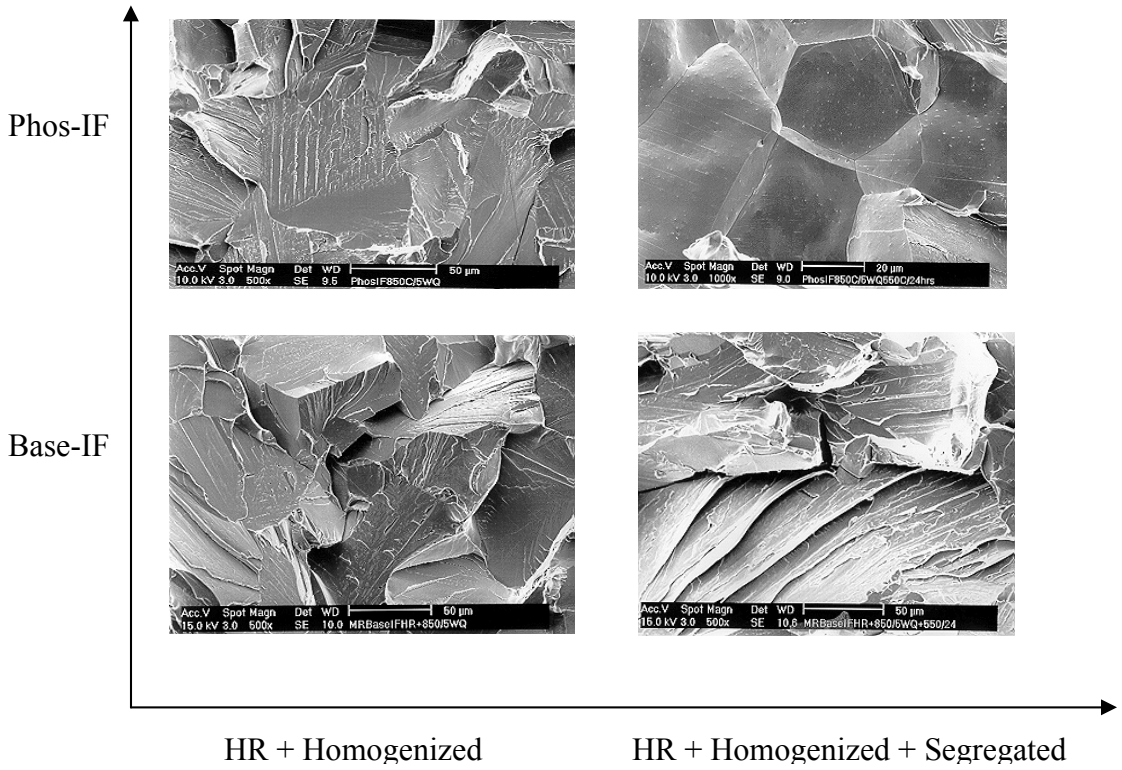

Figure 5.3 Charpy Impact Test Fracture Surfaces

5.1.4.1.2 <u>Quantification of P Segregation to Ferrite Grain Boundaries.</u> To quantify the amount of P segregation to ferrite grain boundaries, AES technique was employed. The following conditions were tested:

a) Phos-IF steel: Hot rolled condition

b) Phos-IF steel: HR + Homogenized

c) Phos-IF steel: HR + Homogenized + Segregated

d) Base-IF steel: HR + Homogenized + Segregated

All the AES samples were fractured at liquid N_2 temperature. The results are shown in Figure 5.4 and 5.5. It is seen from Figure 5.5 (a) that only the Phos-IF steel in the segregated condition shows predominantly intergranular fracture, the rest of the conditions show cleavage fractures.

Even in the Phos-IF steel in the segregated condition, a substantial amount of P segregation is seen only on the intergranular fracture areas, whereas the amount is negligible on the cleavage or transgranular area. For the Phos-IF steel in the segregated condition, the amount of P measured on the intergranular facets ranges between 3.3 to 6.6 at%. Since the results are reported for only one of the two fractured intergranular facets, the actual amount of P at the grain boundary has to be doubled [146]. Thus, the range of total atomic P at the grain boundaries ranges between 6.6 to 13.2 at%, with an average value of 10.3 at% and a standard deviation of 2.57%.

Thus, AES results confirm that the homogenizing heat treatment results in a negligible amount of P segregation to the grain boundaries even in the Phos-IF steel. Additionally, the segregation heat treatment results in substantial segregation of atomic P to grain boundaries in the Phos-IF steel.

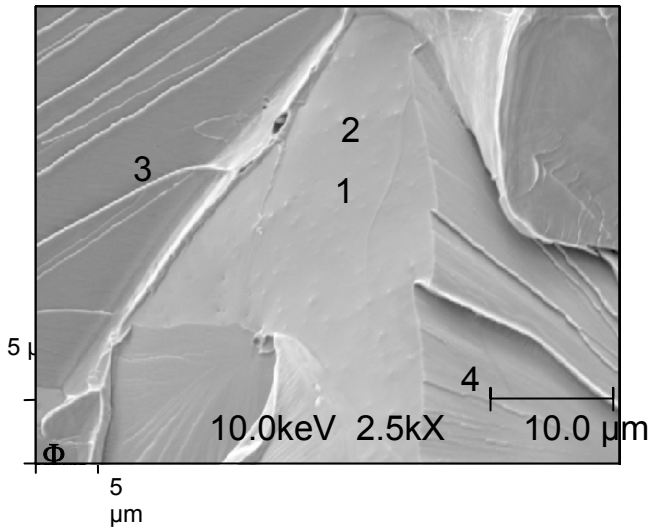

Base-IF: HR + Homogenized + Segregated

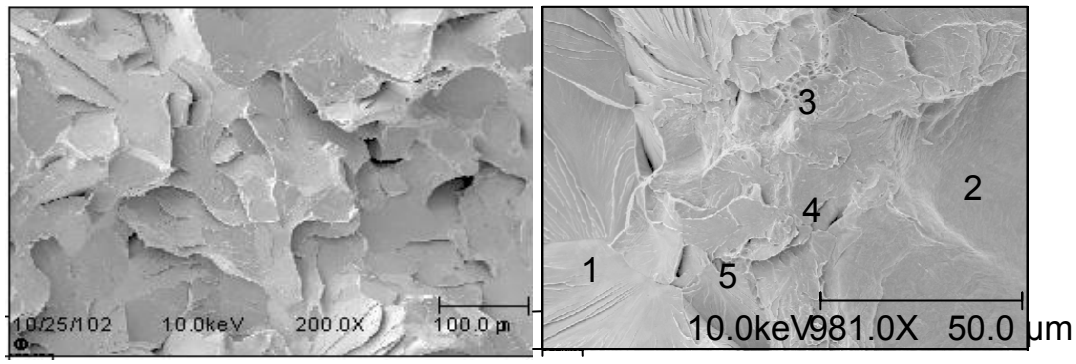

Phos-IF: HR

Phos-IF: HR + Homogenized

Figure 5.4 AES Results: Representative Fracture Surfaces: Test Temperature = -196°C

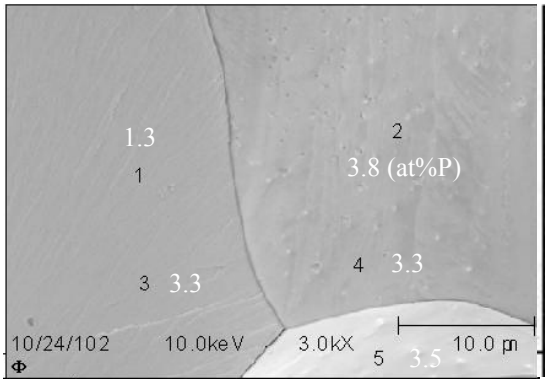

(a) Fracture surface at –196^{0}C temp

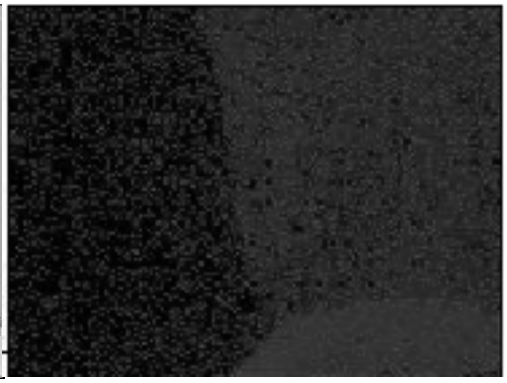

(b) Elemental map showing P segregation to GB

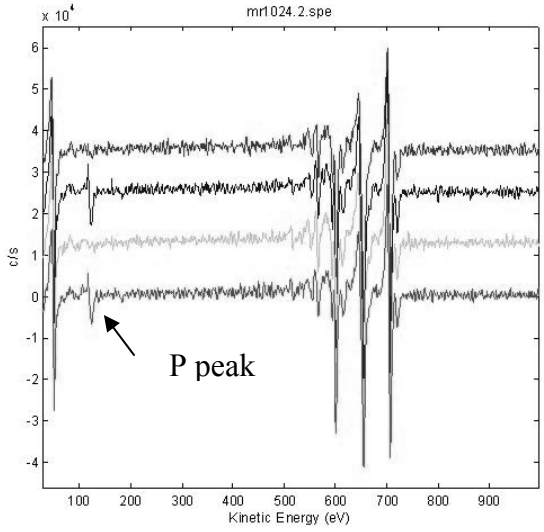

Cleavage

Intergranular facet

Cleavage

Intergranular facet

(c) Presence of prominent P peaks in AES KE plot

Figure 5.5 AES Results for Phos-IF Steel in HR + Homogenized + Segregated Condition

5.1.4.2 <u>Precipitation of FeTiP Precipitates During Processing.</u> In addition to determining the segregation of atomic P to the ferrite grain boundaries, it was necessary to determine if the presence of excess solute P at the grain boundaries resulted in the precipitation of FeTiPs at the grain boundaries. Thus, the evolution of FeTiP precipitates during various stages of processing was tracked by using SEM and STEM. The results have been tabulated in Table 5.7. It is seen from the table that, a few FeTiPs are observed at a few ferrite grain boundaries in the Phos-IF steel only after the segregation heat treatment. The size range of these precipitates is 50-200 nm. There were no FeTiPs observed in the matrix of the Phos-IF steel after any heat treatment. The Base-IF steel did not show the presence of any FeTiPs throughout the various processing schedules.

Table 5.7 Evolution of FeTiP Precipitates During Processing

Processing Stage	Base IF Steel			Phos IF Steel		
	20 μm	53 μm	103 μm	15 μm	39 μm	63 μm
Hot Rolled	N	N	N	N	N	N
Grain Size Annealed	N[1]	N[1]	N[2]	Y*[1]	N[1]	N[2]
$P_{Homogeneous}$	N	N	N	N	N	N
$P_{Segregated}$	N	N	N	Y*	Y*	Y*

1 : Annealed at 750°C / 30 mins **2 : Annealed at 850°C / 30 mins**

*** Very few FeTiP ppts observed only at ferrite grain boundaries**
Size range: 50-200 nm.

Based upon the available Ti and P in solution, it was estimated that the maximum amount of P that could be tied up as FeTiP precipitates in the Phos-IF steel would be 90 ppm with a maximum volume fraction of FeTiP precipitates being $5x10^{-4}$. The morphology of the FeTiPs

observed at the grain boundaries is shown in Figure 5.6. It is seen that the FeTiP precipitates are elongated in shape and show equal atomic percents of Ti and P in the SEM-EDX spectrum. In addition to the presence of FeTiPs, a few other types of precipitates were also found on the ferrite grain boundaries especially in the segregated condition. These were determined to be TiS, $Ti_4C_2S_2$, TiN, MnTiS. A few of these precipitates are shown in Figure 5.7. It should be pointed out that TiC precipitates were conspicuously absent in all conditions.

The use of STEM was also made to identify the precipitation behavior in the homogenized and segregated conditions. STEM-EDS technique was attempted to determine the presence of solute P at the ferrite grain boundaries especially in the Phos-IF segregated condition. The results from the STEM analysis have been presented in Tables 5.8 (a) and (b). Using the STEM-EDX technique, an attempt was made to measure the amount of solute P at the ferrite grain boundaries especially in the Phos-IF steel. It can be seen that from the tables that P at grain boundaries could not be detected using this technique. Some representative micrographs of grain boundaries observed in the STEM are shown in Figure 5.8. It can be seen from the figure that the boundaries are devoid of any precipitates especially FeTiPs. It should be pointed out that TiC precipitates and oxide particles were conspicuously absent in all conditions.

5.1.4.3 Use of TEM to study Grain Boundary Character and Precipitation at Grain Boundaries. TEM studies were performed to determine the grain boundary structure, especially to identify the presence of grain boundary ledges in the homogenized and segregated samples. The representative micrographs in the Phos-IF segregated condition are shown in Figure 5.9. Grain boundary ledges and grain boundary dislocations were readily seen in the segregated Phos-

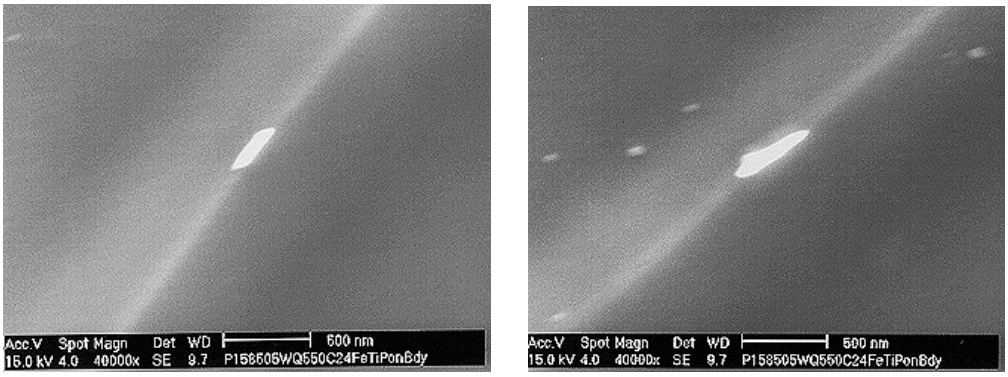

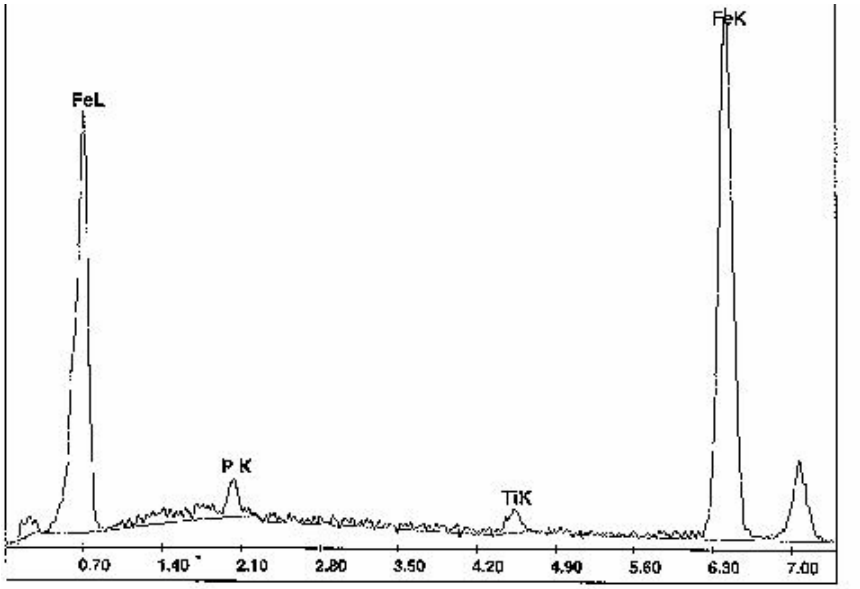

EDAX ZAF Quantification (Standardless)
Element Normalized

Element	Wt %	At %	K-Ratio	Z	A	F
P K	1.48	2.64	0.0112	1.1010	0.6826	1.0018
TiK	1.80	2.06	0.0194	1.0016	0.9791	1.0994
FeK	96.72	95.30	0.9640	0.9983	0.9984	1.0000
Total	100.00	100.00				

Figure 5.6 FeTiP Precipitates at Boundaries and the EDX Spectrum from the Precipitates

Table 5.8 (a) Summary of Results from Use of STEM Technique

Phos-IF Steel (Homogenized)		
Grain Size	Precipitation	Segregation of P to GB
15 μm	TiN: ~ 700 nm to 1 μm H: 8-10 ppts. 10-70 nm **FeTiP: None in matrix and at GB** TiC: None	**Not detectable** at both high and low angle grain boundaries at several locations along GB
39 μm	TiN: ~ 800 nm to 1 μm H: 8-10 ppts. 10-70 nm **FeTiP: None in matrix and at GB** TiC: None	**Not detectable** at both high and low angle grain boundaries
63 μm	TiN: ~ 700 nm to 1 μm H: 8-10 ppts. 10-70 nm **FeTiP: None in matrix and at GB** TiC: None TiS: Some	**Not detectable** at both high and low angle grain boundaries

Table 5.8 (b) Summary of Results from Use of STEM Technique

Phos-IF Steel (Segregated)		
Grain Size	Precipitation	Segregation of P to GB
15 μm	TiN: ~ 700 nm to 1 μm H: ~10 ppts. 30-100 nm **FeTiP: None** TiC: None Oxide particles: None Ppts mainly in matrix	**Not detectable** checked 2 low angle and 3 high angle gbdys.
39 μm	TiN: ~ 800 nm to 1 μm H: ~10 ppts. 30-100 nm **FeTiP: None** TiC: None Oxide particles: None Ppts mainly in matrix	**Not detectable** checked ~ 8 high angle gbs. 2 H ppts at gbs
63 μm	TiN: ~ 700 nm to 1 μm H: ~10 ppts. 30-100 nm **FeTiP: None** TiC: None TiS: Some ppts seen Oxide particles: None Ppts mainly in matrix	**Not detectable** checked ~ 5 high angle gbs.

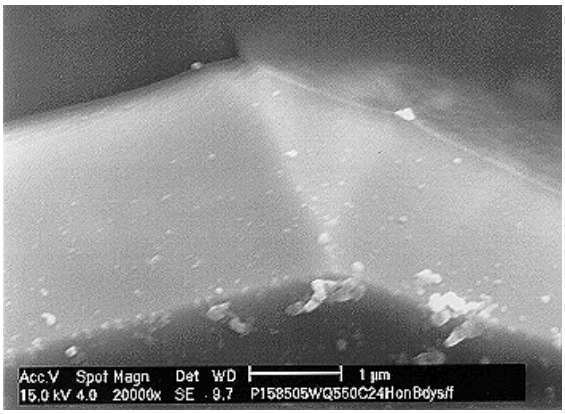

(a)

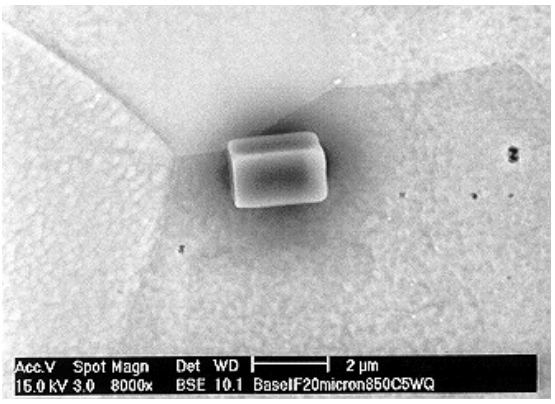

(b)

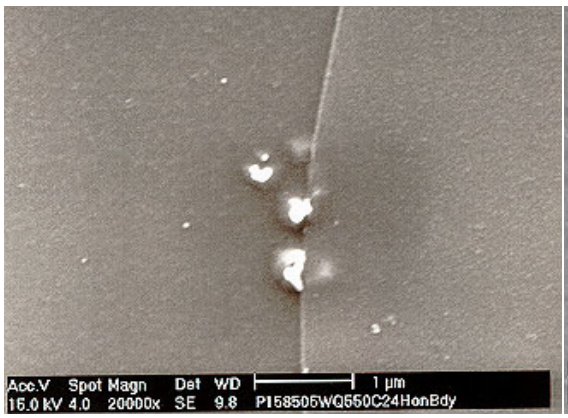

(c)

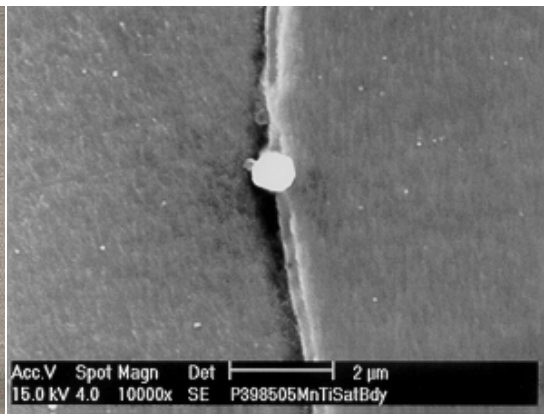

(d)

Figure 5.7 Typical Precipitates Observed at Ferrite Grain Boundaries

a) H (b) TiN (c) H on grain boundaries (d) MnTiS

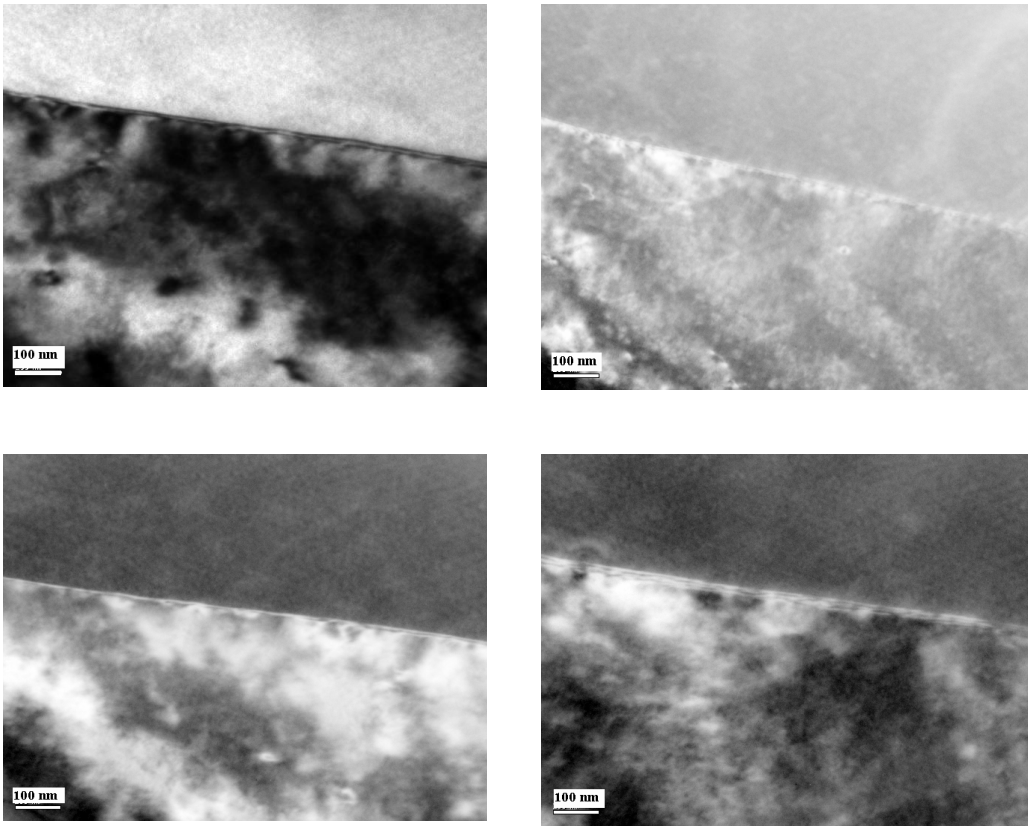

Figure 5.8 STEM Analysis of Grain Boundaries in Phos-IF Segregated Condition

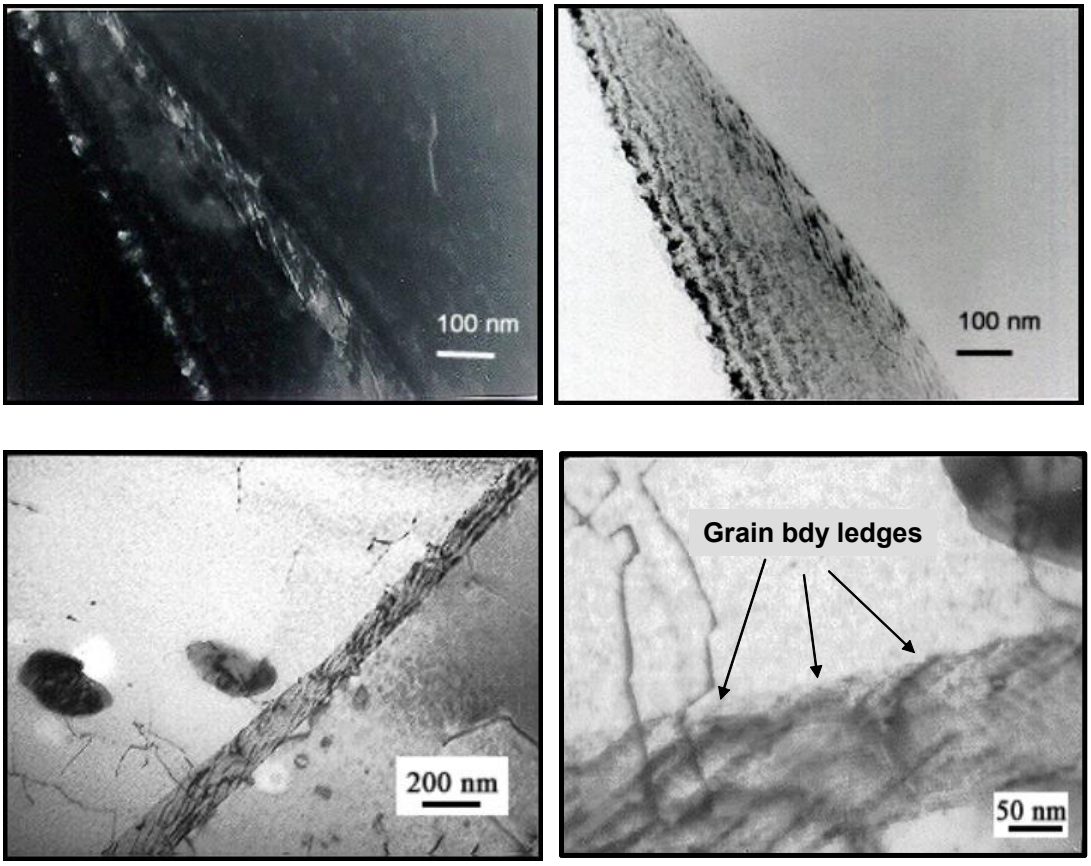

Figure 5.9 TEM Studies of Grain Boundary Ledges in the Phos-IF 15 μm Segregated Condition

IF steel. Some H precipitates were also seen in the vicinity of the boundaries as seen in Figure 5.9.

5.1.4.4 <u>Status of C through Different Stages of Processing.</u> As mentioned previously, the presence of solute C in the matrix can hinder the segregation of P to ferrite grain boundaries through a competitive segregation mechanism at the grain boundaries. The presence of solute C can also bring about significant solid solution strengthening of the matrix. Thus, the presence of solute C can introduce variability in the strength due to the above effects. In order to quantify the amount of C in solution throughout the different stages of processing, "internal friction" tests were performed and the results are presented in Figure 5.10 and tabulated in Table 5.9. It can be seen that the large grain sizes in both the Base-IF and Phos-IF steels show the presence of solute C in the homogenized condition, whereas, in all the other conditions, C is completely stabilized. It should be noted that the large grain sizes in both the steels were annealed at a higher temperature of 850^{o}C for 30 mins prior to the homogenizing heat treatment as compared to the lower annealing temperature of 750^{o}C employed for the small and intermediate grain sizes. The higher annealing temperature seems to have dissolved some C-rich precipitates presumably $Ti_4C_2S_2$.

5.1.5 Microhardness and Macrohardness Measurements

Micro and macrohardness measurements were performed to determine the solid solution strengthening and the grain boundary hardening due to P. The methodology has been shown earlier in Figure 4.1.

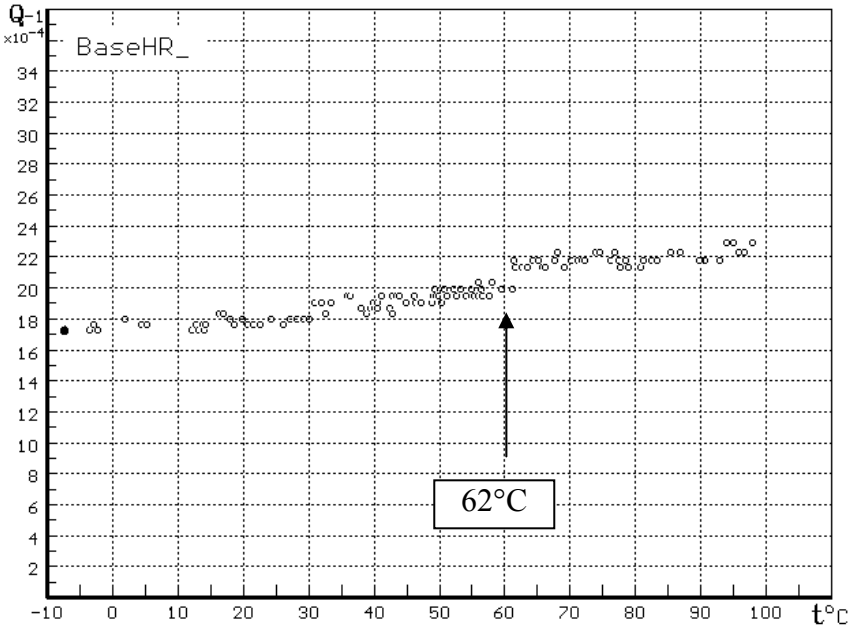

(a) Base-IF: Hot Rolled Condition, Absence of Solute C

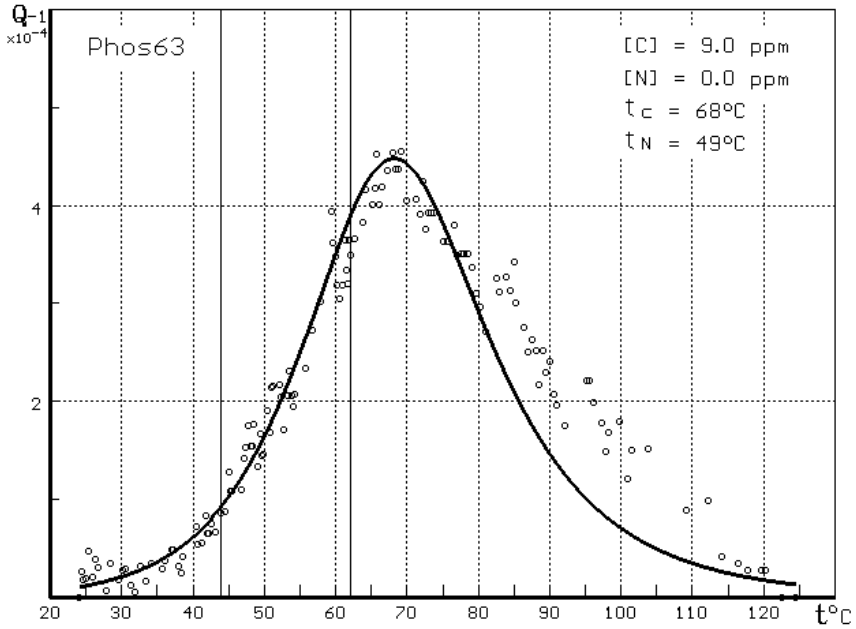

(b) Phos-IF: 63 mm Grain Size, Homogenized Condition

~ 9 ppm Solute C Present in Matrix

Figure 5.10 Internal Friction Results

Table 5.9 Internal Friction Results for Determination of Solute C in Matrix

Steel	Grain Size	Solute C in matrix (ppm)		
		Hot Rolled/As-annealed	Homogenized	Segregated
	μm			
Base-IF	39	HR: 0 ppm	X	X
Phos-IF	25	HR: 0 ppm	X	X
Base-IF	20	As-ann: 0 ppm	0	0
Base-IF	53	As-ann: 0 ppm	0	0
Base-IF	103	As-ann: 15 ppm	15	0
Phos-IF	15	As-ann: 0 ppm	0	0
Phos-IF	39	As-ann: 0 ppm	0	0
Phos-IF	63	As-ann: 9 ppm	9	0

5.1.5.1 Macrohardness Measurements of As-annealed Steels. The results for the macrohardness in the grain-size-annealed or as-annealed condition for all the three grain sizes in the two steels are shown in Figure 5.11. It can be seen from the figure that the dependence of macrohardness on $d^{-1/2}$ is linear in both the steels and is similar to Hall-Petch type of behavior. The macrohardness thus fits the following equation:

$$HVN = H_o + k_h d^{-1/2} \tag{5-1}$$

where, H_o = Intercept on the HVN axis

k_h = H-P slope for macrohardness, units of $(kg/mm^2)(\mu m^{1/2})$

d = grain size, μm

The linear dependence of the macrohardness on $d^{-1/2}$ has been observed by several researchers in both ferrous as well as non-ferrous alloys[178-180].

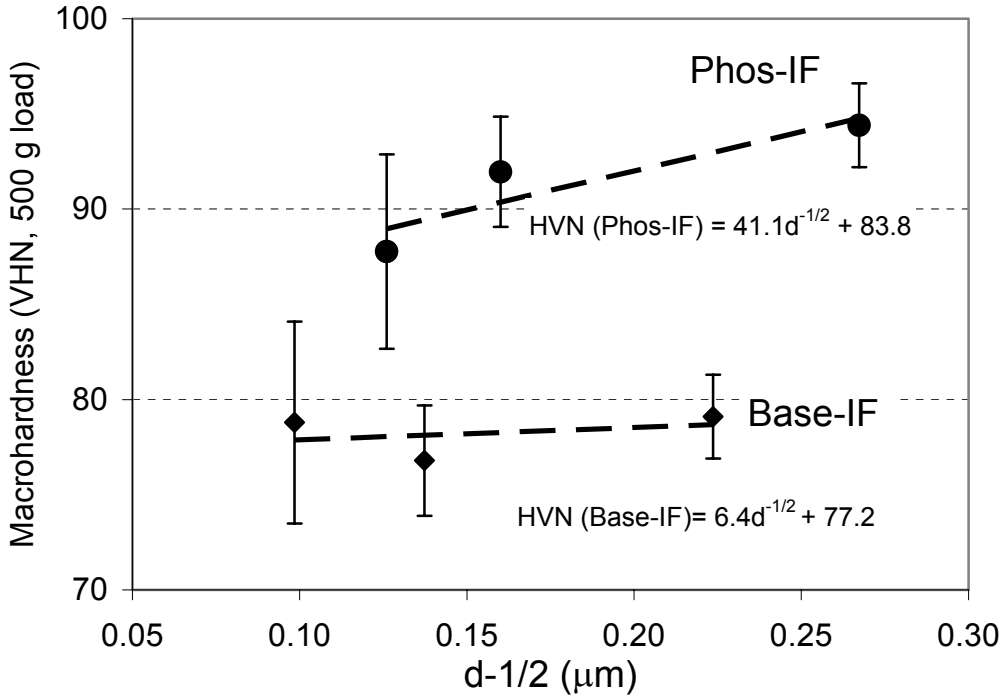

Figure 5.11 Macrohardness of As-annealed Base-IF and Phos-IF Steel

5.1.5.2 Microhardness Measurements: Grain Center (GC) vs. Grain Boundary Hardness (GB). After the as-annealed macrohardness measurements were done, microhardness measurements were performed in both steels in the homogenized and segregated conditions. The results of the grain center and grain boundary hardness measurements are shown in Figures 5.12 and 5.13. From Figure 5.12, it is evident that the grain center microhardness values for the Phos-IF steel is always higher, in all the processing conditions, as compared to those in the Base-IF steel. These microhardness measurements see no interference from the grain boundaries and, hence, this result indicates that solute P in the matrix brings about solid solution strengthening. Figure 5.13 indicates the grain boundary hardening phenomenon due to P segregated to ferrite grain boundaries. It is seen that only in the Phos-IF steel, the grain boundary microhardness, (GB), is higher than the grain center microhardness (GC). This increment of ~ 5 VHN in the microhardness, results from the segregation of atomic P to the grain boundaries. This increment is conspicuously absent in the Base-IF steel.

5.1.5.3 Macrohardness Measurements in the Homogenized and Segregated Condition. Macrohardness measurements, using a 500 g load, were performed in both the IF steels in the homogenized and segregated condition. The results are shown in Figure 5.14. There are several features to be noted in Figure 5.14. This plot is similar to a Hall-Petch plot, except that the macrohardness (kg/mm^2) is plotted vs. $d^{-1/2}$ ($\mu m^{-1/2}$). It can be seen that the slope, k_h, has units of (kg/mm^2)($\mu m^{1/2}$). The value of k_h, in the Base-IF steel increases from 17 (kg/mm^2)($\mu m^{1/2}$) in the homogenized condition to 21.1 (kg/mm^2)($\mu m^{1/2}$) in the segregated condition, an increase of 24%. On the other hand, in the Phos-IF steel, the value of k_h values

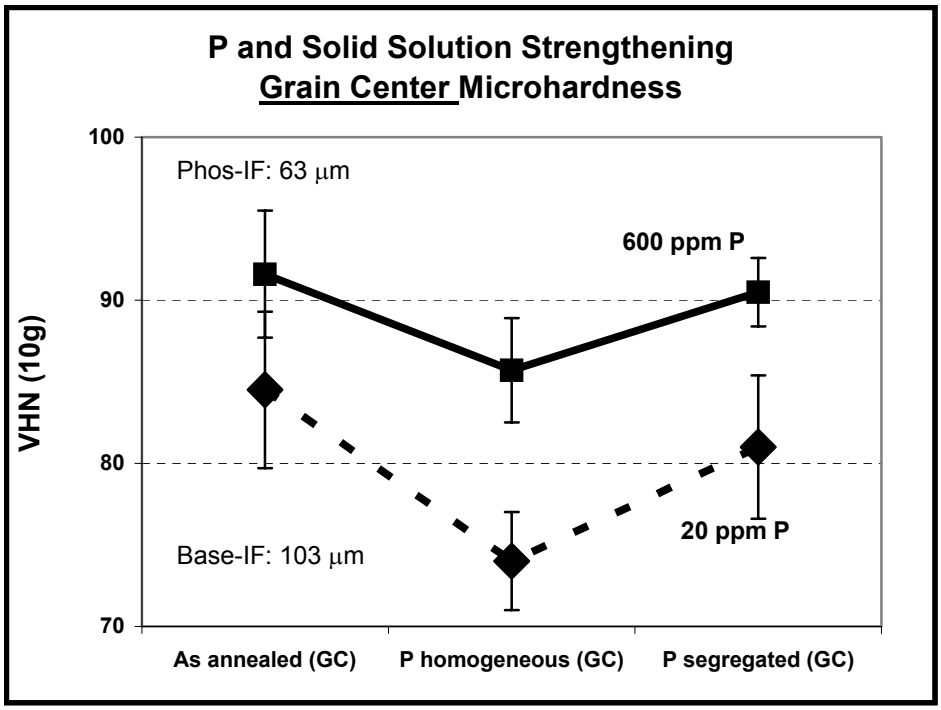

Figure 5.12 Grain Center Microhardness Measurements Indicating Solid Solution Strengthening Due to Solute P in Ferrite Matrix

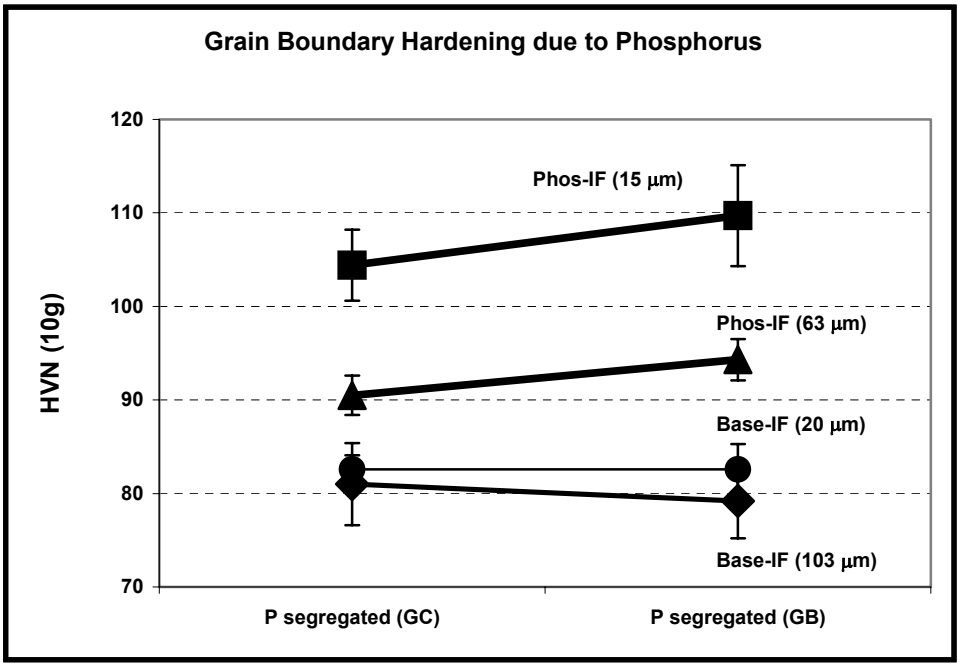

Figure 5.13 Grain Center and Grain Boundary Microhardness Measurements Indicating Grain Boundary Hardening Due to Atomic P at Grain Boundaries

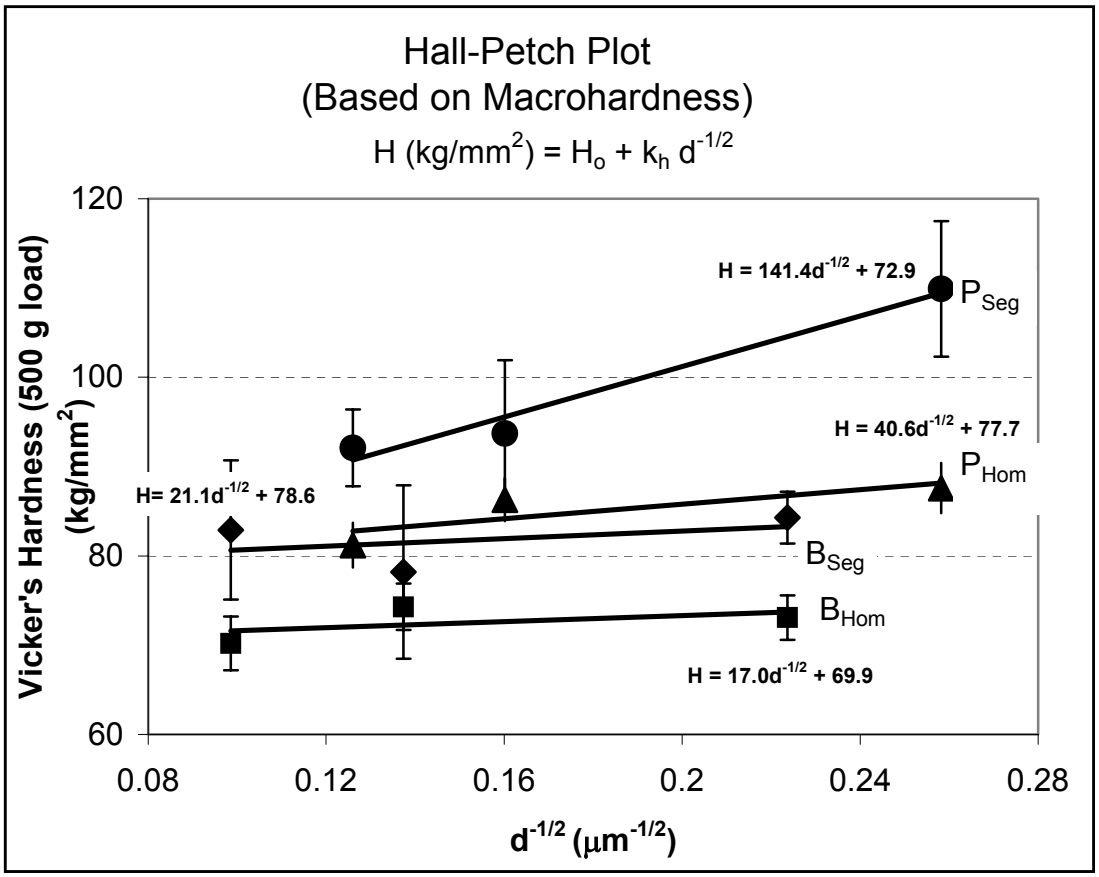

Figure 5.14 Macrohardness vs. $d^{-1/2}$ Plot for Both IF Steels in the Homogenized and Segregated Conditions

increases from 40.6 (kg/mm^2)(μm$^{1/2}$) in the homogenized condition to 141.4 (kg/mm^2)(μm$^{1/2}$) in the segregated condition, an increase of ~ **250%**. Thus, it is seen that the segregation of atomic P to ferrite grain boundaries results in a phenomenal increase in the k_h value.

5.1.6 Tensile Test Results

Tensile tests were performed in the rolling direction of the sheets for the 12 conditions shown in Table 4.2. Yield strengths obtained for the different conditions were plotted vs. $d^{-1/2}$ and the resulting Hall-Petch (H-P) plots are shown in Figures 5.15 and 5.16 for the Base-IF and Phos-IF steel, respectively. The purpose of the tensile tests was to determine the influence of P segregation on the yield strength of IF steels and its influence on the Hall-Petch slope, k_y. The H-P plots are shown for the as-annealed, homogenized and segregation conditions in both the steels. It should be noted that no significant yield point elongation was observed in any of the tensile tests. The following features are noteworthy in the two figures:

a) In the Base-IF steel, for any given grain size, the yield strength (YS) does not vary significantly between the as-annealed, homogenized and segregated condition.

b) In the Phos-IF steel, for any given grain size, the yield strength is consistently higher in the segregated condition than in the as-annealed and the homogenized condition. Thus for this steel, for any given grain size, $YS_{seg} > YS_{as\text{-}annealed} > YS_{homogenized}$.

c) For any given heat treatment condition, namely as-annealed, homogenized or segregated, the value of k_y is higher for the Phos-IF steel compared to the Base-IF steel.

d) The k_y value of the Base-IF steel remains fairly constant in all processing conditions.

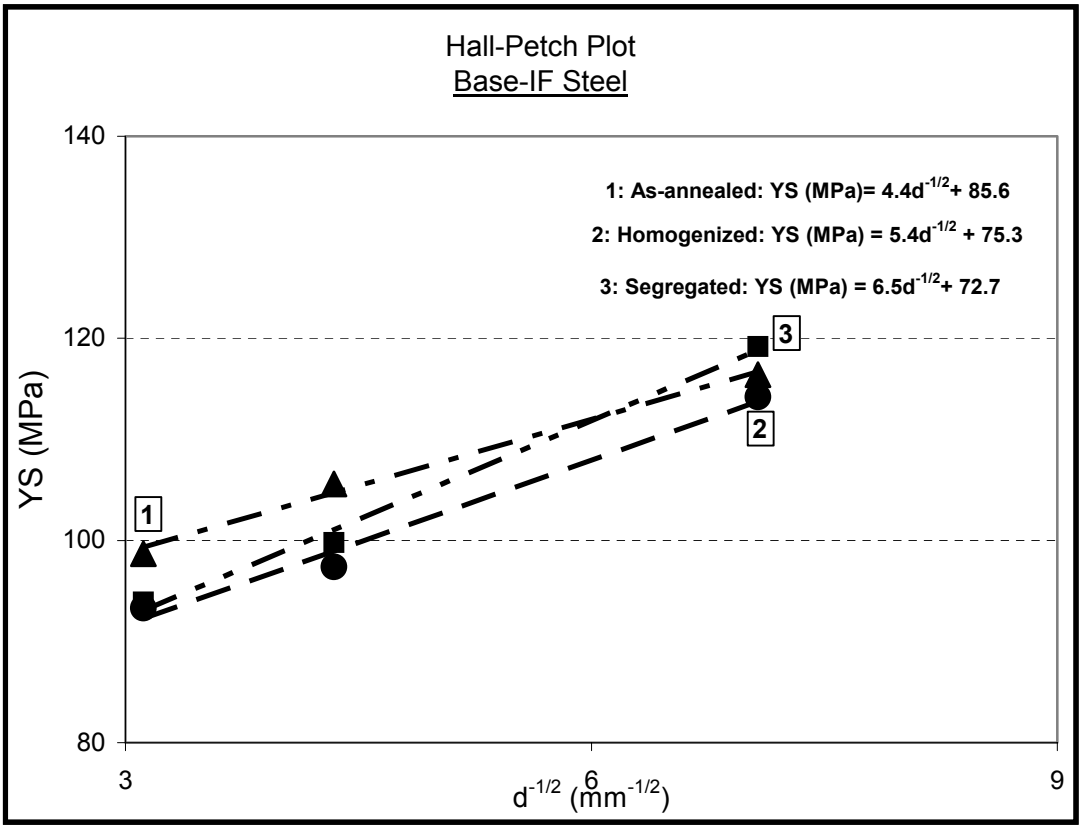

Figure 5.15 Hall-Petch Plot for Base-IF Steel

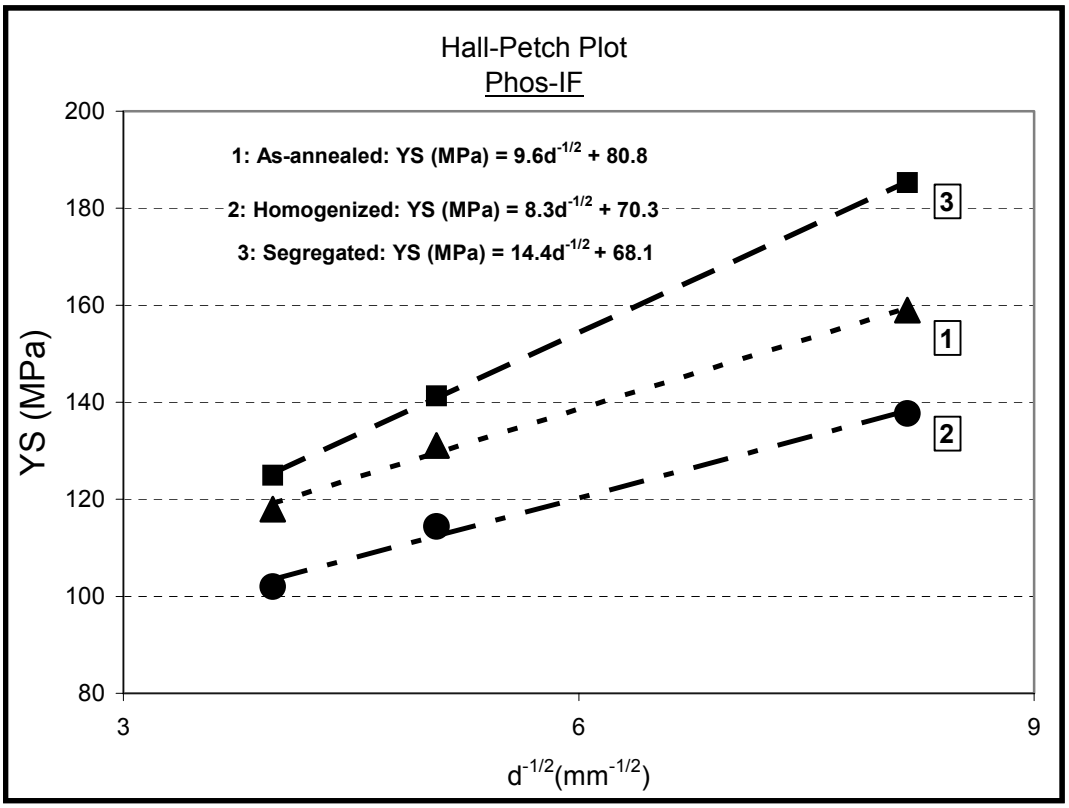

Figure 5.16 Hall-Petch Plot for Phos-IF Steel

e) In both the Base-IF and the Phos-IF, the intercept on the yield strength axis, σ_o, in Figures 5.15 and 5.16, tends to vary inversely with the value of k_y. This result is similar to that observed by Mintz[72] and Johnson[181].

f) The k_y value of the Phos-IF steel in the "Segregated" condition is 73.5% higher than that in the "Homogenized" condition.

g) The segregation of solute P to ferrite grain boundaries, thus, is seen to significantly increase the value of k_y in the Phos-IF steel.

h) In the Phos-IF steel, the increment in the yield strength after the segregation heat treatment is dependent upon the grain size, the increment being 45 MPa in the 15 μm grain size compared to 24 MPa in the 63 μm grain size.

It should be noted that similar results were observed in Figure 5.14, which was a plot of the macrohardness vs. $d^{-1/2}$.

5.1.6.1 Correction to the Measured Value of ky due to Solid Solution Strengthening Contribution of C. From the internal friction results presented in Table 5.9, it is seen that that the 103-micron grain size in the Base-IF steel has 15 ppm C in solution in the as-annealed as well as the in the homogenized condition but 0 ppm C in solution in the segregated condition. Similarly, the 63-micron grain size in the Phos-IF steel has 9 ppm C in solution in the as-annealed and homogenized condition but 0 ppm C in solution in the segregated condition. The excess carbon present in solution will impart a solid solution strengthening contribution (C_{sss}) in the as-annealed and homogenized conditions of the large grain sizes in the two IF steels. In order to compare the true increments in k_y values after P segregation, it is necessary to account for this selective solid solution strengthening contribution due to solute C. Based upon the published

value of k_{sss} for C = 5544 MPa/ 1 wt%, the yield strength increment due to excess C in the 103-micron Base-IF steel is 0.0015 x 5544 MPa = 8.3 MPa. A similar calculation for the 63-micron Phos-IF steel grain size gives the solid solution contribution of solute C, C_{sss} = 5 MPa. The measured values of yield strengths in the as-annealed and homogenized conditions for the two large grain sizes should be corrected for the calculated C_{sss} contribution. This correction modifies the measured values of k_y in Figures 5.15 and 5.16 and the corrected values are plotted in Figures 5.17 and 5.18 and are tabulated in Table 5.10 along with k_h values obtained from Figures 5.11 and 5.14. Figure 5.19 shows the variation of corrected k_y values in both steels. The % difference in the k_y values has also been shown in this figure. It can be seen from Figure 5.19 that the k_y values for the Phos-IF steel are consistently higher than those in the Base-IF steel. Additionally, it can be seen that the k_y value in the segregated Phos-IF steel is 57% higher than that in homogenized Phos-IF steel. Thus, it is seen that the segregation of P to grain boundaries seems to bring about a substantial increase in the Hall-Petch slope.

5.1.7 Texture Hardening Correction to the Measured k_y

As shown in the previous section, a correction to the measured value of k_y was made to account for the excess C present in solution in certain conditions. Another correction that needs to be taken into consideration is the texture hardening correction to the measured value of k_y in the homogenized and segregated condition. The concept behind the necessity for this correction and the methodology followed to perform this correction has been explained previously in section 4.1.1 [c]. The first step required to be done in this correction was to model the dependence of the relative texture hardening contribution to the yield strength of several texture

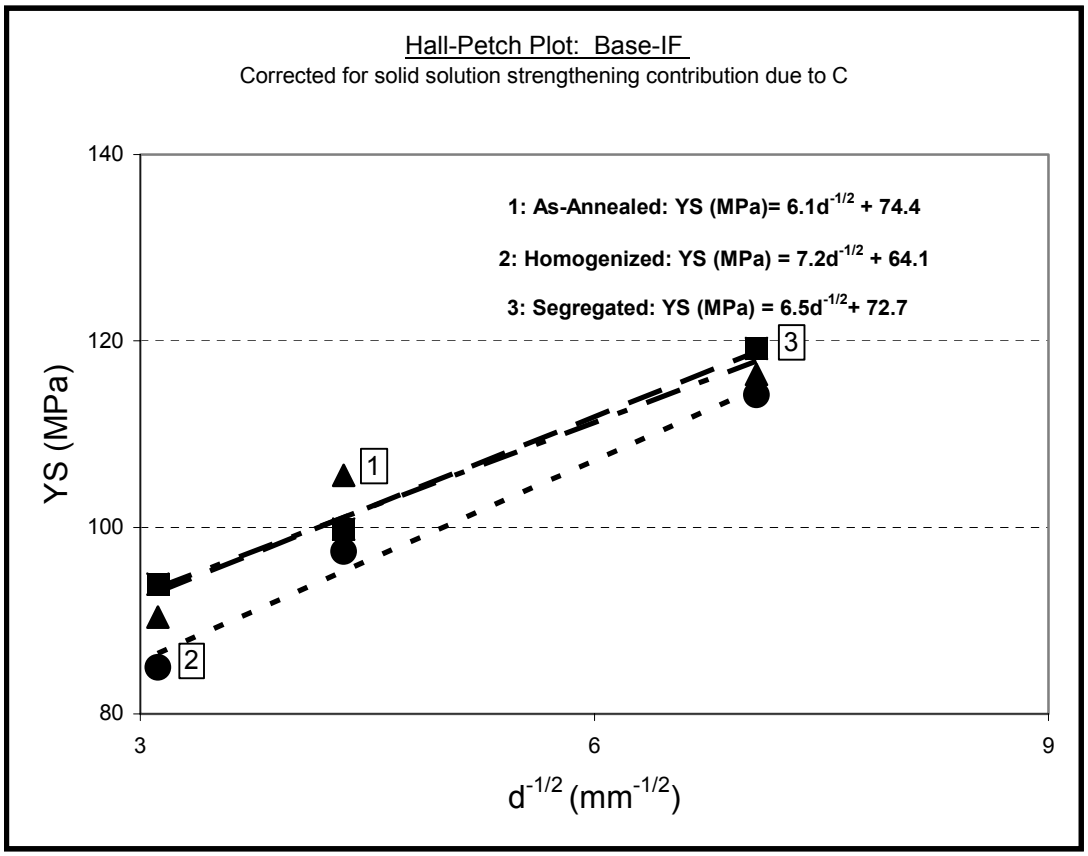

Figure 5.17 Hall-Petch Plot for Base-IF Steel (Corrected for Solid Solution Strengthening Due to C)

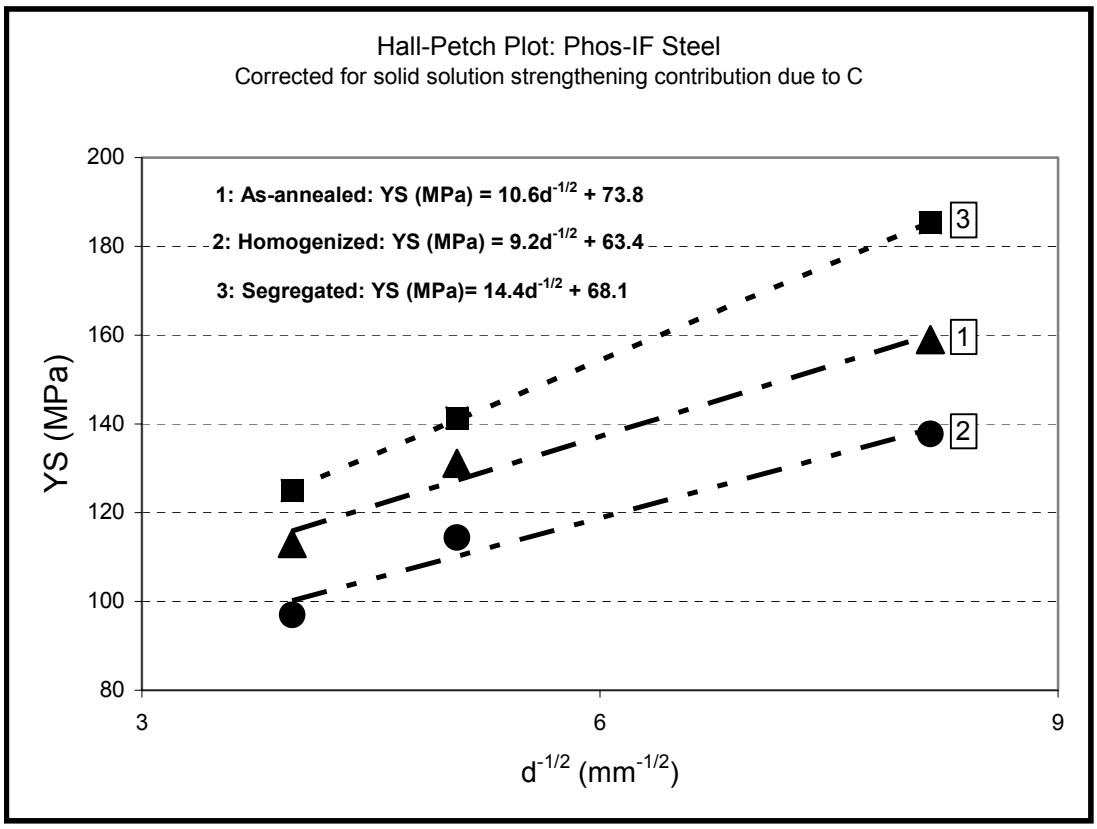

Figure 5.18 Hall-Petch Plot for Phos-IF Steel (Corrected for Solid Solution Strengthening Due to C)

Table 5.10 Hall-Petch Slopes Obtained in Macrohardness and Tensile Testing

Test Condition	k_h (Figure 5.12) $(kg/mm^2).(\mu m^{1/2})$	k_y measured (Fig 5.13 and 5.14) $MPa.mm^{1/2}$	k_y corrected for C_{sss} $(MPa.\ mm^{1/2})$
Base-IF (As-Annealed)	6.4	4.4	6.1
Base-IF (Homogenized)	17.0	5.4	7.2
Base-IF (Segregated)	21.1	6.5	6.5
Phos-IF (As-Annealed)	41.1	9.6	10.6
Phos-IF (Homogenized)	40.6	8.3	9.2
Phos-IF (Segregated)	141.4	14.4	14.4

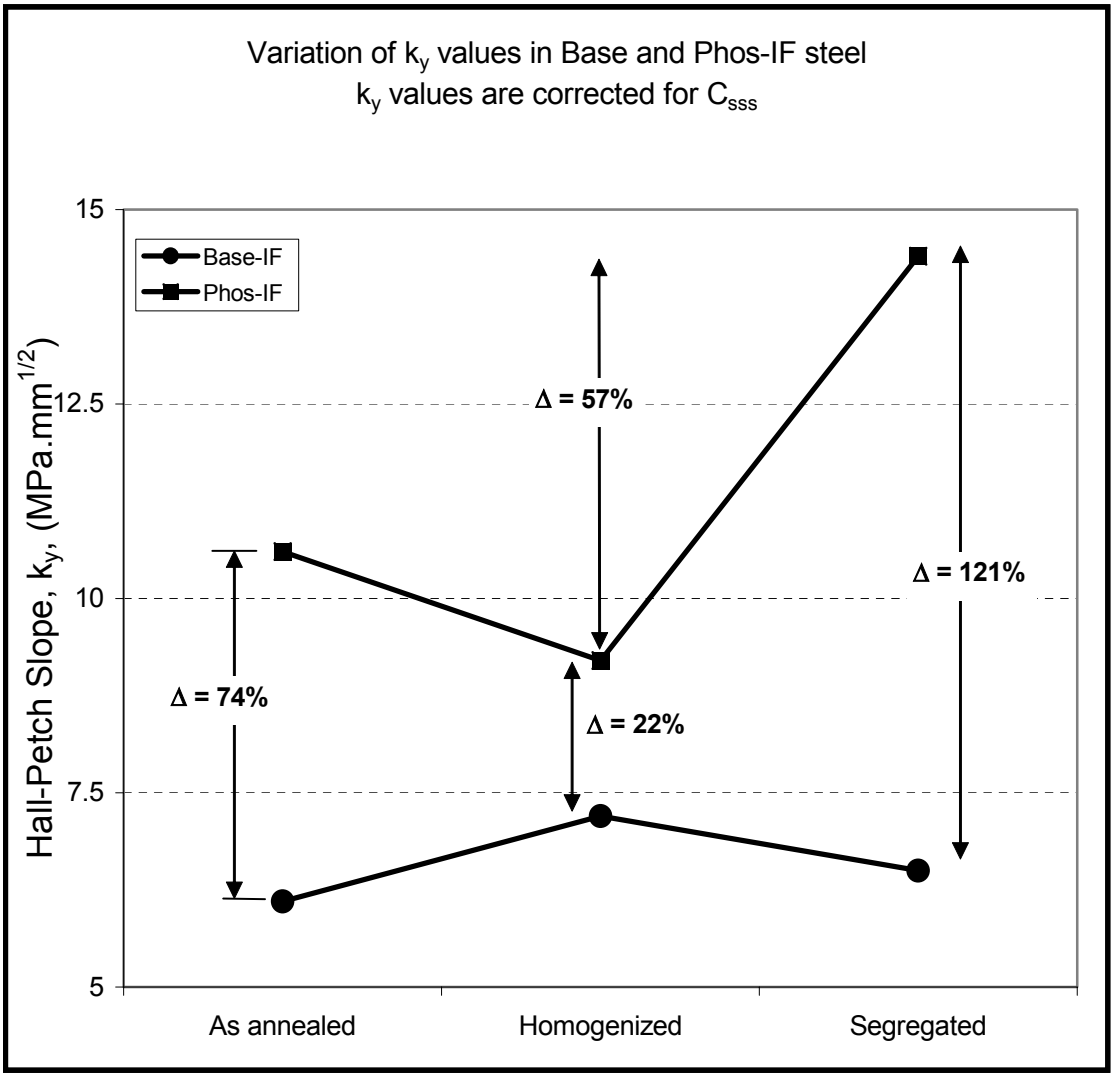

Figure 5.19 Variation of k_y Values in Base-IF and Phos-IF Steel

components in the $\phi_2 = 45^o$ section of the Euler space shown in Figure 2.32. The relative texture hardening contribution was calculated for all the crystallographic texture components along the alpha, gamma and epsilon fibers of the $\phi_2 = 45^o$ section in the Euler space. This calculation was done using the Bishop and Hill approach for predicting yielding in textured sheet metals. The prediction of yielding behavior for each texture component was performed only in the rolling direction of the sheet. The results of this modeling are shown in Figure 5.20. It should be noted that each point along any texture fiber represents a different crystallographic orientation. These orientations are tabulated in Table 5.11. The origin in Figure 5.20 is the relative yield strength of the rotated cube texture, namely, (001)[1-10]. The texture hardening contribution for all the texture components has been shown relative to the strength of this rotated cube texture component. For example, the (111)[1-10] gamma fiber component, when tested in the rolling direction, is expected to be 55% stronger than the (001)[1-10] texture tested in its rolling direction. This figure effectively points out the anisotropy of the texture hardening contribution for the different texture components. The maximum variability of 60% in the texture hardening contribution is seen along the alpha fiber. The variability in the gamma and epsilon fibers is 14% and 38%, respectively. Thus, the gamma fiber is the most isotropic among the three fibers with respect to the texture hardening contribution.

The next step in calculating the texture hardening correction to measured k_y, is to measure the volume fractions of the different texture components in the Base-IF and the Phos-IF steel in homogenized and segregated condition. These measurements were done using the SEM-EBSD technique and the $\phi_2 = 45^o$ ODF sections are shown in Figures 5.21 and 5.22 for all the three grain sizes in the Base-IF and Phos-IF steel in the homogenized condition. Similar measurements were done in the segregated condition. From these ODF sections, the volume

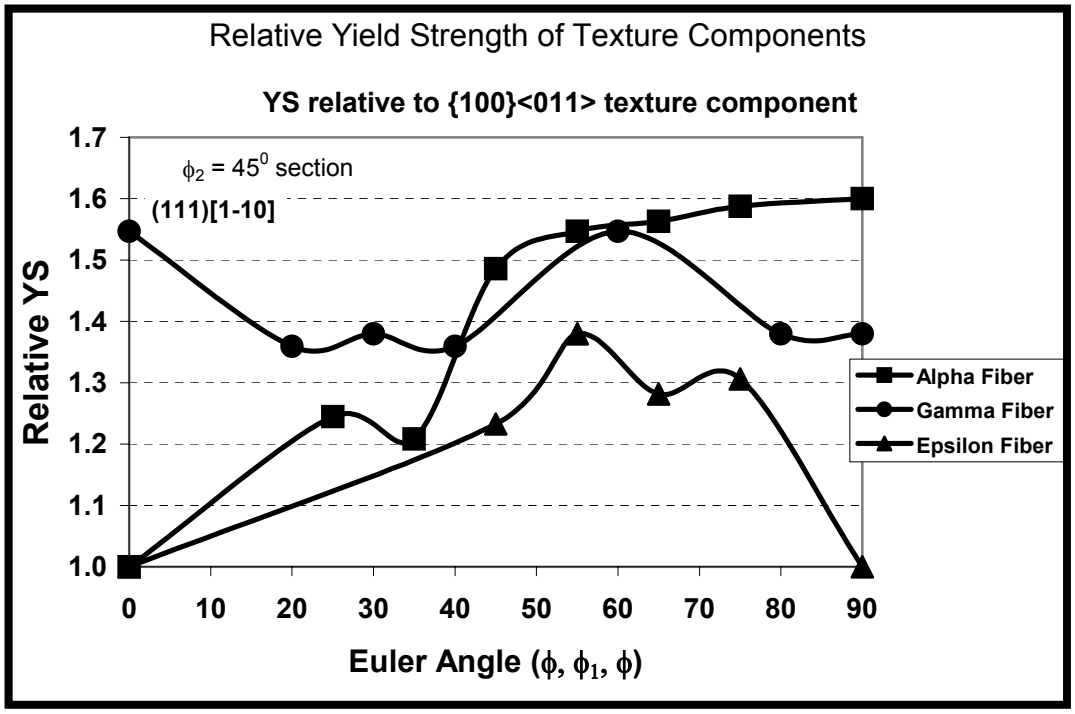

Figure 5.20 Results of the Texture Hardening Modeling for Several Crystallographic Textures in the phi2 = 45^o Section of the Euler Space

Table 5.11 Crystallographic Orientations in the phi2 = 45^{o} Section of the Euler Space

Alpha Fiber		Gamma Fiber		Epsilon Fiber	
Angle (ϕ)	Texture	Angle (ϕ_1)	Texture	Angle (ϕ)	Texture
0	(0 0 1)[1 -1 0]	0	(111)[1-10]	65	(332)[-1 -1 3]
25	(113)[1 -1 0]	20	(111)[2-31]	90	(110)[001]
35	(112)[1 -1 0]	30	(111)[1-21]	45	(223)[-3 -3 4]
45	(223)[1 -1 0]	40	(111)[1-32]	75	(331)[-1 -1 6]
55	(111)[1 -1 0]	60	(111)[0-11]		
65	(332)[1 -1 0]	80	(111)[-1-23]		
75	(221)[1 -1 0]	90	(111)[-1-12]		
85	(331)[1 -1 0]				
90	(110)[1 -1 0]				

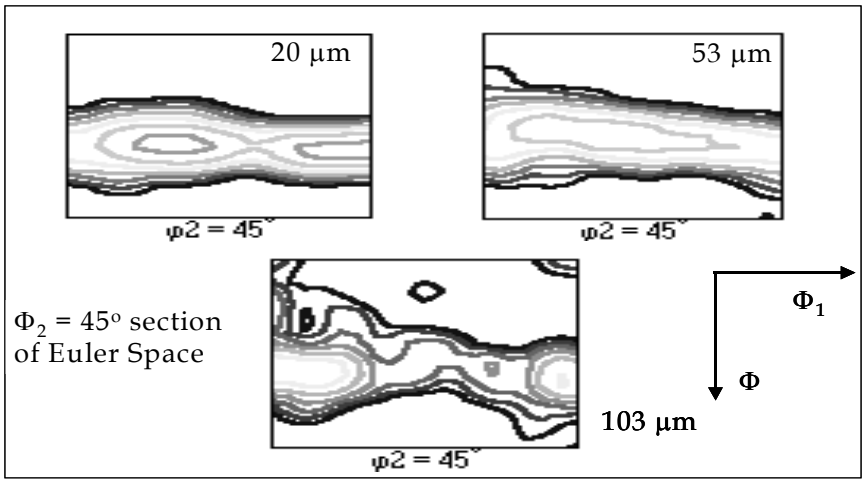

Figure 5.21 phi2 = 45° ODF Section for Three Grain Sizes in Base-IF Steel

(Homogenized Condition)

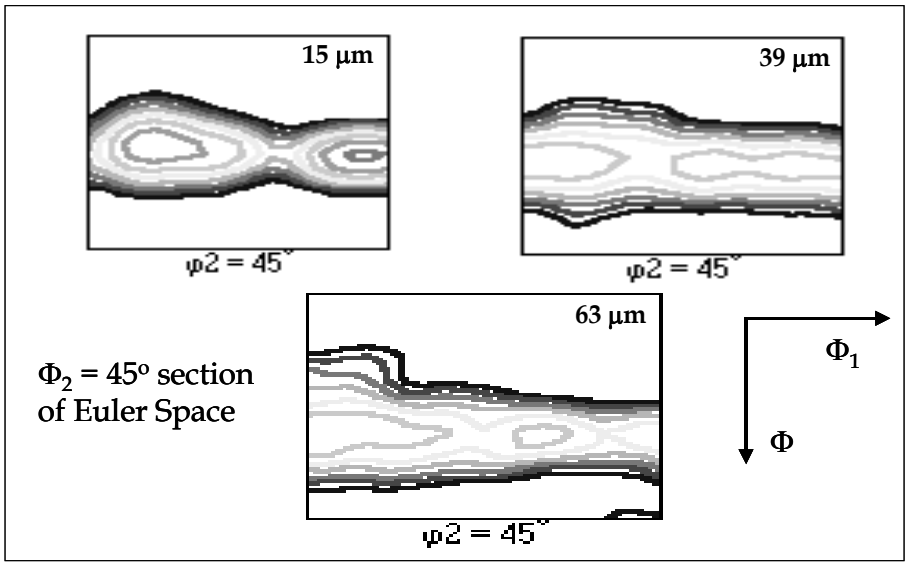

Figure 5.22 phi2 = 45° ODF Section for Three Grain Sizes in Phos-IF Steel

(Homogenized Condition)

fractions of the three fibers were calculated in the two steels and the results for the Base-IF are shown in Figures 5.23 and 5.24 and for the Phos-IF steel in Figures 5.25 and 5.26. It can be seen from all the figures that the volume fractions of texture components vary with different processing routes used to develop the three ferrite grain sizes in both the steels. Also, for a certain nominal grain size, the texture components are different in the homogenized and segregated condition. Combining the results from the texture hardening modeling and the volume fraction data for the two steels, the relative texture hardening contribution in each grain size in both the homogenized and segregated condition of the two IF steels was estimated. The results are shown in Figure 5.27 for the Base-IF steel and in Figure 5.28 for the Phos-IF steel. For the Base-IF steel, the texture hardening contribution has been shown relative to the 103 micron grain size in the segregated condition. For the Phos-IF steel, the texture hardening contribution has been shown relative to the 63 micron grain size in the segregated condition. These data can be used to calculate an upper bound correction as follows: It can be assumed that the texture hardening contribution for a randomly oriented IF steel sheet is 40 MPa, which is the value of the Peierl's-Nabarro force reported in steels[182]. Based upon this assumption, an upper bound estimate of the texture hardening contribution to yield strength in each grain size can be made. The results are shown in Table 5.12 and the corrected values of k_y are shown in Figures 5.29 and 5.30 for the Base-IF steel. Thus, by using the modeling results and by measuring volume fractions of the texture components, the texture hardening correction to measured value of k_y can be estimated.

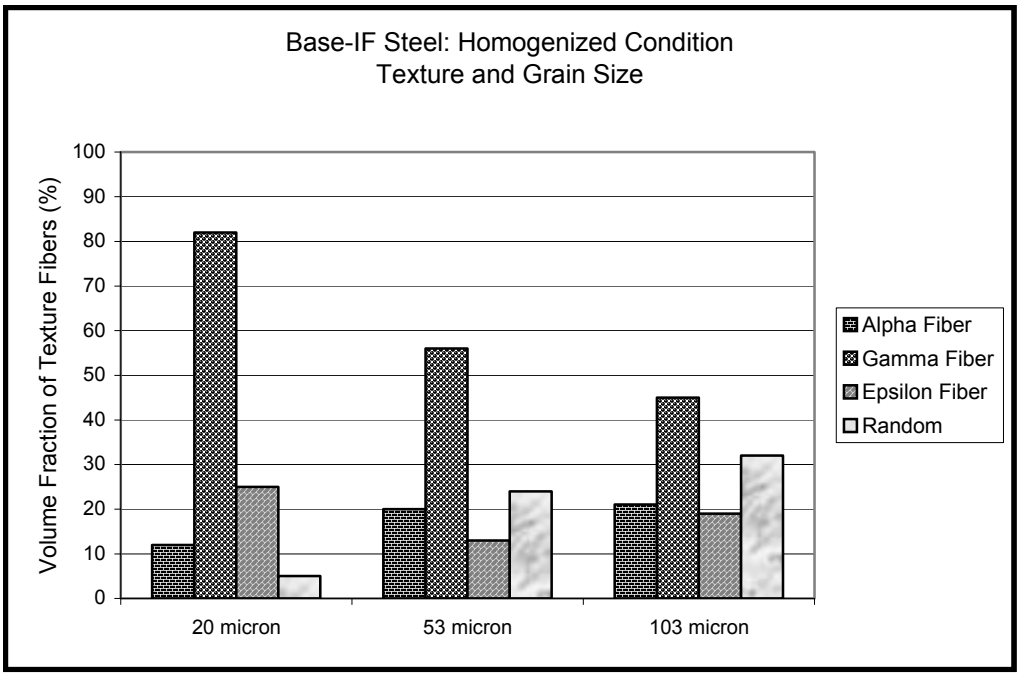

Figure 5.23 Volume Fractions of Texture Components in Base-IF Homogenized Condition

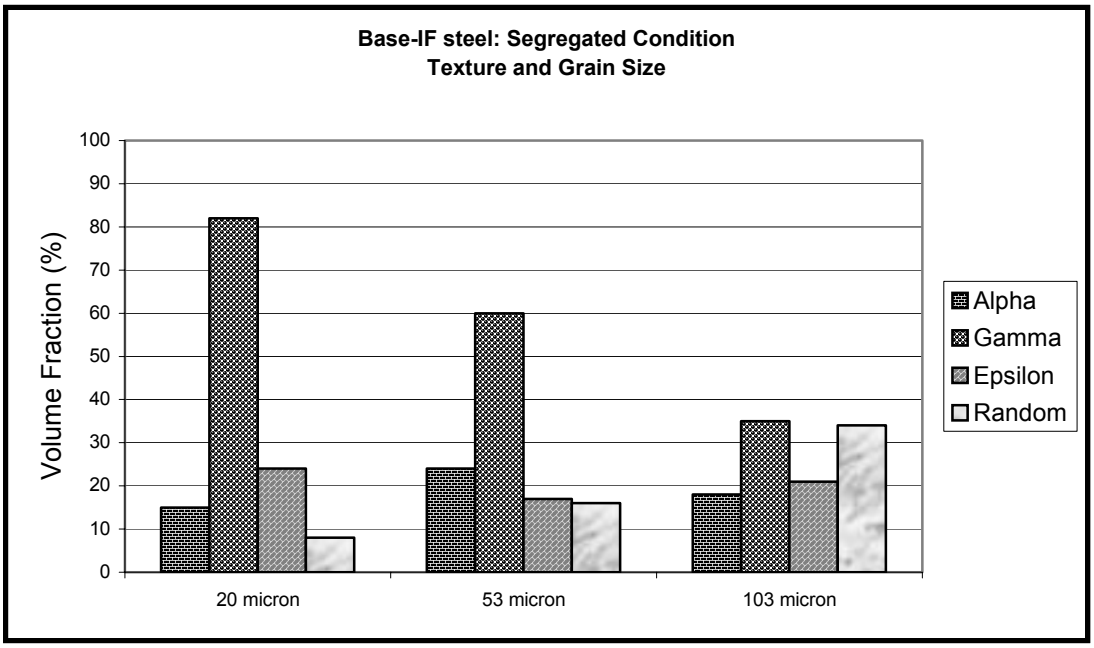

Figure 5.24 Volume Fractions of Texture Components in Base-IF Segregated Condition

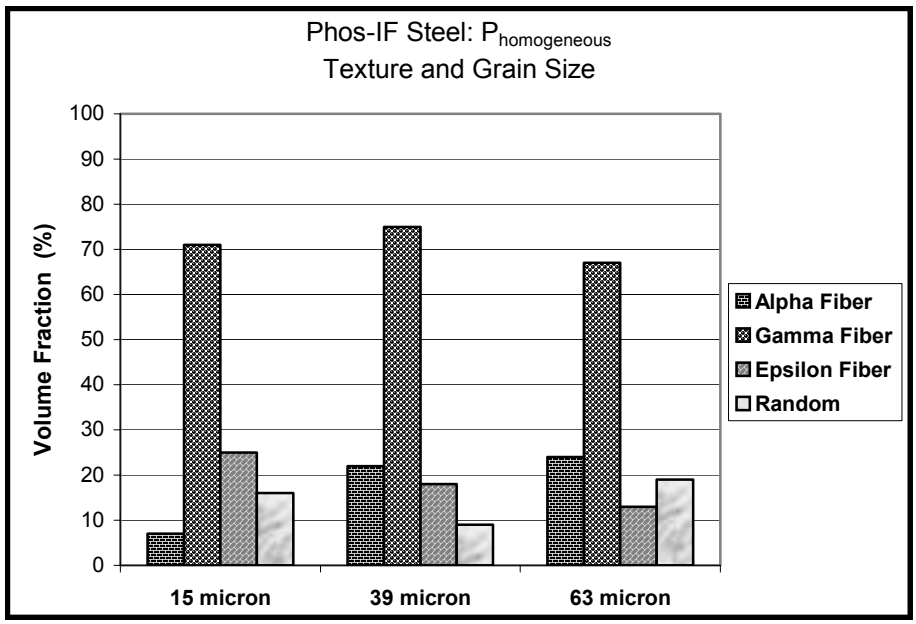

Figure 5.25 Volume Fractions of Texture Components in Phos-IF Homogenized Condition

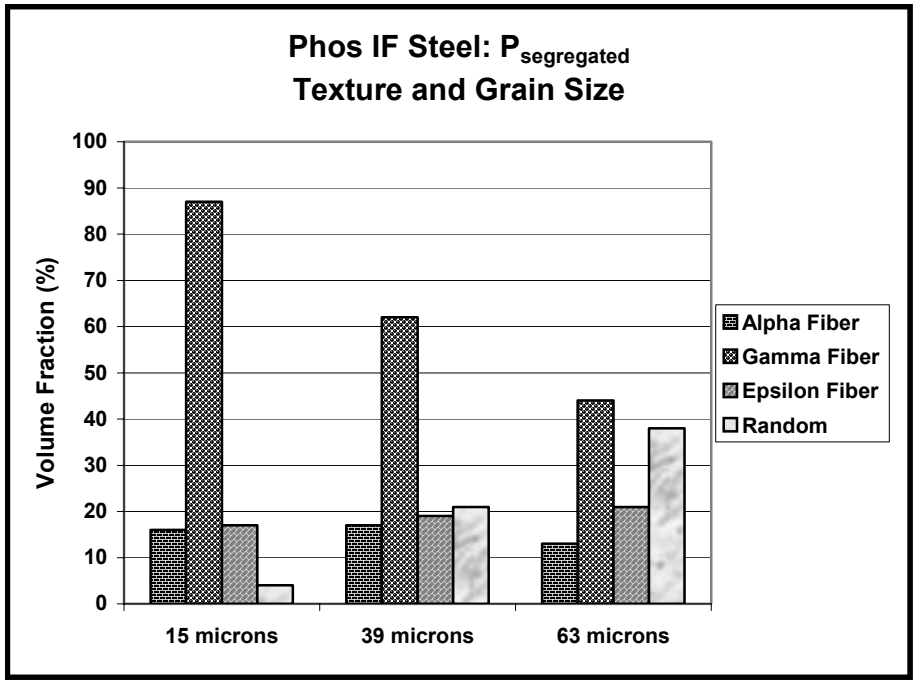

Figure 5.26 Volume Fractions of Texture Components in Phos-IF Segregated Condition

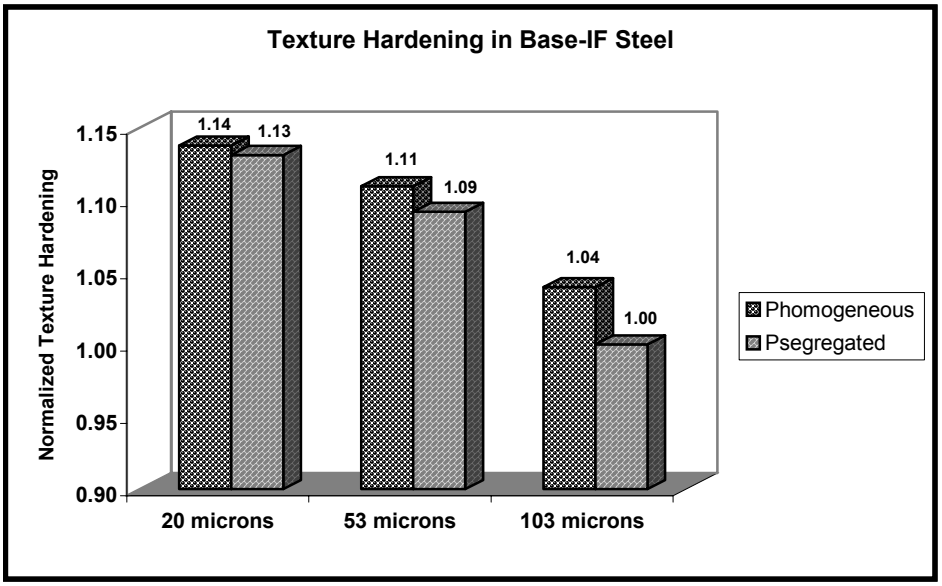

Figure 5.27 Texture Hardening Contribution in Base-IF Steel

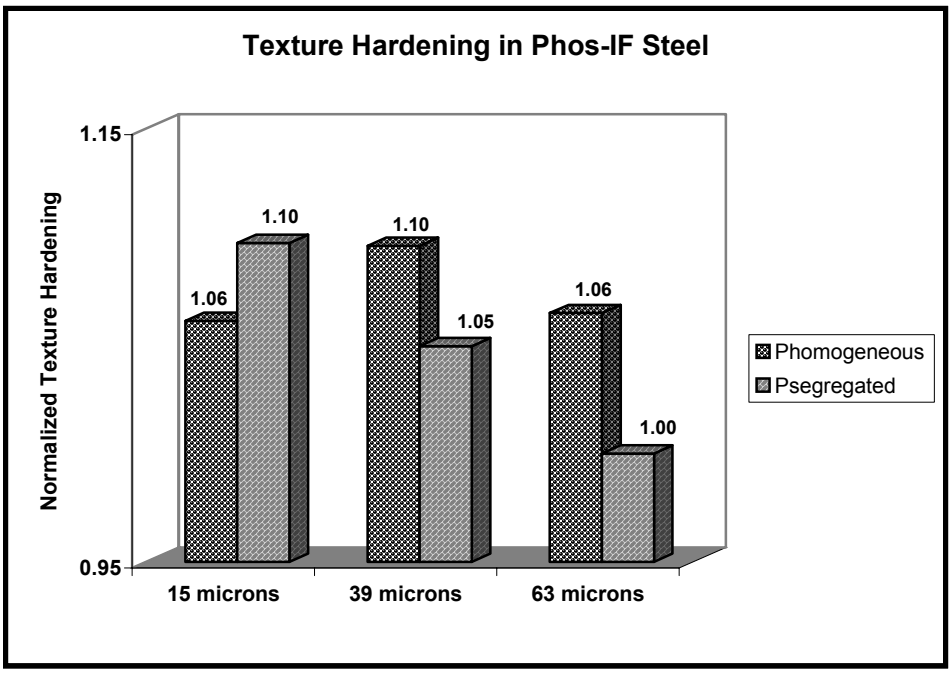

Figure 5.28 Texture Hardening Contribution in Phos-IF Steel

Table 5.12 Upper Bound Estimate of the Texture Hardening Contribution in Each Grain Size

Texture hardening contribution				
Base-IF	(MPa)		Phos-IF	MPa
20 μm (Homog)	46.1		15 μm (Homog)	44.9
20 μm (Seg)	45.7		15 μm (Seg)	46.6
53 μm (Homog)	44.8		39 μm (Homog)	46.6
53 μm (Seg)	44.0		39 μm (Seg)	44.5
103 μm (Homog)	42.0		63 μm (Homog)	44.9
103 μm (Seg)	40.4		63 μm (Seg)	42.4

The k_y values, with and without the texture hardening correction, are shown in Table 5.13. It is thus seen that texture hardening corrections are significantly larger in the Base-IF steel compared to the Phos-IF steel.

5.1.8 Role of FeTiP Precipitates in Affecting the Yield Strength of IF Steels

Thus far it has been shown that the segregation of solute or atomic P to ferrite grain boundaries results in a localized increment of the microhardness in the vicinity of the grain boundaries as well as an increase in the Hall-Petch slope, k_y. It was seen that in the Phos-IF steel segregated condition, a small volume fraction of FeTiPs is precipitated at the ferrite grain boundaries. From the tensile tests, macrohardness results and AES results, it is concluded that almost all the P at the grain boundaries is in the form of solute P in the Phos-IF steel segregated condition. In order to determine the effect of a large volume fraction of FeTiPs at the grain boundaries, it was necessary to use two additional IF steels. Both these IF steels had higher Ti contents and Nb was added to one of the steels. The chemical compositions of these IF steels are shown in Table 5.14.

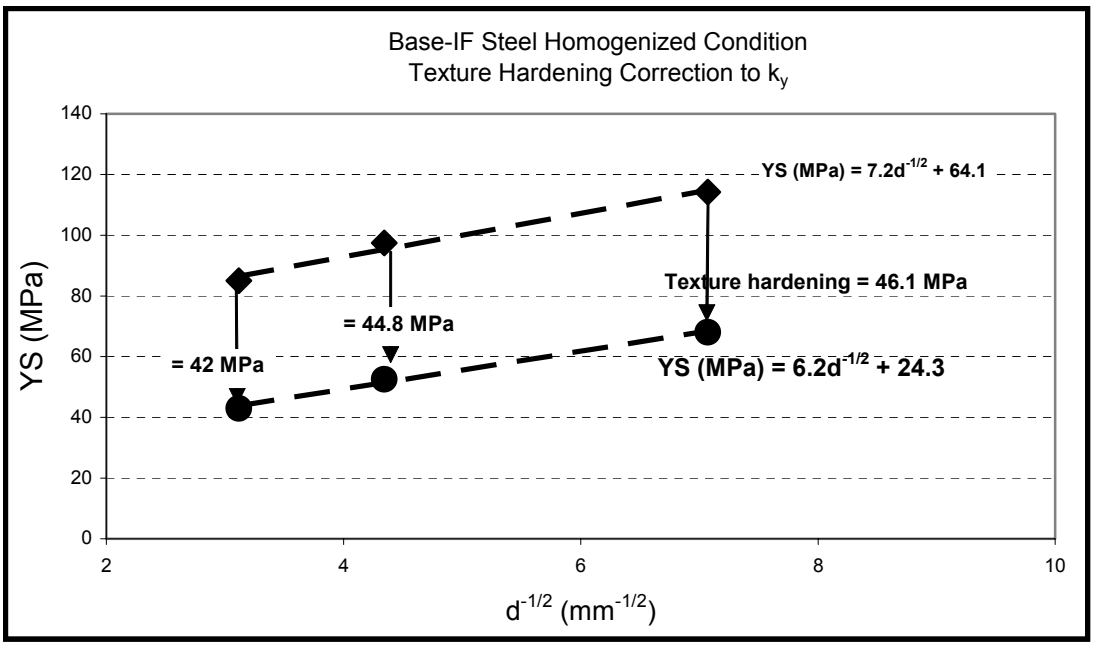

Figure 5.29 Texture Hardening Correction to k_y in Base-IF Homogenized Condition

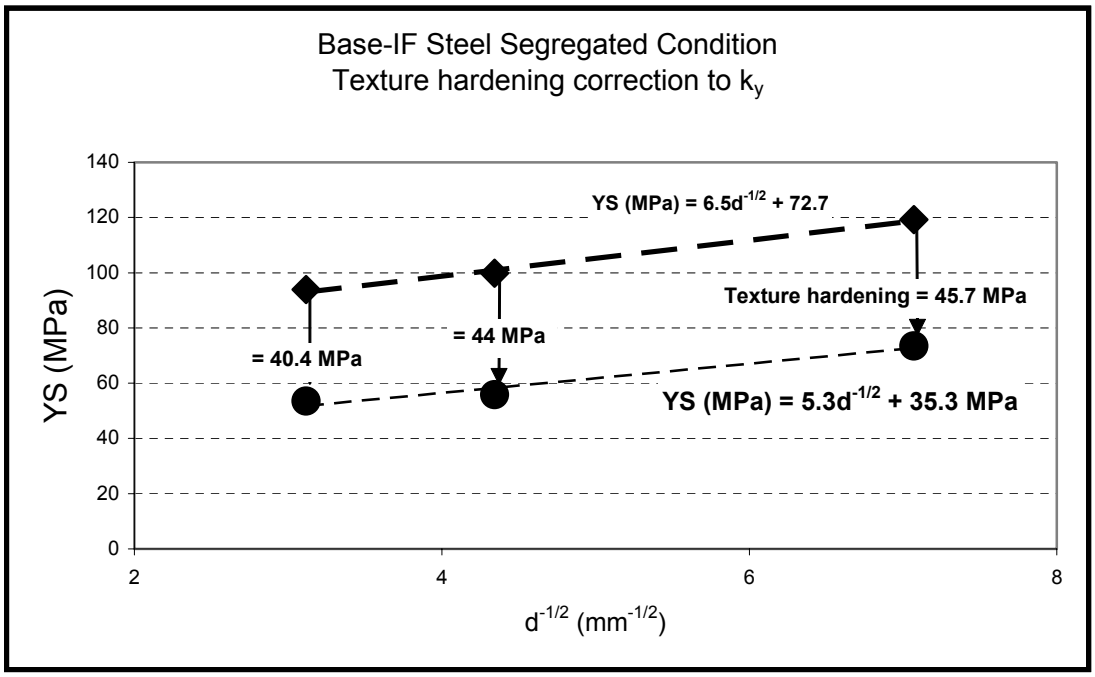

Figure 5.30 Texture Hardening Correction to k_y in Base-IF Segregated Condition

Table 5.13 Change in k_y After Texture Hardening Correction

Condition	k_y (MPa.mm $^{1/2}$) Without texture hardening correction	k_y (MPa.mm $^{1/2}$) With texture hardening correction	% change in k_y
Base-IF Homog	7.2	6.2	-14
Base-IF Segregated	6.5	5.3	-18.5
Phos-IF Homog	9.2	9.4	2.2
Phos-IF Segregated	14.4	13.4	-6.9

Table 5.14 Chemistry of Steels Used for Studying Effect of FeTiPs on Strength

Steel Designation	Ti (ppm)	Nb (ppm)	P (ppm)
BrTiP	600	0	600
BrTiNbP	600	300	600

It should be noted that the Ti levels in these steels are 600 ppm compared to the 390 ppm in the Base-IF and Phos-IF steels. The BrTiNbP steel additionally contains 300 ppm Nb. These steels were received in the hot rolled condition. The hot rolling process for both BrTiP and BrTiNbP steels consisted of coiling at 620^{o}C unlike the hot rolling schedule followed in the Base-IF and Phos-IF steels. These steels were subjected to the same homogenizing and segregation heat treatments after hot rolling, to develop the two locations of solute P as in the Base-IF and Phos-IF steels. The ferrite grain sizes were measured in both the steels after hot

rolling, homogenizing and segregation heat treatments. Macrohardness measurements were performed after the different heat treatments to determine the effect of P segregation on mechanical properties. Due to the higher Ti and Nb contents of these steels, it was expected that the volume fraction of the phosphide precipitates would be much higher as compared to the Base-IF and Phos-IF steels. SEM technique was used to determine the presence of phosphide precipitates on the boundaries and in the matrix. The results from the macrohardness tests are shown in Figure 5.31. It is seen from this figure that the presence of a significant volume fraction of FeTiP and FeTiNbP precipitates on the ferrite grain boundaries in both BrTiP and the BrTiNbP IF steels in the segregated condition, results in a significant decrease in the macrohardness. On the other hand, the presence of solute P at the ferrite grain boundaries in the segregated Phos-IF steel results in a considerable increment in the macrohardness.

Thus, the precipitation of phosphides on the grain boundaries results in a loss of strength in IF steels. The extent of phosphide precipitation in the BrTiP and BrTiNbP steels is shown in Figure 5.32 and 5.33.

5.2 Objective 2: Crystallographic Texture and Springback Behavior of IF Steels

The experimental approach employed in this objective has been explained in section 4.2.1.1. The results are presented below.

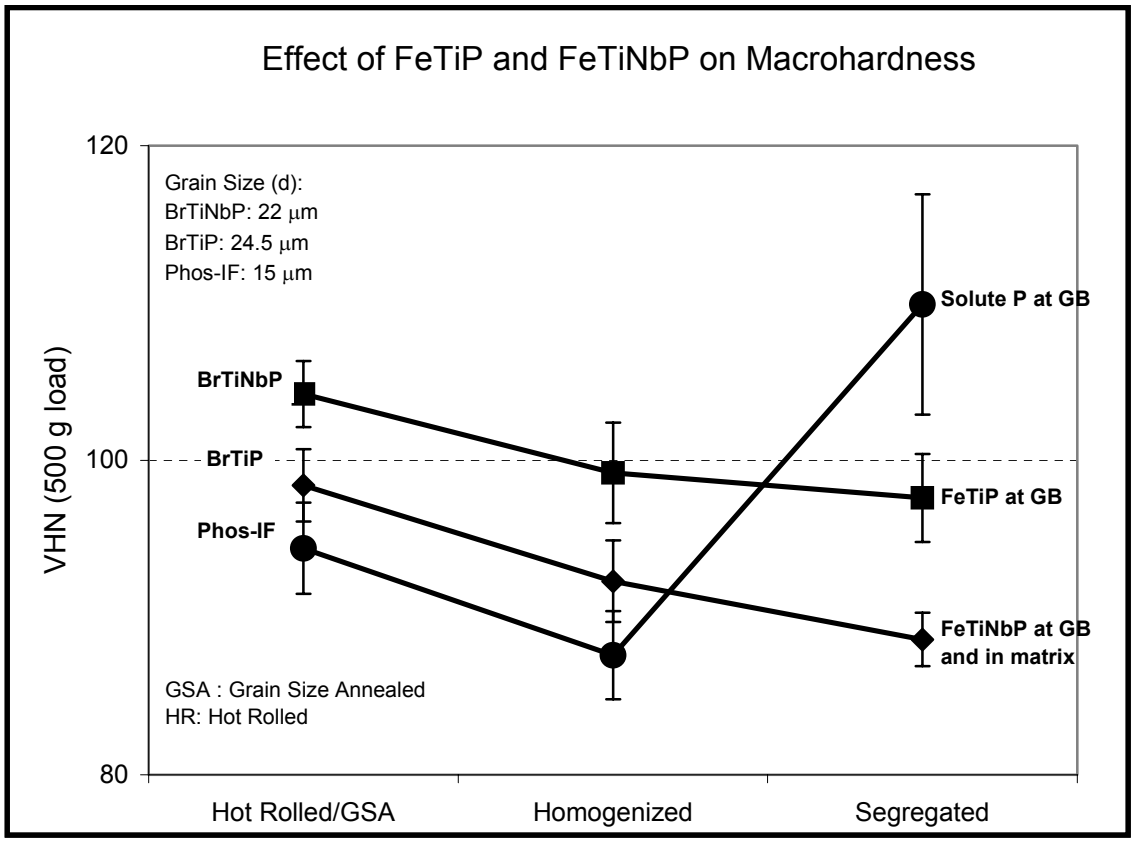

	300Ti-20P-0Nb	300Ti-600P-0Nb	600Ti-600P-0Nb	600Ti-600P-0Nb
Hot Rolled/GSA	N	N	N	N
Homogenized	N	N	**Y (GB)**	**Y (at GB, in Matrix)**
Segregated	N	**Y(Very few at GB)**	**Y (GB)**	**Y (at GB, in Matrix)**

Figure 5.31 Effect of FeTiP and FeTiNbP Precipitation on Macrohardness

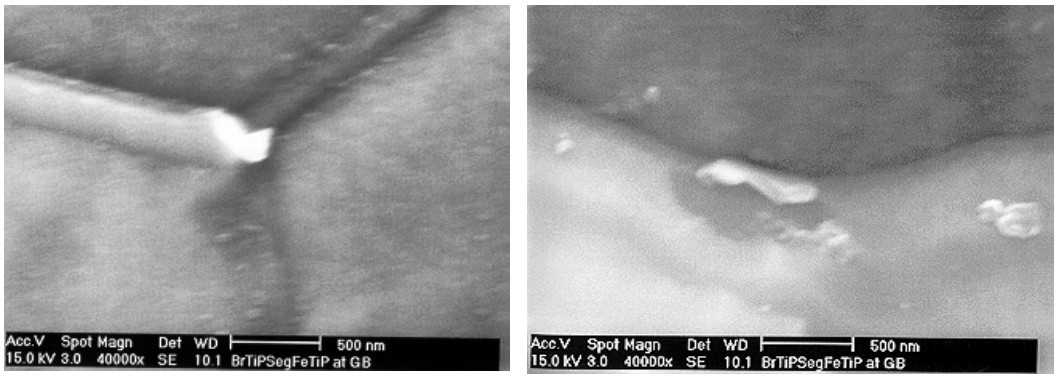

Figure 5.32 FeTiP Precipitates at Grain Boundaries in BrTiP Steel

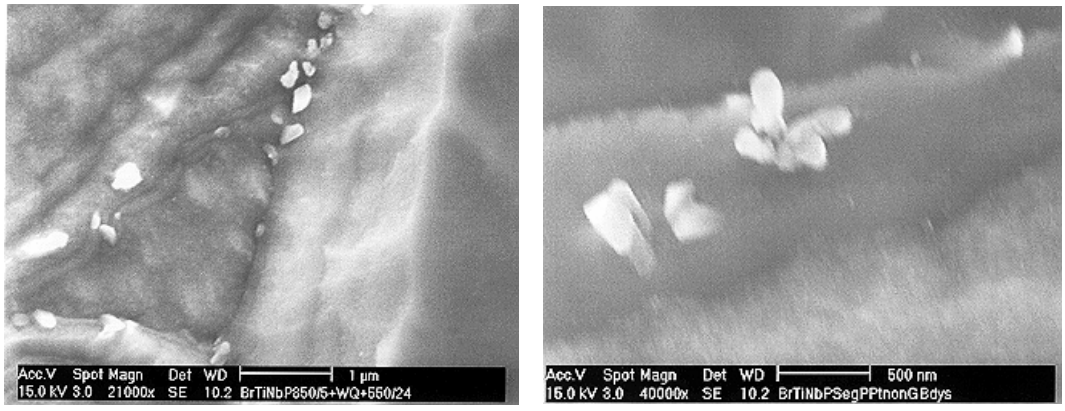

Figure 5.33 FeTiNbP Precipitates at Grain Boundaries in BrTiNbP Steel

5.2.1 Effect of Crystallographic Texture on the Elastic Anisotropy of IF Steel Sheets

The first step in this modeling was to determine the different crystallographic directions as a function of angle θ with the rolling direction for a particular crystallographic texture (hkl)[uvw]. Several textures from the $\phi_2 = 45^o$ section of the Euler space were chosen and the results are shown for certain representative textures in Table 5.15.

Table 5.15 Crystallographic Directions in the Plane of the Sheet for Certain Textures (hkl)[uvw] in IF Steel Sheets

Texture	Directions in plane of sheet				
(111)[110]	0 = 1,-1,0	(110)[110]	0 = 1,-1,0	(110)[001]	0 = 0,0,1
Gamma fiber	12 = 7,-9,2	Alpha Fiber	8 = 5,-5,1	Epsilon Fiber	10 = -1,1,7
	20 = 2,-3,1		20 = 2,-2,1		25 = -1,1,3
	30 = 1,-2,1		35 = 1,-1,1		35 = -1,1,2
	45 = 1,-4,3		45 = 2,-2,3		45 = -2,2,3
	60 = 0,-1,1		55 = 1,-1,2		55 = -1,1,1
	75 = -1,-3,4		65 = 1,-1,3		70 = -2,2,1
	83 = -2,-3,5		75 = 1,-1,5		80 = -4,4,1
	90 = -1,-1,2		82 = 1,-1,9		90 = -1,1,0
			90 = 0,0,1		

The next step is to determine the elastic modulus, E and Poisson's ratio, ν, and, hence, the plane-strain elastic modulus, E', in each of these directions for all the crystallographic textures. Based upon these calculations, the polar plots of E' vs. θ for different textures can be plotted and the results are in Figure 5.34 and Figure 5.35 for certain textures belonging to the alpha, gamma and epsilon fibers. It can be seen from Figure 5.34 that, for the γ-fiber texture components, the profiles of E' vs. θ are almost circular. This means that the value of E' is nearly constant in the plane of the sheet implying that the γ-fiber components are elastically isotropic. On the other hand, all the α-fiber and ε-fiber components are characterized by large elastic anisotropy since

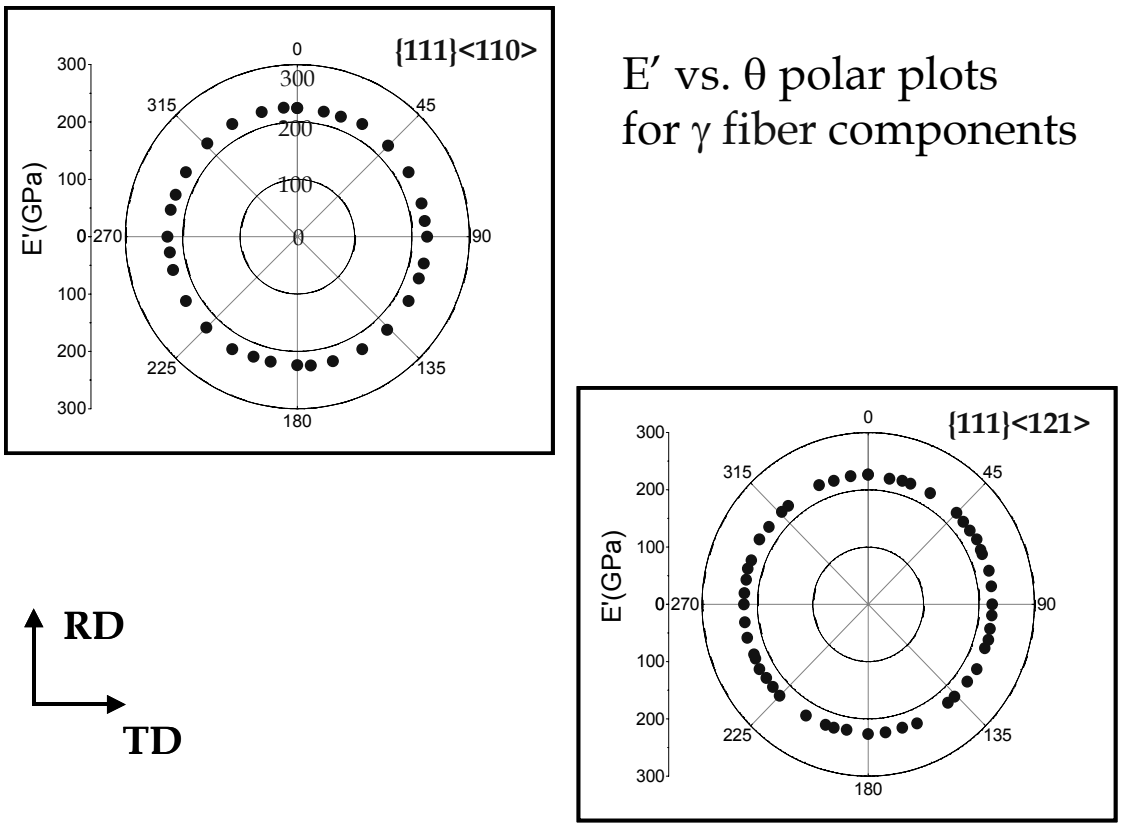

Figure 5.34 Polar Plots of Plane Strain Elastic Modulus, E', vs. Theta for Gamma Fiber Components

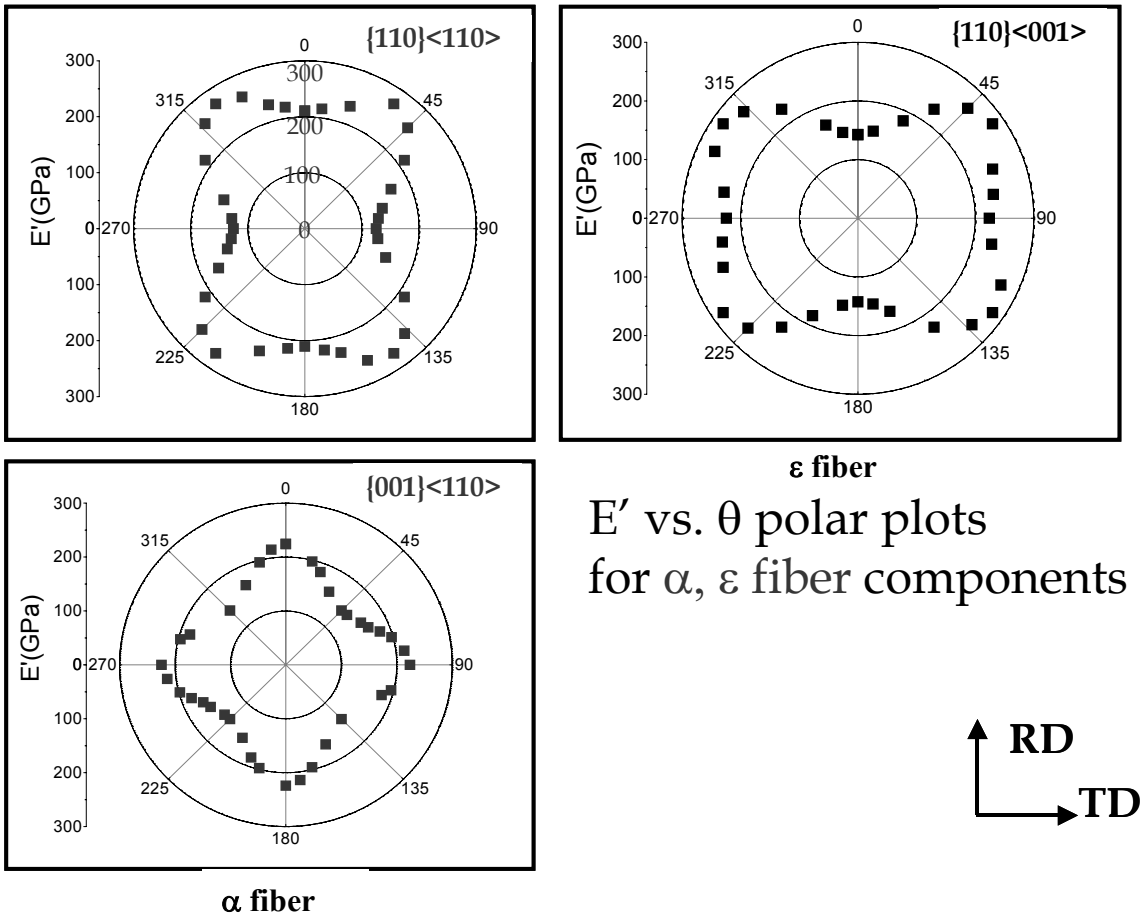

Figure 5.35 Polar Plots of Plane Strain Elastic Modulus, E', vs. Theta for Alpha and Epsilon Fiber Components

the profiles of E' vs. θ are non-circular and considerably distorted, indicating that the value of E' changes substantially in the plane of the sheet for these texture components. Based upon these polar plots, the amount of springback in each direction was calculated for a nominal sheet thickness of 0.025 inches, initial bend angle (α_o) of 45^o, initial radius of curvature (r_o) of 1.5 inches and two nominal yield strength levels of 150 MPa and 250 MPa in the RD. The resulting polar plots of S vs. θ are shown in Figures 5.36 and 5.37. It is seen from Figure 5.36 that the profiles of S vs. θ for gamma fiber components are circular, indicating that the in- plane variability of springback, S, is minimal for the gamma fiber components. This is a direct result of the excellent elastic isotropy shown by the gamma fiber components. It is also seen that as the nominal level of yield strength increases from 150 MPa to 250 MPa, the amount of springback increases.

It is seen from Figure 5.37 that the high elastic anisotropy associated with the alpha and epsilon fiber components results in a high degree of in-plane variability of springback for these texture components. The data from the polar plots can be used to calculate the values of the normal and planar anisotropy of E' and S for each texture using equations 4-4 through 4-7. These values are tabulated in Table 5.16 and can be used to compare the in-plane springback variability exhibited by the different crystallographic textures. It can be seen from the table that the gamma fiber components show minimum variability in springback, followed by epsilon fiber components and then by alpha fiber components.

The data of Table 5.16 point out the following interesting features of springback behavior:

a) To minimize S_{bar} in IF steel sheets, crystallographic textures with high values of E'_{bar} should be developed, since S_{bar} is inversely proportional to the value of E'_{bar}.

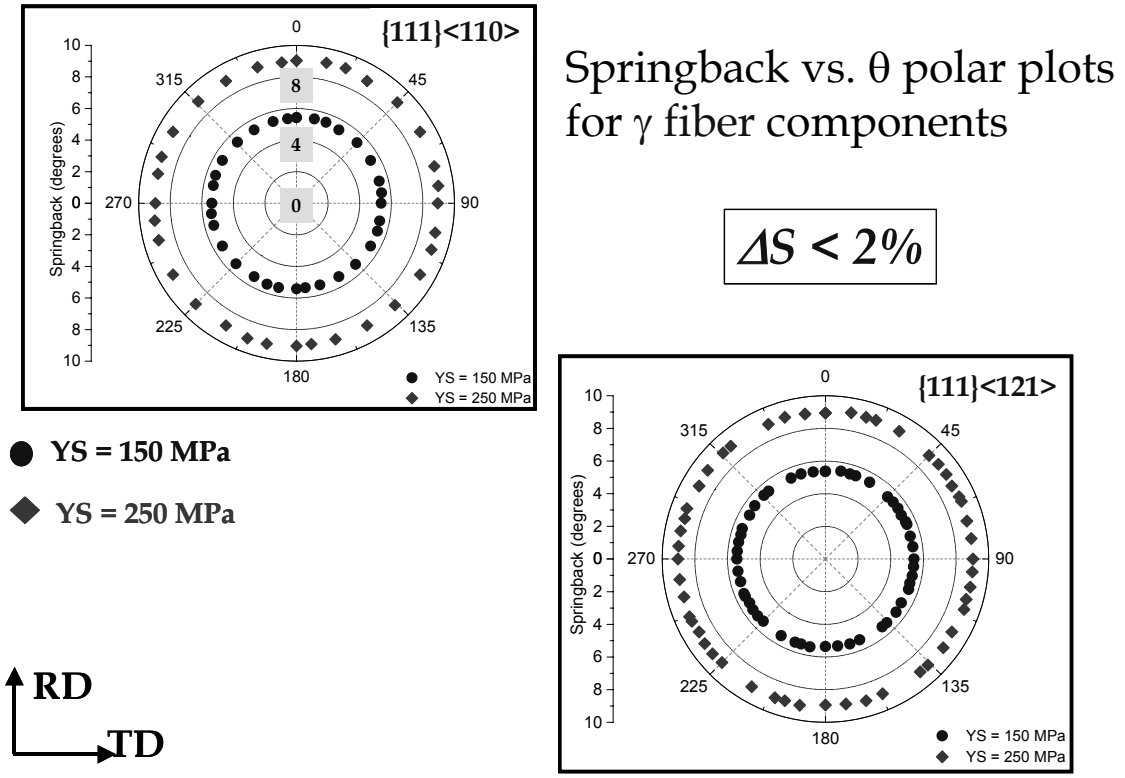

Figure 5.36 Polar Plots of Springback, S, vs. Theta for Gamma Fiber Components

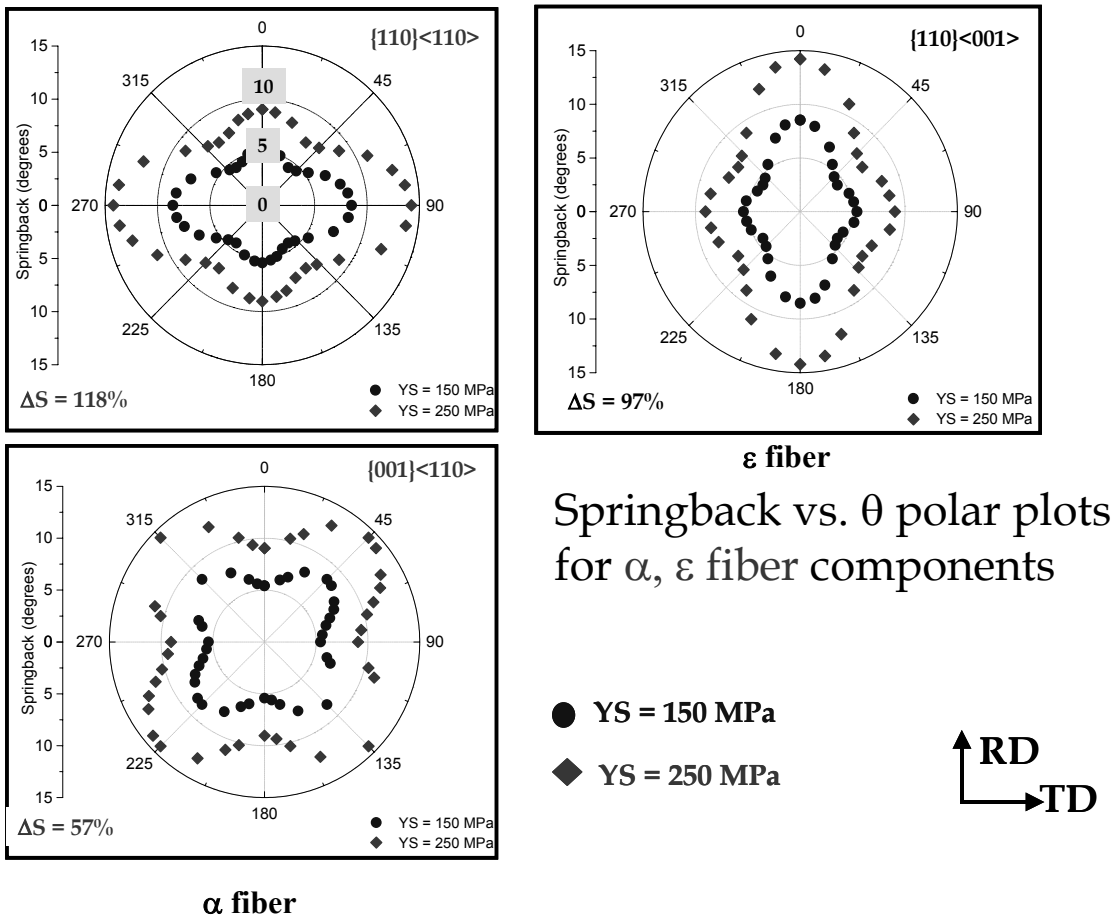

Figure 5.37 Polar Plots of Springback, S, vs. Theta for Alpha and Epsilon Fiber Components

b) The amount of springback, S_{bar}, tends to be lower for γ-fiber components than for the α and ε-fiber components.

c) Crystallographic textures that show higher values of elastic anisotropy, (ΔE'), also show higher values of springback variability, (ΔS).

d) The variability in springback is small for all the γ-fiber components (1.7 - 1.8 %) but is considerably large for the α and ε-fiber components, (20 - 118%).

Table 5.16 Effect of Texture on the In-plane Variability of Springback in IF Steel Sheets

Texture Component	Parent Fiber	E'_{bar} GPa	ΔE' GPa	S_{bar} degrees	ΔS degrees	Variability in Springback $(S_{max} - S_{min}) / S_{min}$ (%)
{111}<110>	Gamma	224.8	1.1	5.41	-0.03	1.7
{111}<112>	Gamma	225.6	-0.5	5.39	0.01	1.8
{111}<231>	Gamma	223.8	-0.9	5.42	0.02	1.8
{554}<225>	Epsilon	224.4	-23.8	5.44	0.61	20
{332}<113>	Epsilon	238.3	-69.4	5.23	1.59	49
{110}<001>	Epsilon	224.1	-81.5	5.78	2.39	97
{113}<110>	Alpha	200.9	77.9	6.29	-2.42	56
{001}<110>	Alpha	183.3	81.7	6.97	-3.11	57
{337}<110>	Alpha	210.8	75.9	5.98	-2.10	58
{110}<110>	Alpha	224.1	-81.5	5.78	2.39	118

In the above analysis and results, it was assumed that the IF steel sheet is comprised of a single ideal texture (hkl)[uvw]. Industrially processed IF steel sheets are characterized by a mixture of different crystallographic textures. It is known that the gamma fiber components,

namely, the {111}<uvw> texture components, impart excellent deep drawability to IF steel sheets, whereas, the alpha fiber components, especially the {001}<110>, impart poor deep drawability. Based upon the above polar plots and using a simple law of mixtures, it is possible to calculate the in-plane springback for different mixtures of the gamma fiber component, {111}<110>, and the alpha fiber component, {001}<110>. The results are shown in Figure 5.38. It can be seen from this figure that the variability in springback, measured as an angular change, is the least for the gamma fiber component, {111}<110>. As the volume fraction of the {001}<110> alpha fiber component is increased, the in-plane variability of springback also increases. Thus the data from the polar plots can be used to calculate the springback for different mixtures of texture components observed in industrially processed IF steel sheets.

5.2.2 Modeling of Springback Behavior in Draw-bend Test Applications using FEM

In addition to modeling the effects of crystallographic texture in plane-strain bending applications, FEM was performed to simulate the springback in a draw-bend test. The details of the draw-bend test are shown in Figures 2.28 and 2.29. The FEM was performed by Dr. Dipo Onipede and Carlos Gomes at the Mechanical Engineering department of the University of Pittsburgh, using the LS-DYNA application software. The objective was to determine the effects of elastic and plastic anisotropy in affecting the springback parameters in a draw-bend test namely, the angles θ_1, θ_2 and the radius of curvature, ρ. From the variation of these springback parameters, a welding gap was calculated in terms of the displacement of the end point of the strip as shown in Figure 4.7. The results have been tabulated in Tables 5.17 and 5.18. Table 5.17 shows the dependence of the springback parameters and the corresponding welding gap on the

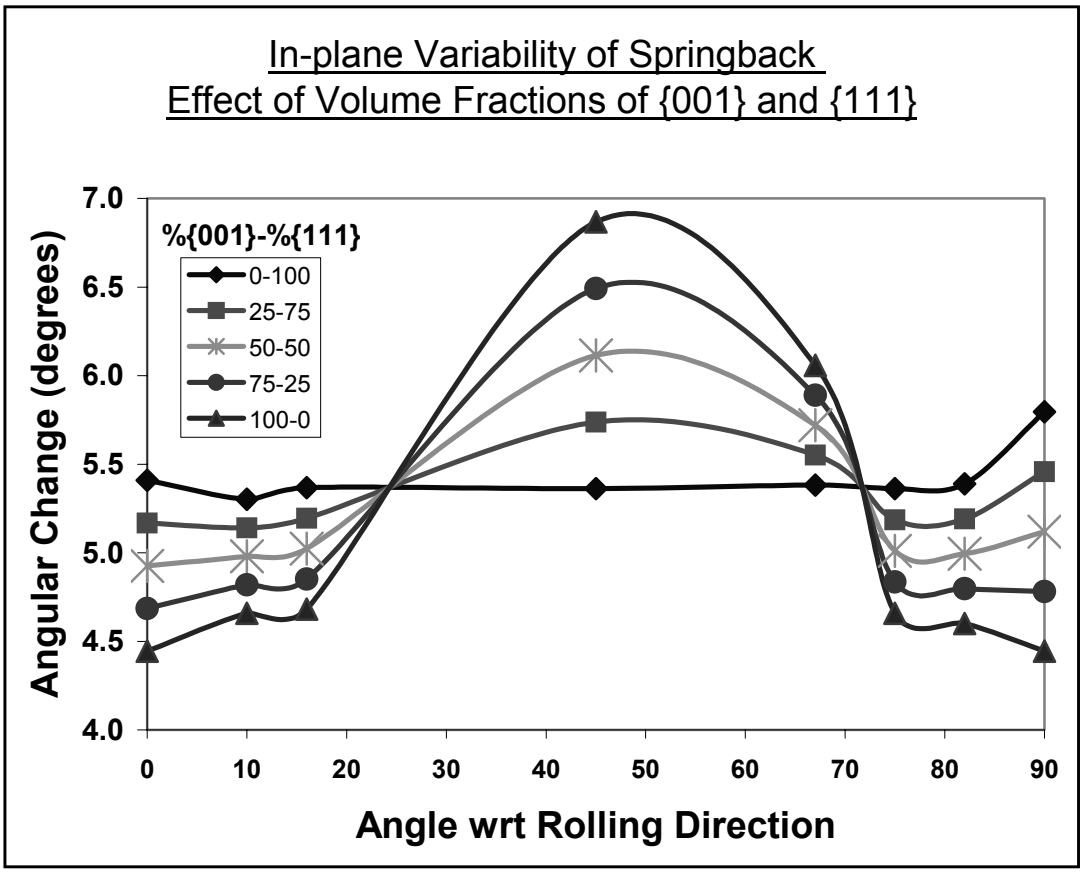

Figure 5.38 Effect of Volume Fractions of Alpha and Gamma Fiber Components on Springback

yield strength of the strip, the testing of which is simulated in the draw-bend test using FEM. Table 5.18 shows the dependence of the welding gap on the elastic properties of the strip. The resulting profiles of the strips after simulation of the draw-bend test have been shown in Figures 5.39 and 5.40. The dependence of the welding gaps ΔX and ΔY on the yield strength and elastic properties are shown in Figures 5.41 and 5.42. It can be readily seen from the Figure 5.41 that, for a given yield strength, the displacements, ΔX and ΔY of the end point of the strip decrease considerably as the plane strain elastic modulus, E', increases. A 100% increase in E' reduces ΔX by 75% and reduces ΔY by 118%. Similarly from Figure 5.42, it is seen that for a given values of E', as the yield strength increases from 150 to 350 MPa, the welding gap, ΔX, increases by 133% and ΔY increases by 165%.

Thus, the prediction of springback parameters using FEM also yields similar results in draw-bend applications as in plane-strain bending applications. Springback is minimized in sheet steels having high elastic moduli and low yield strengths.

Table 5.17 Effect of Yield Strength on Springback Parameters in the Draw-bend Test

							Welding Gap	
YS (MPa)	**E(GPa)**	**ν**	θ_1	θ_2	θ_2-θ_1	ρ (mm)	ΔX mm	ΔY mm
150	207	0.3	94.4	85.0	9.4	417.3	4.6	9.2
200	207	0.3	96.1	83.4	12.7	311.7	6.1	12.5
250	207	0.3	98.6	81.8	16.8	242.3	8.1	16.7
300	207	0.3	100.5	80.2	20.5	202.7	9.3	20.5
350	207	0.3	102.8	78.6	24.3	171.8	10.7	24.4

Table 5.18 Effect of Elastic Properties on Springback Parameters in the Draw-bend Test

							Welding Gap	
E'(GPa)	**E(GPa)**	**ν**	θ_1	θ_2	θ_2-θ_1	ρ (mm)	ΔX mm	ΔY mm
142	**125**	**0.35**	105.7	76.5	29.1	147.0	11.9	29.4
181	**165**	**0.3**	101.8	79.1	22.7	189.1	10.1	22.7
227	**207**	**0.3**	99.2	81.4	17.8	240.3	8.5	17.7
238	**225**	**0.23**	98.6	81.9	16.7	252.9	8.1	16.6
258	**248**	**0.2**	97.8	82.4	15.4	277.7	7.5	15.3
280	**272**	**0.17**	96.9	83.1	13.7	307.4	6.8	13.5

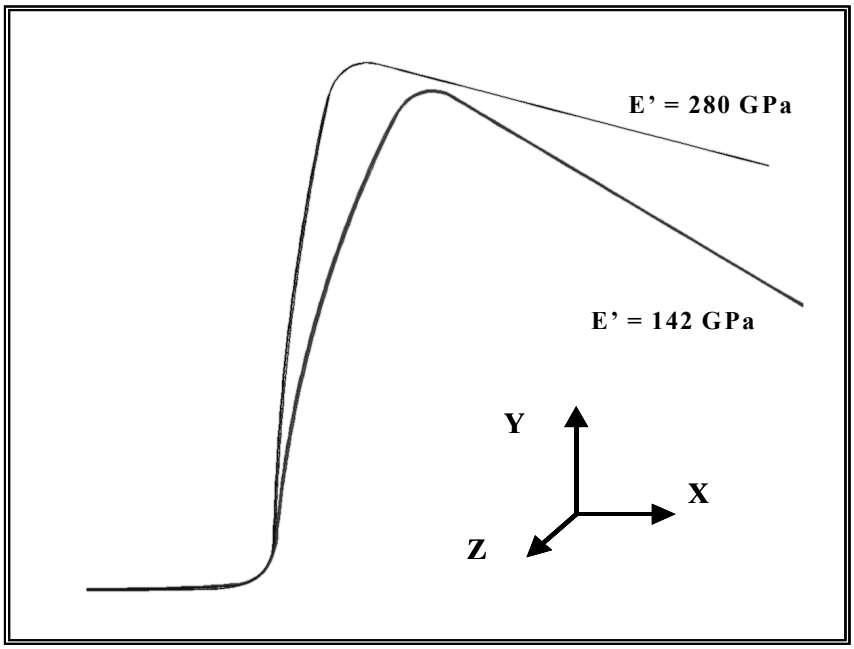

Figure 5.39 Effect of Plane Strain Elastic Modulus on the Profiles of Strip in a Draw-bend Test

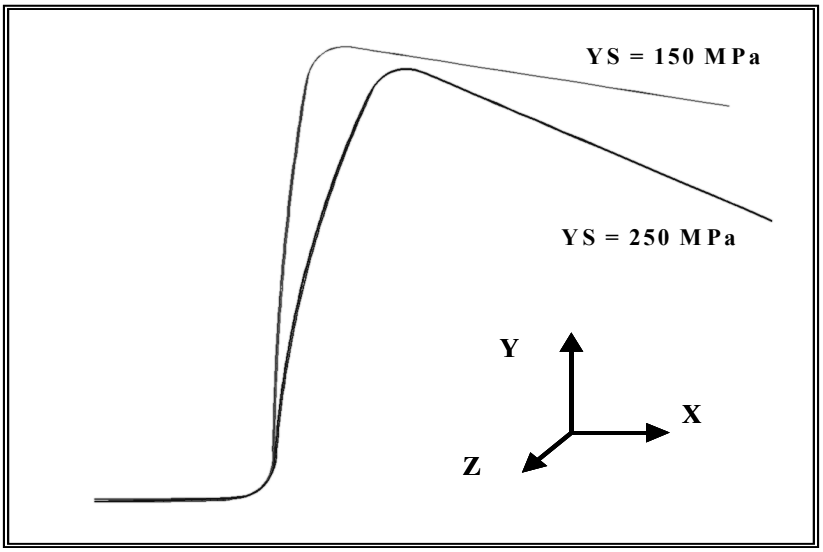

Figure 5.40 Effect of Yield Strength on the Profiles of Strip in a Draw-bend Test

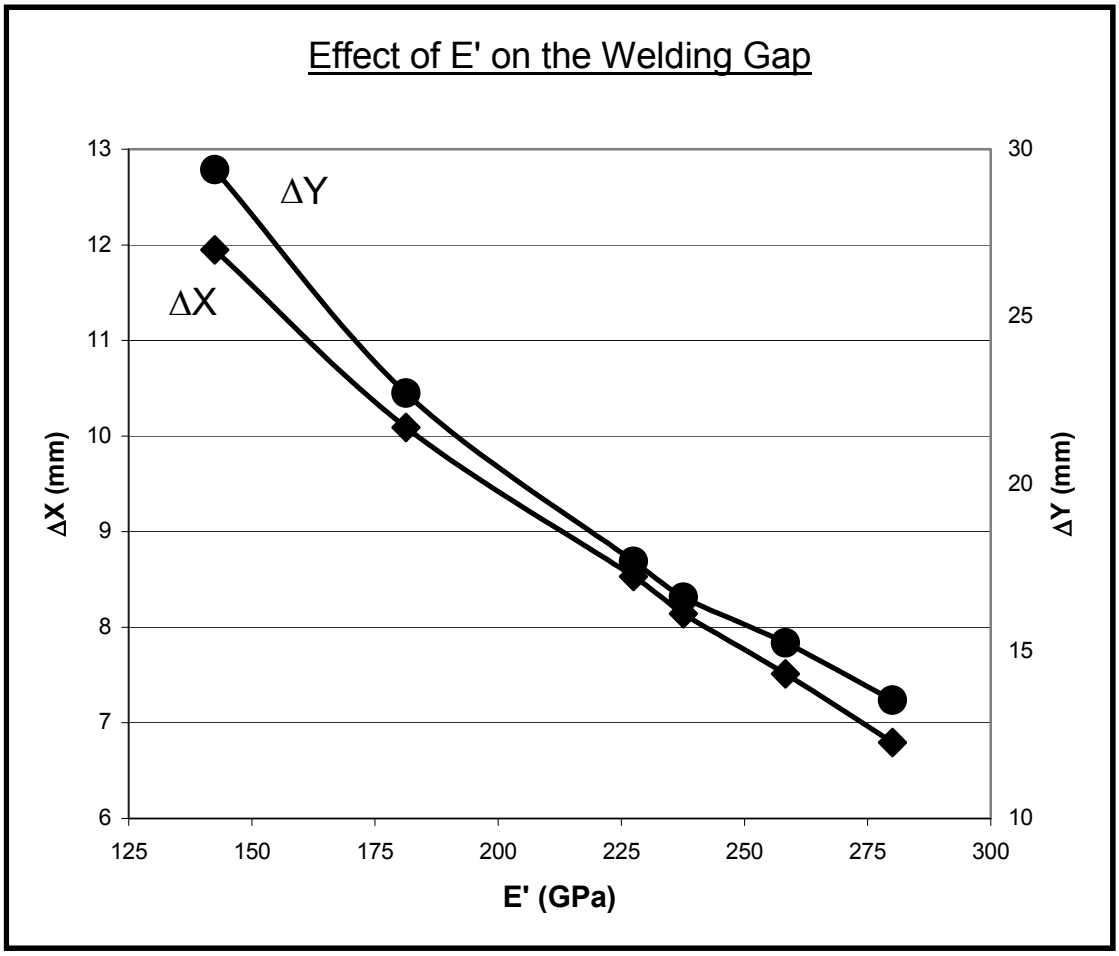

Figure 5.41 Effect of Plane Strain Elastic Modulus on the Welding Gap

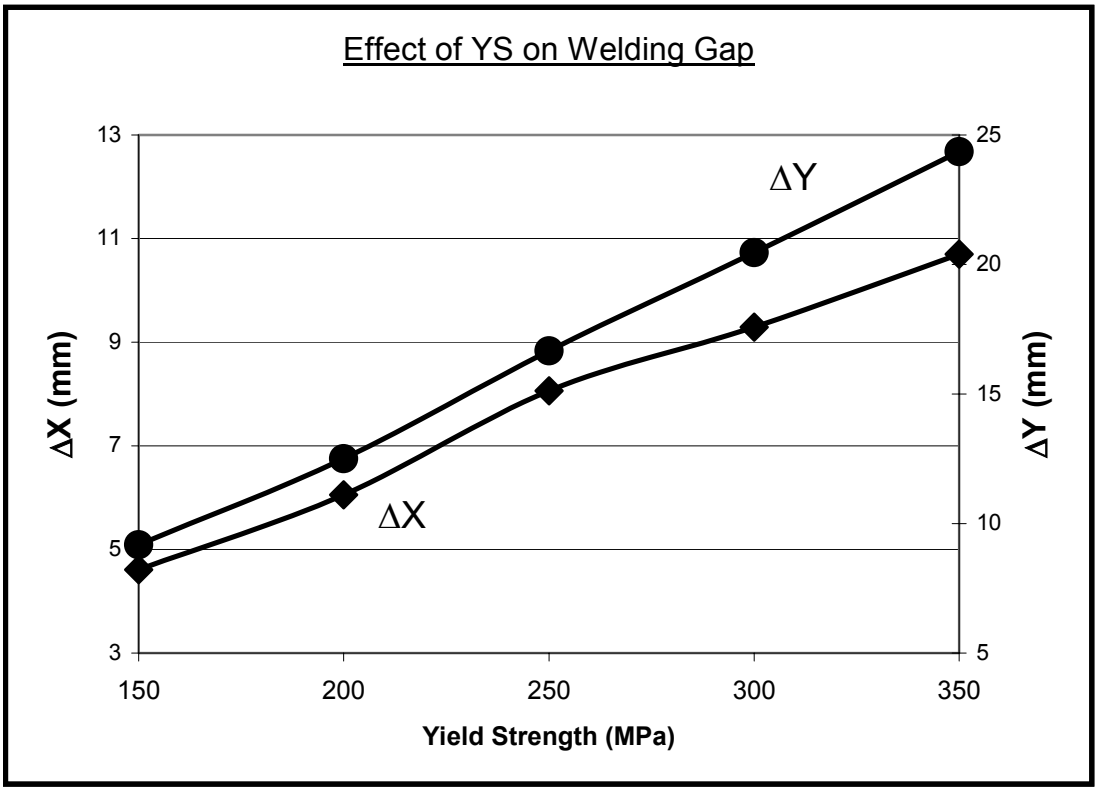

Figure 5.42 Effect of Yield Strength on the Welding Gap

6.0 DISCUSSION

The complex role of phosphorus in affecting the yield strength of IF steels has been thoroughly investigated in Objective 1 of this research. As mentioned earlier, the complexity of the role of P in affecting the strength arises from the variability in the location of P and the relative distribution of P between these locations. These different locations of P are shown in Figure 2.19. In this research, the strengthening due to the presence of solute P in the ferrite matrix, at the ferrite grain boundaries and as phosphide precipitates either at grain boundaries, or in the matrix, has been carefully studied. The hypothesis in this objective was that the segregation of solute P to ferrite grain boundaries brings about a localized increment in the grain boundary microhardness and results in an increase in the Hall-Petch slope, k_y, in IF steels.

Based upon all the results presented in the previous section, the following is a discussion of the various effects that P additions can bring about in IF steels.

6.1 Phosphorus and Solid Solution Strengthening

Based upon the microhardness measurements shown in Figure 5.10, it can be seen that the grain center microhardness of the Phos-IF steel is always higher than that of the Base-IF steel in the largest grain size developed in the two steels. This observation indicates that P brings about solid solution strengthening. From the tensile test results, it is possible to estimate the solid solution strengthening due to solute P. In order to estimate this contribution, it is necessary to compare the tensile properties of the steels at the same grain sizes. Based upon the k_y values shown in Figure 5.17, the yield strength values for the Base-IF 15 μm, 39 μm and 63 μm are shown in Table 6.1.

Table 6.1 Yield Strength Values of Base-IF and Phos-IF at Same Grain Sizes (Calculated From k_y Values in Figure 5.17 and 5.18)

Steel condition	As-annealed YS (MPa)	Homogenized YS (MPa)	Segregated YS (MPa)
Base-IF **(15 μm)**	124.2	122.9	125.8
Base-IF **(39 μm)**	105.3	100.6	105.6
Base-IF **(63 μm)**	**98.7**	92.8	98.6
Phos-IF **(15 μm)**	159	137.7	185.3
Phos-IF **(39 μm)**	131.1	114.4	141.3
Phos-IF **(63 μm)**	**113**	97	125

The solid solution strengthening due to solute P can be calculated from the differences in the yield strength between the Base-IF (63 μm) as-annealed and the Phos-IF (63 μm) as-annealed conditions. This difference is 113-98.7 = 14.3 MPa for a 600 ppm difference in bulk P content. Thus the k_{sss}^{P} value is = 2.38 MPa/0.01 wt% P. It should be noted that this calculation can be done only for the 63 μm grain size since the annealing temperature used is the highest, namely, 850^{o}C/30 mins. This high annealing temperature ensures that in the Phos-IF steel, the maximum amount of solute P is displaced away from the grain boundaries, thus retaining almost all the phosphorus in the ferrite matrix. Additionally, the values after the homogenizing treatment cannot be used for this calculation because of the water quenching employed after the homogenizing heat treatment, which might have precluded the ability of solute P to bring about its potential solid solution strengthening effect. From Figure 5.12, it is seen that the presence of

600 ppm bulk P in Phos-IF steel results in an increment of ~ 10 kg/mm^2 in the grain center microhardness as compared to the Base-IF steel. Thus, in terms of the grain center microhardness, solute P brings about 1.67 kg/mm^2/0.01 wt% P increase in the matrix microhardness. This result is additional evidence of solute P bringing about solid solution hardening in IF steels.

6.2 Phosphorus and Grain Boundary Hardening

It is seen that 600 ppm P brings about 14.3 MPa of solid solution strengthening. Based upon the yield strength values obtained in the segregated condition, it is also possible to estimate the grain boundary hardening brought about by P segregation to the grain boundaries.

It is seen that for a particular grain size in the segregated condition, the total difference in the yield strength between the Phos-IF steel (Homogenized) and Phos-IF steel (Segregated) condition is given as:

$$\Delta YS_{Phos,GBH} = YS_{P,Segregated} - YS_{P,Homogenized} \quad (6\text{-}1)$$

Thus for the 63 μm grain size,

$\Delta YS_{Phos,GBH}$ = 125-97 = 28 MPa

Similarly, $\Delta YS_{Phos,GBH}$ for 39 μm grain size = 27 MPa

and $\Delta YS_{Phos,GBH}$ for 15 μm grain size = 47.6 MPa

The relative split in the SSS vs. GBH contribution due to P is shown in Figure 6.1. It can be readily seen from Figure 6.1 that the GBH contribution can be ~ 3.5 times higher than the solid solution strengthening contribution especially in the finer grain sizes.

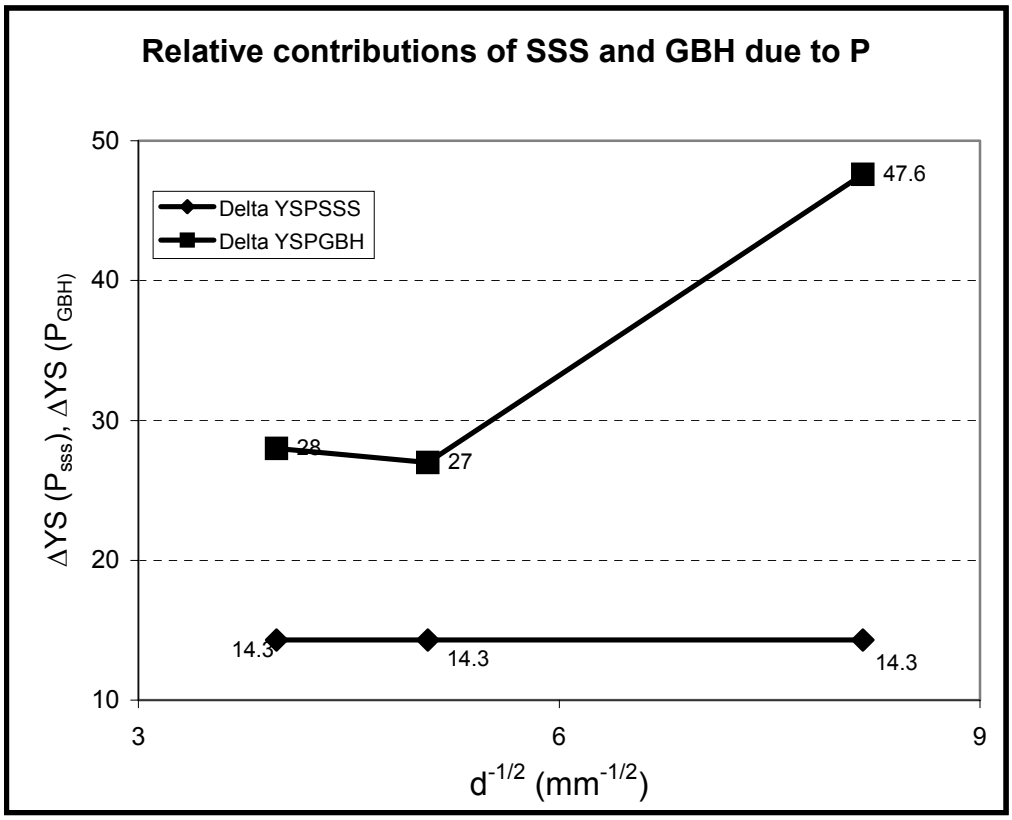

Figure 6.1 Relative Split in the Solid Solution Strengthening and Grain Boundary Hardening

The effectiveness of atomic P at the grain boundaries in bringing about grain boundary hardening is shown below. In the 15 μm Phos-IF segregated condition steel, the grain boundary hardening increment is 47.6 MPa. From the AES results presented in section 5.1.4.1.2, the average value of the P segregation to ferrite grain boundaries at a segregation temperature of 550^{o}C is 10.3 at %. Thus, in the 15 μm grain size, the segregation of P to ferrite grain boundaries would bring about 47.6 MPa/10.3 at% = **4.62 MPa/ at % P segregated**. Assuming that the grain boundary segregation of P is the same in all the three grain sizes in the segregated condition, the grain boundary hardening contribution in the 39 μm grain size comes out to be 27 MPa/10.3 at% = **2.62 MPa/ at % P segregated.** Similarly, this contribution in the 63 μm grain size comes out to be 28 MPa/10.3 at% = **2.72 MPa/ at % P segregated**. It is thus seen that the efficiency of solute P to bring about grain boundary hardening strongly depends upon the grain size of the IF steels. The above grain boundary hardening values, hence, need to be normalized by $d^{-1/2}$ values in the three grain sizes. These normalized values for grain boundary hardening due to solute P at the grain boundaries are shown in Table 6.2. It can be seen from Table 6.2 that the average value of grain boundary hardening due to solute P is ~ **18.6 MPa.μm$^{1/2}$/ at% P segregated**.

In summary, it is seen that the total increment in yield strength due to the addition of P to IF steels has two components:

a) Grain size independent solid solution strengthening, determined to be 2.38 MPa/ 0.01 wt% P.

b) Grain size dependent grain boundary hardening, determined to be 18.6 MPa.μm$^{1/2}$/ at% P segregated. It should be noted that the grain boundary hardening increment is also strongly dependent upon the grain boundary character and the amount of P segregated to the ferrite grain boundaries.

Table 6.2 Grain Boundary Hardening Contribution Due to P Segregation

Grain Size (μm)	$d^{-1/2}$ ($\mu m^{-1/2}$)	Total grain boundary hardening contribution (MPa)	Normalized grain boundary hardening contribution (MPa/at%P/$d^{-1/2}$) (MPa.$\mu m^{1/2}$/ at%P)
15	0.25	47.6	18.5
39	0.16	27	16.4
63	0.13	28	20.9

The difference in the k_y values between the Base-IF and Phos-IF steel is evident in Figure 5.19. It is seen that the k_y values in the Phos-IF steel are significantly higher than in the Base-IF steel in all conditions of P location, the difference being the highest in the segregated condition (Δk_y = 121%). It should be noted that in the homogenized condition, where there is negligible solute P at the grain boundaries in Phos-IF steel, the difference in the k_y values is the least, 22%.

The difference in the k_y values of the Phos-IF steel in the homogenized and segregated condition is also considerably large (57%). This means that for the same bulk P content of 600 ppm, the grain size strengthening contribution to the yield strength can vary by 57% for a given grain size. This has important implications in the IF steel sheet processing. It is seen that by controlling the degree of P segregation to the grain boundaries, the yield strength variability can be controlled.

It is also seen that in the Phos-IF steel, the lowest value of k_y observed is 9.2 MPa.mm $^{1/2}$, in the homogenized condition. This maybe due to the lack of solute P at the grain boundaries and also due to the subsequent water quenching. This result is similar that obtained by Cottrell[69] and also by Hook[183]. Hook observed a drop in yield strength in low carbon steel sheets after water

quenching due to the generation of mobile dislocations in the water quench. The generation of mobile dislocations also eliminated the YPE in ultra-low carbon steel sheets.

In addition to bringing about the increase in the yield strength, the segregation of P to grain boundaries also brings about a localized increase in the grain boundary microhardness as shown in Figure 5.13. It is seen that only in the Phos-IF steel in the segregated condition, the grain boundary microhardness is higher than the grain center microhardness. It should be noted that this increase is statistically different as validated by the f-test and is due to the segregation of solute P to ferrite grain boundaries. This increase is absent in the Base-IF steel and also in the Phos-IF steel in the homogenized condition. It should be pointed out that the microhardness measurements were performed using a load of 10 gm in the Vicker's hardness test. This was the minimum load that could be used in this equipment. If a lower load could have been used, the increment seen in the grain boundary microhardness would have been higher due to the reduced "dilution" from the matrix microhardness.

6.3 FeTiP Precipitation and Strengthening of IF Steels

The role of FeTiP and FeTiNbP precipitation in affecting the strength of IF steels has been shown in Figure 5.31. It is seen that when solute P at the grain boundaries is scavenged by the precipitation of FeTiP and FeTiNbP at the grain boundaries, a loss in grain boundary hardening occurs and this reflects in a drop in the bulk macrohardness and would also result in a corresponding loss in the yield strength. It is worthwhile to note the following features regarding this precipitation:

a) The extent of the phosphide precipitation depends strongly on the amounts of Ti and Nb in the steel. For the same segregation heat treatment of 550^{o}C/24 hrs, the Phos-IF steel

with bulk Ti and P contents of 390 ppm and 600 ppm did not show abundant FeTiP precipitation at the grain boundaries. The BrTiP steel had higher Ti levels of 600 ppm and the BrTiNbP had 300 ppm Nb in addition to 600 ppm Ti. The higher alloying content in both these steels resulted in abundant FeTiP and FeTiNbP precipitates at the grain boundaries for the same segregation heat treatment, thereby resulting in a drop in the bulk macrohardness values after the segregation heat treatment.

b) Nb seems to aid the precipitation of the phosphide precipitates. This observation can have significant implications in alloy design of P-bearing IF steels.

c) It is not necessary to have phosphide precipitation in the ferrite matrix to observe a drop in the yield strength. Presence of sufficient volume fractions of phosphide precipitates at the grain boundaries can result in substantial losses in the grain boundary hardening potency of solute P.

6.3.1 Calculation of Scavenging of Solute P by FeTiP Precipitation

It is possible to estimate the number of FeTiP precipitates of a certain size that are needed to scavenge all the solute P from the grain boundary facets for different grain sizes in the Phos-IF steel. This estimation is shown below:

Assumptions:

a) Morphology of the FeTiP ppts is ellipsoidal.

b) Maximum dimensions of the ellipsoid, as seen in SEM observations are

   a = b = 600 nm, c= 150 nm.

c) Grain shape is tetrakaidecahedron.

d) 1 monolayer P segregation in all grain sizes after segregation heat treatment.

e) All the P atoms that precipitate to form FeTiP are obtained solely from the grain boundary facet and not from the matrix.

Based upon these assumptions, the number of FeTiP precipitates of the above dimensions needed to scavenge one hexagonal face of the tetrakaidecahedron grain can be estimated. This estimation is shown in Table 6.3.

Table 6.3 Scavenging of Solute P at Grain Boundaries by FeTiP Precipitation

Grain Size (μm) Linear Intercept	Surface Area of one hexagonal face of the tetrakaidecahedron (μm^2)	Grain boundary Area scavenged by largest FeTiP ppt.(μm^2)	No. of ppts needed to scavenge one full face
15	130	48	3
39	878	48	18
63	2292	48	48

Thus, it is seen from the above table that the number of FeTiP precipitates needed to scavenge solute P from the grain boundaries is smaller for finer grain sizes. It should also be noted that in Figure 5.31, the grain sizes of the BrTiP and BrTiNbP IF steels are 24.5 and 22 μm, respectively. Hence, the probability that solute P has been completely scavenged from the grain boundaries is relatively high in these steels.

Thus, in summary, the addition of P to IF steels brings about the following effects on strength:

1) P in ferrite matrix: Solid Solution Strengthening

$$+ \Delta YS = k_{SSS} * (\% P_{matrix})$$

$$k_{sss} = 2.38 \text{ MPa}/0.01 \text{ wt\% P}$$

2) P segregated to ferrite grain boundaries: Grain Boundary Hardening

$+\Delta YS = k_y * (d^{-1/2})$

$k_y = f(\%\ P\ at\ GB) = k'_{GBH} * (at\ \%\ P\ at\ GB)$

$k'_{GBH} = 18.6\ MPa.\ \mu m^{1/2}/at\%\ P\ at\ GB$

3) P in FeTiP:

$-\Delta YS = f\ (\%\ P\ in\ FeTiP)$

FeTiP (matrix): $-\Delta YS = -\ ksss * (\%\ P\ in\ FeTiP)$

FeTiP (at GB): $-\Delta YS = -\ k'_{GBH} *(at\ \%\ P\ at\ GB\ scavenged\ by\ FeTiP)* (d^{-1/2})$

The effect of solute P and FeTiP precipitation (in matrix and at grain boundaries) has been shown schematically in Figure 6.2. It should be noted that the C curves for the solute P segregation and the subsequent precipitation of the FeTiP at the grain boundaries and in the ferrite matrix will depend on the chemistry of the IF steel. From the observations in this work, the locations of the four steels namely Base-IF, Phos-IF, BrTiP and BrTiNbP used in this research have been shown relative to the C curves.

The extent of P segregation to the grain boundaries will depend, among other factors, upon the rate of cooling after the homogenization heat treatment. In this research, the specimens were water quenched after the homogenization heat treatment of 850^{o}C/5 mins. The water quenching was done for the following reasons:

a) To prevent any P segregation to grain boundaries during the cooling.
b) To accelerate the kinetics of P segregation to grain boundaries during the subsequent segregation heat treatment.

The use of slower cooling rates after homogenization can affect the kinetics and, hence, the extent of P segregation immediately after homogenization and also during subsequent segregation, thereby affecting the precipitation of FeTiP at the grain boundaries. The use of

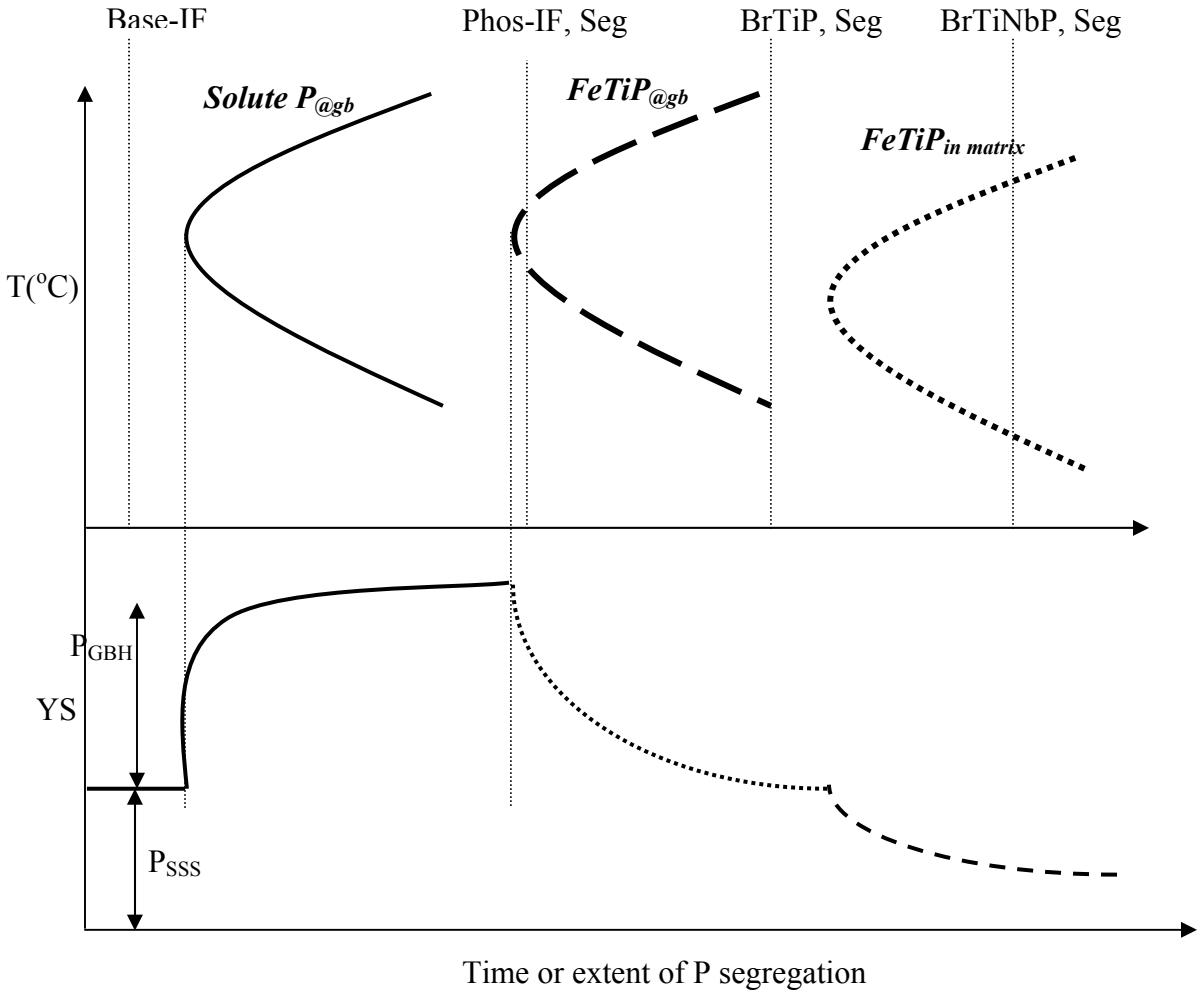

Figure 6.2 Effect of Solute P and FeTiP Precipitation on the Yield Strength of IF Steels

higher cooling rates will suppress the segregation of P during the cooling after homogenization. But on the same token, higher cooling rates can induce non-equilibrium segregation of solute P during subsequent segregation heat treatments.

6.4 Mechanism of Grain Boundary Hardening

It has been shown that the segregation of P to ferrite grain boundaries results in a significant increase in the Hall-Petch slope, k_y, and also the local grain boundary microhardness. This observation is strongly supportive of the earlier work done by Braunovic, Leslie, Spitzig and Wilson, which has been described earlier in section 2.3.6.2 and 2.3.6.3. The findings in this work also tend to support Li's theory of the role of grain boundary ledges in initiating slip at the grain boundaries. As seen from the TEM observations in Figure 5.9, grain boundary ledges are readily observed in the segregated condition of the Phos-IF steel. The segregation of solute P is expected to cause the following effects:

a) The grain boundary ledge density increases, and consequently the density of dislocations emitted by these ledges in the vicinity of the grain boundaries also increases.
b) On subsequent straining, the increased dislocation density near the boundaries will result in rapid forest hardening or strain hardening.
c) The solute P atoms at the grain boundaries will pin the dislocations causing additional solute hardening at the grain boundaries.

Thus, grain boundary strengthening is postulated to be a combination of dislocation forest hardening and solute P hardening of the dislocations emitted by the grain boundary ledges. This mechanism of grain boundary hardening has been shown schematically in Figure 6.3. It should be noted that the grain boundary hardening will be higher for finer grain sizes on account of the

inherently high geometrically necessary dislocation densities at the grain boundaries in fine grain sized samples. A similar result was obtained by Ainslie et al[184]. during their studies on sulfur segregation in ferrite. These researchers observed that the presence of excessive solute sulfur at the grain boundaries resulted in a substantially higher dislocation density networks at the ferrite grain boundaries compared to that at the grain centers. These dislocation networks at the grain boundaries act as efficient traps for the sulfur atoms in the vicinity of the boundary.

6.5 Thermo-mechanical Processing and Corrections to the Hall-Petch slope, k_y

One of the main objectives in this work was to determine the change in k_y value with or without P segregation to ferrite grain boundaries. Different processing routes were used in this research to develop the three ferrite grain sizes in each IF steel and the conditions of P location as described previously. In addition to the different grain sizes that were produced by employing these processing routes, it was also observed that the microstructure of the three grain sizes was different in at least the following two ways, namely:

a) the distribution of solute carbon

b) the relative volume fractions of crystallographic texture components in each grain size.

Each of these microstructural variables, which are directly controlled by the processing variables, can affect the Hall-Petch slope, k_y.

In essence,

$$k_y^{measured} = f(\text{Csss, texture hardening, segregated P})$$

Hence in order to determine the change in k_y solely due to the segregation of P, it was necessary to account for the changes in k_y due to solute C and texture variations. Examination of

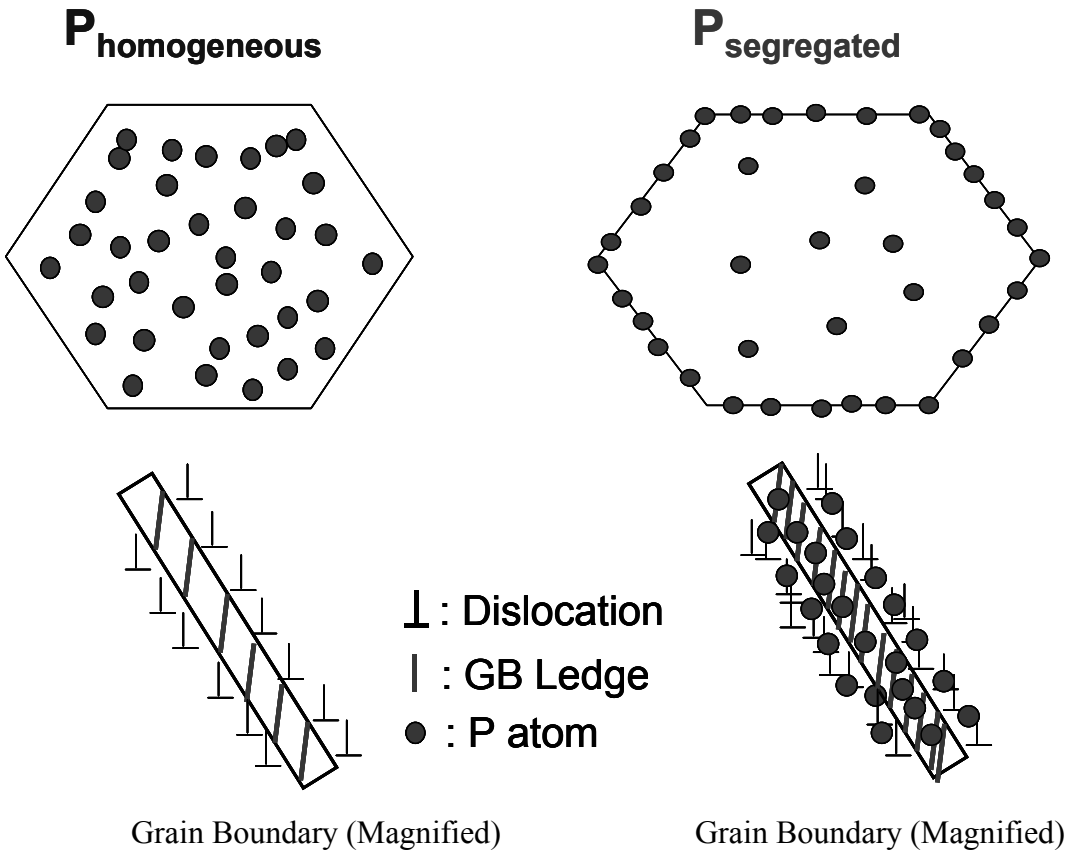

Figure 6.3 Schematic of Grain Boundary Hardening Mechanism Due to P Segregation

Table 5.10 shows that the correction in k_y, due to the solid solution strengthening of C can be as high as 39%. The presence of solute C thus can introduce changes in the value of k_y as well as compete with P for segregation to the ferrite grain boundaries.

Thus, the variability of solute C can result in the variability in the strength of IF steels through its direct influence on k_y, and indirectly, through its influence on P segregation. The texture hardening correction to k_y has been largely overlooked in the Hall-Petch literature to date. In this work, an upper bound estimate of this correction was made by the use of texture hardening modeling and measurement of crystallographic texture components using the EBSD technique. It is seen from Table 5.13 that the texture hardening correction to k_y can be as high as 19%. Thus, it is to be noted that the changes in processing can result in changes in the relative volume fractions of the texture components. The variability in texture can introduce variability in the yield strength of IF steels. It should be noted that IF steels can develop extremely strong textures. Therefore, the texture hardening contribution to yield strength would be higher in IF steels than in other high strength steels that rely upon precipitation or multiphase strengthening mechanisms. Hence, the texture hardening correction to k_y would be most significant in IF steels.

6.6 Relationship between k_y and σ_o, in the Hall-Petch Plot

A striking feature of the Hall-Petch plots shown in Figures 5.17 and 5.18 is the relation between the value of slope k_y and the intercept on the Y axis, σ_o. These values are shown for the different conditions in Table 6.4.

Table 6.4 Values of k_y and σ_o in the Hall-Petch Plots

Test Condition	Ordinate intercept of the Hall-Petch Plot, σ_o (MPa)	k_y corrected for C_{sss} (MPa. $mm^{1/2}$)
Base-IF (As-Annealed)	74.4	6.1
Base-IF (Homogenized)	64.1	7.2
Base-IF (Segregated)	72.7	6.5
Phos-IF (As-Annealed)	73.8	10.6
Phos-IF (Homogenized)	63.4	9.2
Phos-IF (Segregated)	68.1	14.4

The k_y and the corresponding σ_o values for the various conditions have been plotted in Figure 6.4. It is seen from Figure 6.4 that, in the Base-IF steel, the value of σ_o varies inversely with the k_y value. This trend is not so evident in the Phos-IF steel. A similar behavior was

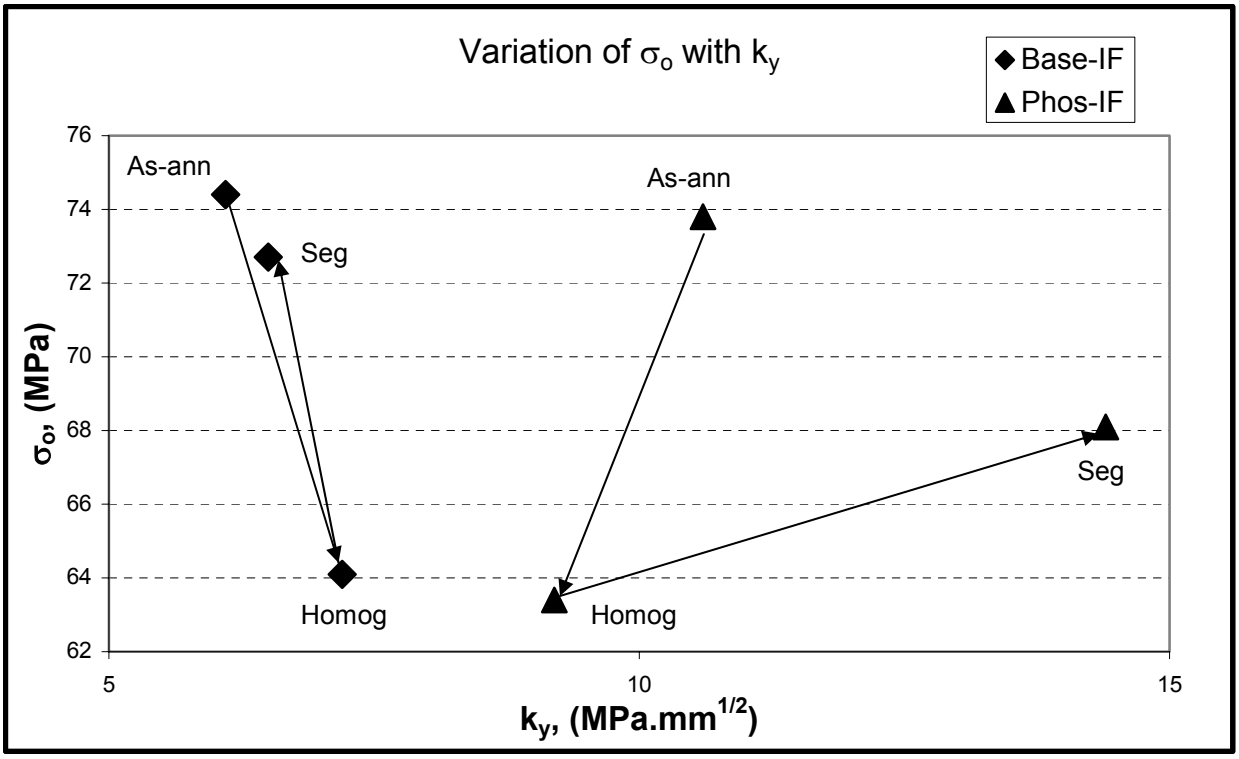

Figure 6.4 Variation of σ_o with k_y for Base-IF and Phos-IF Steel

observed by Mintz and Johnson in ferrous alloys. It is assumed that the value of σ_o, represents the yield strength of the single crystal. Johnson[181] and Mintz[72] argued that this extrapolation is not accurate. As the grain sizes gets larger compared to the specimen thickness or diameter, the Hall- Petch relation is seen to diverge from the linear dependence and the value of k_y decreases rapidly to approach a value of zero at large grain sizes. Johnson argued that in such relatively large grain sizes, the specimen no longer remains a polycrystal, but becomes a "multiple" crystal specimen. In this case, the majority of the grains may be surface grains and may not be fully subject to the mutual constraints exerted by the grains in a polycrystalline sample. Thus, the extrapolation to the yield strength axis does not necessarily give the single crystal yield strength value and has to be interpreted with caution.

Figure 6.4 brings about an interesting point. In the Base-IF steel, homogenizing after the as-annealed heat treatment increases the value of k_y but decreases the value of σ_o. In the subsequent segregation heat treatment, the values of k_y and σ_o almost recover to those in as-annealed condition. On the other hand, in the Phos-IF Steel, the homogenization heat treatment decreases the value of k_y as well as σ_o. Subsequent segregation heat treatment increases the values of k_y as well as σ_o. The value of k_y in the segregated condition is much higher than that in the as-annealed condition, whereas the value of σ_o is lower than that in the as-annealed condition. The changes in the values of σ_o and k_y are shown in Tables 6.5 and 6.6 for both the IF steels.

Table 6.5 Change in σ_o and k_y in the Base-IF Steel with Change in Processing

Change in Processing	Change in σ_o, $\Delta\sigma_o$, %	Change in k_y, Δk_y, %
As-annealed to Homogenized	-13.8	+18
Homogenized to Segregated	+13.4	-9.7

Table 6.6 Change in σ_o and k_y in the Phos-IF Steel with Change in Processing

Change in Processing	Change in σ_o, $\Delta\sigma_o$, %	Change in k_y, Δk_y, %
As-annealed to Homogenized	-14.1	-13.2
Homogenized to Segregated	+7.4	+56.5

Thus, it can be concluded from Figure 6.4 that the variability of σ_o and k_y is much higher in the Phos-IF steel compared to the Base-IF for the same processing schedules. This also implies that the properties of the Phos-IF steel are more sensitive to processing conditions compared to those in the Base-IF steel.

6.7 Industrial Implications

One of the most important findings in this research is that P segregation to ferrite grain boundaries brings about effective grain boundary hardening in IF steels, the extent of which depends upon the amount of P segregated to the grain boundaries. In the Phos-IF steel, for the grain size of 15 μm, the yield strength varies by as much as 48 MPa, depending upon the segregation of P. Thus, varying the amount of P segregation to the grain boundaries through

appropriate processing routes can provide a tool in controlling the yield strength of P-bearing IF steels. It is known that the segregation of P in IF steels occurs predominantly during coiling of the hot band. Controlling the processing variables such as the cooling rate after the finishing temperature and the coiling temperature, the degree of P segregation can be controlled. Higher cooling rates through the transformation temperature can promote non-equilibrium segregation of P to ferrite grain boundaries as would high coiling temperatures. Depending upon the chemistry of the IF steel, high coiling temperatures would also promote the precipitation of FeTiP at grain boundaries. The chemistry of IF steels is also an important factor in affecting the precipitation of FeTiP. All these factors would then affect the variability in the strength of IF steels in the hot band. This variability in the strength has been schematically shown and summarized in Figure 6.5. It is known that the segregation of P to ferrite grain boundaries results in the undesirable phenomenon of Cold Work Embrittlement (CWE). The scavenging of solute P atoms at the grain boundaries by the FeTiP or FeTiNbP precipitates could be an effective tool to counteract CWE.

The extensive segregation of P to grain boundaries also occurs during the annealing of IF steel sheets, particularly during batch annealing compared to continuous annealing. Since continuous annealing cycles use higher temperatures than conventional batch annealing cycles, the segregation of P to grain boundaries is expected to be higher in batch annealing. It is usually observed that the grain sizes developed in batch annealing are larger than those in continuous annealing. Also, continuously annealed IF steel sheets are seldom fully recrystallized, whereas batch annealed IF steel sheets are fully recrystallized. Inspite of these two factors, batch annealed IF steels show the same yield strength levels as continuously annealed IF steels. This could be due to the higher grain boundary hardening contribution in the batch annealed IF steels[151, 185].

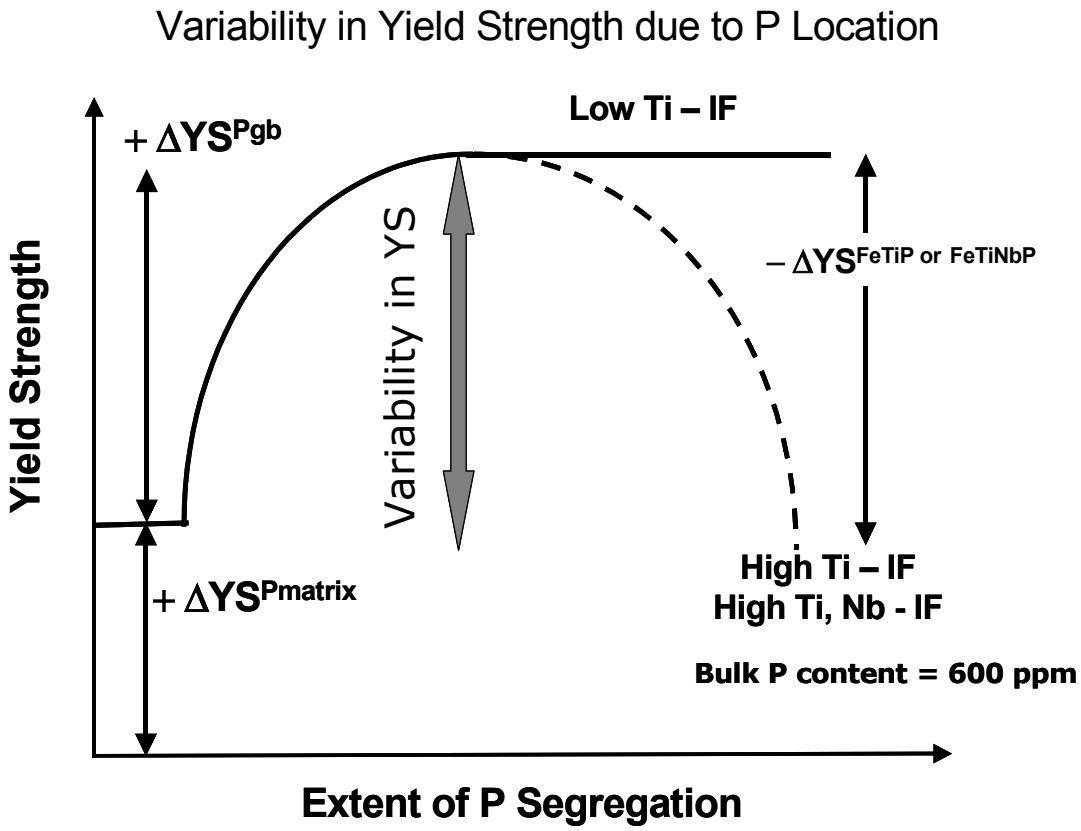

Figure 6.5 Schematic of Variability in Yield Strength of IF Steels Due to Extent of P Segregation

Use of different annealing schedules during recrystallization can also vary the distribution of solute C and the evolution of crystallographic texture. These factors, as mentioned previously, can also introduce variability in the mechanical properties.

6.8 Crystallographic Texture and Springback Behavior of IF Steels

On the basis of theoretical modeling, it has been categorically shown that crystallographic texture can impart significant elastic anisotropy in the plane of IF steel sheets and hence can be used as an effective tool in controlling the in-plane variability of springback. It is seen from Figures 5.34 through 5.37 and Table 5.16 that the gamma fiber components show elastic isotropy, hence isotropic in-plane springback behavior, whereas the large elastic anisotropy of the alpha and epsilon fiber components results in a significantly anisotropic springback behavior. Table 5.16 rates the various texture fiber components based upon the maximum variability of in-plane springback behavior. It is thus seen that gamma fiber components are best suited for isotropic springback behavior. There are several implications of the above findings for the IF steel sheet industry. Firstly, control of elastic anisotropy via control of the crystallographic texture may be a powerful approach in reducing the variability of springback in IF steel sheets. Of special benefit may be the goal of producing strong γ-fiber components compared to the α and ε-fiber components. It is known that the presence of strong γ-fiber orientations also results in high R_{bar} and low ΔR values in IF steel sheets and, hence, excellent deep drawability, whereas α and ε-fiber components impart poor deep drawability to IF steel sheets. It thus turns out that by optimizing the processing in such a way as to obtain strong intensities of γ-fiber orientations in the IF steels, the sheet steel industry can benefit both in terms

of achieving excellent deep drawability as well as isotropic springback behavior. The use of crystallographic texture in controlling the springback behavior might turn out to be significant especially when the demand for high strength, thinner gauge IF steels is on the rise. In practice, the degree to which the control of the texture of IF steels can be used to reduce springback variability will depend on the extent to which the γ-fiber components can be maximized at the expense of the α and ε-fiber components. The maximization of gamma fiber components and the associated benefits in achieving uniform springback behavior can be made use of in all forming operations. Thus, sheet steels exhibiting isotropic in-plane springback behavior will be highly useful in all sheet forming applications. This has been schematically shown in Figure 6.6.

The finite element modeling results also show that sheet steels having high elastic moduli along the length of the strip will exhibit lower springback as measured by the final welding gaps, ΔX and ΔY. This has been shown in Figure 5.39 and Figure 5.41. Figures 5.40 and 5.42 show the effect of increasing yield strength on the welding gaps and the draw-bend profile of the sheet. Thus, it is seen that even in the draw-bend applications, IF steel sheets with high elastic moduli and low yield strengths along the length of the strip will exhibit lower springback values.

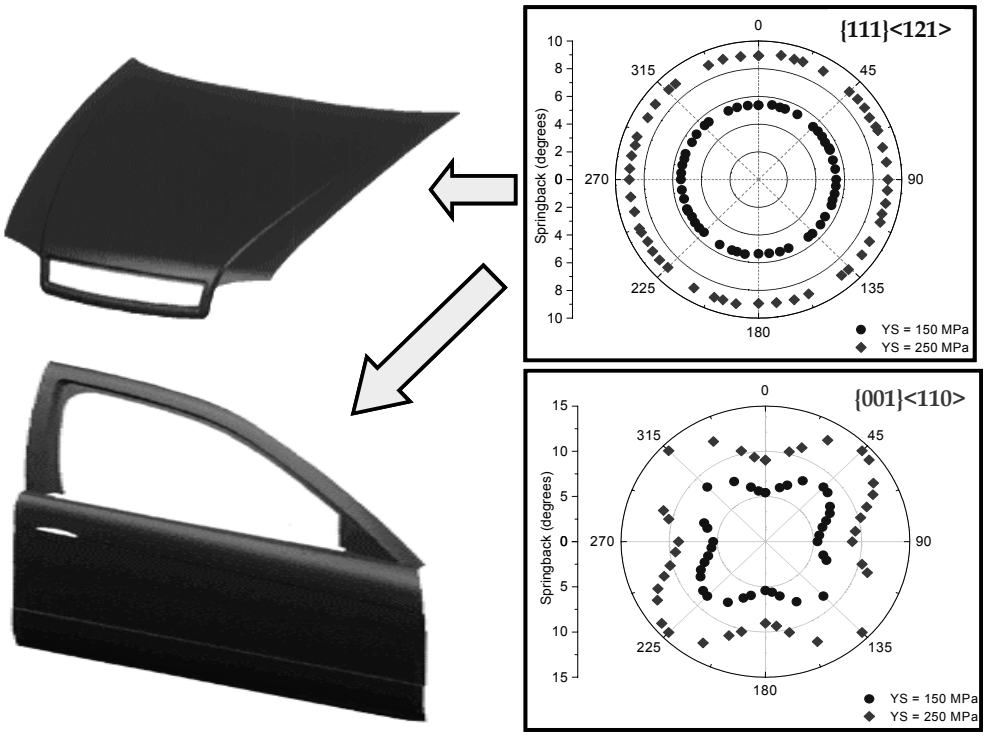

Figure 6.6 Usefulness of Gamma Fiber Components in Other Sheet Forming Applications Due to Isotropic Springback Behavior

7.0 CONCLUSIONS

7.1 Role of Phosphorus in the Small Strain Yielding Behavior of IF Steels

The following conclusions can be drawn from the work done in this objective:

1) Segregation of solute P to ferrite grain boundaries brings about extensive grain boundary hardening, which manifests itself in a substantial increment in the Hall-Petch slope, k_y. The magnitude of this grain boundary hardening is dependent upon the grain size of ferrite and is higher for finer grain sizes.
2) The increment in grain boundary hardening brought about by solute P is highly dependent upon the grain boundary surface area per unit volume, S_v. The increment in the Hall-Petch slope k_y, caused by P segregation, has been determined to be ~18.6 MPa.$\mu m^{1/2}$/ at% P segregated.
3) The segregation heat treatment of 550^{o}C/24 hrs results in an average of 10.3 at % of solute P at the grain boundaries as measured by AES.
4) Solute P in the matrix also brings about solid solution strengthening, the magnitude of which has been determined to be 2.38 MPa/0.01 wt% P.
5) The segregation of P to ferrite grain boundaries also results in an increase in the local grain boundary microhardness.
6) The k_y values in the Phos-IF steel are consistently higher than those in the Base-IF steel for all the heat treatment conditions employed, namely, as-annealed, homogenized and segregated. The maximum difference in the k_y values between the Phos-IF and Base-IF steel is 121% in the segregated P condition.

7) In the Phos-IF steel, the k_y value is the highest for the segregated P condition. This value is 57% higher than the homogenized condition, suggesting that the k_y value is strongly dependent upon the segregation of solute P to ferrite grain boundaries.
8) Grain boundary hardening is caused by the increased dislocation density at the grain boundaries due to the effect of P segregation on the grain boundary ledge density and also due to the solute pinning of the excess dislocations at the grain boundaries.
9) The small volume fraction of FeTiP precipitates, found in the Phos-IF steel after segregation heat treatment, has a negligible effect on the yield strength.
10) Using higher levels of bulk Ti and the addition of Nb results in abundant precipitation of FeTiP and FeTiNbP at the grain boundaries. This precipitation scavenges solute P from the ferrite grain boundaries and results in a substantial loss of grain boundary hardening.
11) Solute Nb is seen to participate in the precipitation of phosphides at the grain boundaries and in the matrix.
12) The different processing routes used to develop the ferrite grain sizes in the Base-IF and Phos-IF steels results in different levels of solute C in the matrix and different crystallographic textures in the grain sizes.
13) The presence of different amounts of solute C in the matrix affects the value of k_y. After accounting for the presence of C and its accompanying solid solution contribution, the correction to k_y can be as high as 39%.
14) The presence of different crystallographic textures in different grain sizes also affects the value of k_y. Modeling the yield strength anisotropy of different crystallographic textures, in conjunction with determining the volume fractions of texture components, provides an effective tool to determine the texture hardening correction to k_y. After accounting for the

texture hardening in each grain size, it is observed that the texture hardening correction to the measured value of k_y can be as high as 19%.

15) The contribution of texture hardening to the overall yield strength is higher in IF steels, due to their ability to develop extremely strong crystallographic textures. Therefore, the texture hardening correction to k_y is expected to be most significant in IF steels.

16) Changing processing routes to vary the grain size can also change other microstructural characteristics, which will impart variability to the yield strength.

17) One of the main sources of yield strength variability in P-bearing IF steels is the relative distribution of P in the matrix, at grain boundaries and in FeTiP precipitates. Alloy and processing design of IF steels can be effectively used to control the distribution of P in ferrite and thereby control the variability in yield strength of IF steels.

7.2 Crystallographic Texture and Small Strain Unloading or Springback Behavior

The following conclusions can be drawn from the work done in this research:

1) Elastic anisotropy, associated with crystallographic texture, can, by itself, introduce a large variability in the springback behavior of IF steel sheets intended for use in plane strain bending applications.

2) γ-fiber texture components exhibit strong elastic isotropy, and, hence, show minimum variability (<2%) in springback in the plane of the IF steel sheet.

3) α-fiber and ε-fiber texture components exhibit large elastic anisotropy and hence show large variability in springback in the plane of the IF steel sheet.

4) In addition to exhibiting excellent deep drawability, the gamma fiber texture components are also ideally suited for isotropic springback behavior.

5) In draw-bending applications, IF steel sheets exhibiting large elastic moduli and low yield strengths along the length of the strip exhibit minimum values of springback as predicted from the final welding gaps.

8.0 FUTURE WORK

Phosphorus and Yield Strength of IF Steels

The segregation heat treatments employed in this work resulted in 10.3 at % solute P at the ferrite grain boundaries in the Phos-IF steel, resulting in a grain boundary hardening contribution of 18.6 MPa..$\mu m^{1/2}$ / at% P. For a given bulk P content, the amount of solute P at the grain boundaries can be varied by using different segregation heat treatments. By measuring the corresponding changes in the grain boundary hardening contribution to the yield strength, the dependence of the grain boundary hardening contribution on the amount of solute P at the boundaries can be mapped.

Crystallographic Texture and Springback Behavior

The theoretical modeling in plane-strain bending applications as well as in draw bend testing shows that the gamma fiber components exhibit isotropic springback behavior. Experimental verification of this model by developing widely different crystallographic textures in IF steel sheets through appropriate processing would give valuable insight in the springback behavior of these sheet steels.

BIBLIOGRAPHY

BIBLIOGRAPHY

1. K. Ushioda, N.Y., K. Koyama, O. Akisue. "Application of ULC Steels to the development of Super-formable Sheet Steels, Solution-Hardened High Strength Sheet Steels and Bake-hardenable Sheet Steels". in IF.IFS 94. 1994. Tokyo: Iron and Steel Institute of Japan.

2. Hudd, R.C., "Some aspects of Annealing of Low Carbon Strip Steel." Metals and Materials, 1987(February): p. 71-76.

3. Leslie, W.C., The Physical Metallurgy of Steels. 1981, McGraw Hill. p. 27-28.

4. Hutchinson, W.B., Nilsson, K.I., Hirsch, J. "Annealing Textures in ULC Steels" in Metallurgy of Vacuum Degassed Steels. 1989. Indianapolis: TMS, Warrendale, PA. pp. 109-126

5. Okamoto, A., Takahashi, M. "Effects of a Small Amount of Carbon on the Recrystallization Texture Formation in Steel" in Proceedings of 6th Int. Conf. On Textures of Materials. 1981: ISIJ. pp. 730-748

6. Takahashi, M., Okamoto, A., Ino, S. and Nakata, T., "Effect of Nitrogen Content on the Deep Drawability of Rimmed Low Carbon Cold Rolled Steel Sheet" Trans. ISIJ, 1979. Vol. 19: p. 144-151.

7. Ono, S., O. Nozoe, T. Shimomura and K. Matsudo. "Annealing Textures in ULC Steels" in Metallurgy of Continuously Annealed Sheet Steel. 1981. Indianapolis: AIME, Warrendale, PA. pp. 99-116

8. Whiteley, R.L. et al., "Relationship among Texture, Hot Mill Practice and the Deep Drawability of the Sheet Steel", in Hot Rolled Products III. 1962, Interscience, NewYork. p. 47-63.

9. Held, J.F. in Mechanical Working and Steel Processing IV. 1965: Met. Soc. AIME, New York.

10. Hutchinson, W.B., "Development and Control of Annealing Texture in Low Carbon Steels" International Materials Reviews, 1984. **Vol. 29**(No.1): p. pp. 25-42.

11. Cahn, R.W., Haasen, P., Kramer, E.J, ed. Materials Science and Technology. Vol. 7. 1991. 299-301.

12. Pickering, F.B., Physical Metallurgy and Design of Steels 1978, Applied Science Publishers. p. 37-43.

13. Mohanty, O.N., Gope, "Car Body Materials in the Coming Years, Prospects of Steel" Tata Tech, 1997. **Vol. 27**: p. 21-28.

14. Gladman, T., in "Physical Metallurgy of Microalloyed Steels" 1997. p. 33-35.

15. Taylor, B., Formability Testing of Sheet Metals, in ASM Metals Handbook. p. 876-899.

16. Lankford, W.T., Trans. ASM, 1950. **42**: p. 1197.

17. Whiteley, R.L., Wise D.E, in Flat Rolled Products III. 1962, Interscience: Newyork. p. 42.

18. Cahn, R.W., Haasen, P., Kramer, E.J, ed. Materials Science and Technology. Vol. 7. 1991. 313-315.

19. Cahn, R.W., Haasen, P., Kramer, E.J, ed. Materials Science and Technology Vol. 7. 1991. pp. 54.

20. I. Gupta, R.D.B. "Metallurgy of Formable Vacuum Degassed Interstitial-Free Steels" in Metallurgy of Vacuum Degassed Steels. 1989. Indianapolis: TMS, Warrendale, PA. pp 43-72

21. S. Satoh, T.O., M. Nishida, T. Erie. "Effects of Alloying Elements and Hot Rolling Conditions on the Mechanical Properties of Continuously Annealed, Extra-low-carbon Steel Sheet"in Proceedings of Technology of Continuously Annealed Cold Rolled Sheet Steels Symposium. 1985. Detroit, MI: TMS-AIME, Warrendale, PA.

22. Hua, M. 1995, University of Pittsburgh.

23. I. Gupta, P., L.T.,Shiang, T.L. "Effects of Alloying Elements and Hot Rolling Conditions on the Mechanical Properties of Continuously Annealed, Extra-low-carbon Steel Sheet" in Hot and Cold Rolled Sheet Steels. 1988. Cincinnati, OH: TMS-AIME, Warrendale, PA. pp. 139-153

24. Aparicio, L.R. 1998, University of Pittsburgh.

25. Katoh, H. in Proceedings of the International Conference on Advances in Physical Metallurgy and Applications of Steel. 1981.pp. 95

26. Goodman, S.R., Mould, P.R., and Siple, J.C. in Proceedings of the International Conference on Advances in Physical Metallurgy and Applications of Steel. 1981. pp.167

27. Pickering, F.B., Physical Metallurgy and Design of Steels. 1978, Applied Science Publishers. pp. 10-14.

28. Pickering, F.B. et al., "An investigation into some Factors which control the strength of carbon steels" in Metallurgical Developments in Carbon Steels: Iron and Steel Institute.

29. Blickwede, D.J., "Strain Hardening and Anisotropy" Metal Progress, 1969. Vol. 1, pp. 84-88.

30. Courtney, T.H., in Mechanical Behavior of Materials, 1990, McGraw Hill. pp. 173-184.

31. Hertzberg, R.W., Deformation and Fracture Mechanics of Engineering Materials 1976, John Wiley and Sons. pp. 39-48.

32. Leslie, W.C., Iron and its Dilute Substitutional Solid Solutions Met Trans., 1972. 3 pp. 5-26.

33. Leslie, W.C., The Physical Metallurgy of Steels 1981, McGraw Hill. pp. 68-70.

34. Dieter, G., Mechanical Metallurgy 1986, McGraw Hill. pp. 203-207.

35. Verhoeven, J.D., in Fundamentals of Physical Metallurgy 1975, John Wiley and Sons. pp. 515-517.

36. Kelly, A. et al., Progress in Materials Science, 1963. Vol. 10 (No. 3).

37. Gladman, T., in Physical Metallurgy of Microalloyed Steels 1997. pp. 47-56

38. Ham, et al., "Dislocation-Particle Interactions", in Strengthening Methods in Crystals 1971, Applied Science Publishers. pp. 2-121.

39. Chawla, et al., in Mechanical Metallurgy, Principles and Applications, 1984, Prentice Hall. pp. 402-437.

40. Hill, R., Proc. R. Soc. London, Ser. B, 1948. Vol. 193, pp. 281-297.

41. Caddell, et al.., in Metal Forming, 1993, Prentice Hall. pp. 272-273.

42. Kozasu, I., Tetsu-to-Hagane, 1975. Vol. 61, pp. 991.

43. Barlat, F., and Lian, J., "Plastic Behavior and Stretchability of Sheet Metals, Part I: A Yield Function for Orthotropic Sheets under Plane Stress Conditions" International Journal of Plasticity, 1989. Vol. 5, pp. 51-66.

44. Hall, E.O., Proc. Phys. Soc., 1951. Vol 64B, pp. 747.

45. Petch, N.J., J. Iron and Steel Inst., 1953. Vol. 174, pp. 25.

46. Gladman, T., in Physical Metallurgy of Microalloyed Steels, 1997. pp. 39-42.

47. Chawla, et al., in Mechanical Metallurgy, Principles and Applications, 1984, Prentice Hall. pp. 494-514.

48. Cottrell, A.H., Trans TMS-AIME, 1958. Vol. 212, pp. 192.

49. Tjerkstra, H.H., "The Effect of Grain Size on the Stress-Strain Curve of alpha-iron and the connection with the Plastic Deformation of the Grain Boundaries" Acta Met, 1961. 9 pp. 259-263.

50. Armstrong, R.W., Codd, I., Douthwaite, R.M., Petch, N.J., Phil. Mag., 1962. **7**: pp. 45.

51. Conrad, H., Acta Met, 1963. Vol. 11, pp. 75.

52. Li, J.C.M., Trans TMS-AIME, 1963. Vol. 227, pp. 139.

53. Li, J.C.M., Chou, Y.T, "The Role of Dislocations in the Flow Stress Grain Size Relationships" Met Trans., 1970. Vol 1, pp. 1145-1159.

54. Brandon, D.G., Acta Met, 1964. Vol. 12, pp. 813.

55. Murr, L.E., Met Trans A, 1975. Vol 6A, pp. 505-513.

56. Worthington, P.J., Smith, E., "The Formation of Slip Bands in Polycrystalline 3% Silicon Iron in the Pre-yield Microstrain Region" Acta Met, 1964. 12, pp. 1277-1281.

57. Price, C.W., and Hirth, J.P., "A Mechanism for the Generation of Screw Dislocations from Grain-Boundary Ledges" Materials Science and Engineering, 1972. Vol. 9**,** pp. 15-18.

58. Hirth, J.P., "The Influence of Grain Boundaries on Mechanical Properties" Met. Trans, 1972. Vol. 3, pp. 3047-3067.

59. Hirth, J.P., Ballufi, R.W, "On Grain Boundary Dislocations and Ledges" Acta Met, 1973. 21, pp. 929-942.

60. Hutchinson, M.M., Pascoe, R.T, "Grain-boundary Strengthening in Copper-base Solid Solutions" Metal Science Journal, 1972. 6, pp. 90-95.

61. Murr, L.E., in Interfacial Phenomena in Metals and Alloys, 1975, Addison-Wesley. pp. 165-258.

62. Bernstein, I.M., Rath, B.B, Surface Science, 1972. Vol 31, pp. 68.

63. Murr, L.E., in Interfacial Phenomena in Metals and Alloys, 1975, Addison-Wesley. pp. 338-344.

64. Hornbogen, E., "Observations of Yielding in an Iron-3.17 At% Phosphorus Solid Solution" Trans of the ASM, 1963. 56, pp. 16-24.

65. Hornbogen, E., Staniek, G., "Grain-size dependence of the mechanical properties of an age-hardening Fe-1%Cu-alloy" Journal of Materials Science, 1974. 9, pp. 879-886.

66. Hu, H., "Effect of Solutes on Luders Strain in Low-Carbon Sheet Steels" Met Trans A, 1983. 14A, pp. 85-91.

67. Wilson, D.V., "Role of Grain Boundaries in the Discontinuous Yielding of Low Carbon Steels" Metal Science Journal, 1967. Vol. 1, pp. 40-47.

68. Wilson, D.V., "Grain-size Dependence of Discontinuous Yielding in Strain-aged Steels" Acta Met, 1968. 16, pp. 743-753.

69. Cottrell, A.H., in "The Relationship between Structure and Mechanical Properties of Metals" 1963, HMSO. pp. 456.

70. Morrison, W.B., Leslie, W.C, "The Yield Stress-Grain Size Relation in Iron Substitution Alloys" Met Trans A, 1973. Vol. 4, pp. 379-381.

71. B. Mintz, H.K., Smith, G.D.W., "Size Strengthening in Steel and its Relationship to Grain Boundary Segregation of C" Materials Science and Technology, 1992 (June).

72. Mintz, B., "Importance of k_y (Hall-Petch slope) in determining strength of steels" Metals Technology, 1984. 11, pp. 265-272.

73. Mintz, B., "Influence of Silicon and Nitrogen on the Impact Properties of As-rolled Mild and Carbon-Manganese Steels" Journal of the Iron and Steel Institute, 1973, pp. 433-439.

74. Mintz, B., "Influence of Manganese on the Impact Transition Temperature of As-rolled Plain Carbon Manganese Steels" Metals Technology, 1974, pp. 226-232.

75. Mintz, B., Turner, P.J, Met Trans A, 1978. 9A, pp. 1611.

76. Floreen, S et al., Acta Met, 1969. Vol. 17, pp. 1175.

77. Seybolt, A.U., Westbrook, J.H, "Oxygen-induced Grain Boundary Hardening in NiGa". Acta Met, 1964. 12, pp. 449-460.

78. Braunovic, M., Haworth, C.W., Weiner, R.T, "Grain-boundary Hardening in Iron and Iron Alloys" Metal Science Journal, 1968. 2, pp. 68-73.

79. Braunovic, M., Haworth, C.W., "Further Studies of Grain-boundary Hardening in Iron and Iron Alloys" Metal Science Journal, 1970. 4, pp. 85-89.

80. Braunovic, M., Haworth, C.W., "Grain-boundary Hardening and Elastic Recovery of Micro-indentations" Journal of Materials Science, 1972. 7, pp. 763-770.

81. Braunovic, M., Haworth, C.W., "On the Phenomenon of Grain-boundary Hardening in Iron" Journal of Materials Science, 1974. 9, pp. 809-820.

82. Aust, K.T., Hanneman, R.E, Niessen, P., Westbrook, J.H, "Solute Induced Hardening near Grain Boundaries in Zone Refined Metals" Acta Met, 1968. Vol. 16, pp. 291-302.

83. Braunovic, M., Haworth, C.W., "The Petch Relation and Grain Boundary Hardening" Canadian Metallurgical Quarterly, 1974. 13(1), pp. 211-214.

84. Bloom, T.A., Fosnacht, D.R., Haezebrouck, D.M, "The Influence of Phosphorus on the Properties of Sheet Steel Products and Methods used to control Phosphorus Levels in Steel Product Manufacturing-Part I" I&SM, 1990, pp. 35-41.

85. Spitzig, W.A., Sober, R.J., "Effect of Phosphorus on the Mechanical Properties of Hot-rolled 0.1C-1.0 Mn Steel Strip″ Met Trans A, 1977, 8A, pp. 1585-1590.

86. Spitzig, W.A., Sober, R.J., "Effect of Phosphorus on the Mechanical Properties of Normalized 0.1 Pct C, 1.0 Pct Mn Steels" Met Trans A, 1977. 8A, pp. 651-655.

87. Spitzig, W.A., "The Effects of Phosphorus on the Mechanical Properties of Low-carbon Iron" Met Trans A, 1972. Vol. 3, pp. 1183-1188.

88. Matsuoka Takashi, Y.K., "Metallurgical Aspects in Cold Rolled High Strength Steel Sheets" Met Trans A, 1975. 6A, pp. 1613-1622.

89. Gerber, B. "Microalloyed, Vacuum Degassed High Strength Steels with Special Emphasis on IF Steels" in 39th MWSP Conference, 1997. Indianapolis, ISS, pp. 159-164

90. Hopkins, B.E., Tipler, H.R, "The Effect of Phosphorus on the Tensile and Notch-impact Properties of High-purity Iron and Iron-carbon alloys" Journal of the Iron and Steel Institute, 1958, pp. 218-237.

91. Nilsson, K.I., Johansson, E. "Development of IF-steels on ULC Basis for EDDQ and High-strength Applications using CAL and HDG Lines" in Metallurgy of Vacuum Degassed Steels, 1989, Indianapolis: TMS, Warrendale, PA, pp. 143-160

92. Pradhan, R, "Metallurgical Aspects of a Batch-annealed Bake-hardening Steel" in Metallurgy of Vacuum Degassed Steels, 1989, Indianapolis, TMS, Warrendale, PA. pp. 309-325

93. Tokunaga, Y., Kato, H. "Application of Interstitial-free (IF) Steel Sheets to Automobile Parts" in Metallurgy of Vacuum Degassed Steels, 1989. Indianapolis, TMS, Warrendale, PA, pp. 91-108

94. Pradhan, R., "Cold Rolled Interstitial Free Steels: A Discussion of Some Metallurgical Topics" in IF.IFS 94.,1994, Tokyo, Iron and Steel Institute of Japan, pp. 165-177

95. Meyer, L., Bleck, Wolfgang., Muschenborn, Wolfgang, "Product-oriented IF Steel Design" in IF.IFS 94, 1994, Tokyo, Iron and Steel Institute of Japan, pp. 1-20

96. Irie, T., Satoh, S., Hashiguchi, K., Takahashi, I., Hashimoto, O., "Metallurgical Factors Affecting the Formability of Cold-rolled High Strength Steel Sheets" Trans ISIJ, 1981, 21, pp. 793-801.

97. Hoydick, D.P., Osman, T.M.,. "Influence of Phosphorus Content on the Recrystallization Behavior and Mechanical Properties of Boron-bearing Ti-Nb Fully Stabilized Steels" in 40th MWSP Conference. 1998, Pittsburgh, PA, ISS, pp. 195-204

98. Lanteri, S et al., "Influence of Mn and P on Precipitation in High Strength IF Steels" in 38th MWSP Conference, 1996, Cleveland, ISS, pp. 431-441

99. Lanteri, S., "Study of Mechanical Properties and Precipitation in High Strength IF Steels" in 40th MWSP Conference, 1998, Pittsburgh, PA, ISS, pp. 189-194

100. Mizui, A et al., "Texture Formation in ULC Ti added Cold Rolled Sheet Steels" in Metallurgy of Vacuum Degassed Steels, 1989. Indianapolis, TMS, Warrendale, PA, pp. 161-180

101. Rege, J., Garcia, C.I., DeArdo, A.J., "The Segregation Behavior of Phosphorus and its Role in the Cold Work Embrittlement and Annealing Behavior of Ti-stabilized Interstitial-free Steels" in 39th MWSP Conference, 1998. Indianapolis, IN, ISS, pp. 149-158

102. Sakata, K., Okuda, K., Furukimi, O., "Discussion of Solid Solution Strengthening Mechanism of Phosphorus in Steel" Tetsu-to-Hagane, 1998, 84 (8), pp. 26-32.

103. Xianjin, W., Yanwei, M., Yonglin, K., Di. T, "Development and research of automobile steel sheets in China. in Modern LC and ULC Sheet Steels for Cold Forming: Processing and Properties" 1998, Aachen, Germany, Verlag Mainz, pp. 27-38

104. Li, W., Sheng, Y.M., Min, L.J., "Effect of Ti Content on FeTiP Precipitate Behavior in High-Strength P and Mn-added Ti+Nb-IF Steels" in Modern LC and ULC Sheet Steels for Cold Forming: Processing and Properties, 1998, Aachen, Germany, Verlag Mainz, pp. 473-477

105. Luo, S., Liu, B., Zhong, D., "Effect of Composition and Processing Parameters on Microstructure and Formability of P Bearing IF Steels" in Modern LC and ULC Sheet Steels for Cold Forming: Processing and Properties, 1998, Aachen, Germany, Verlag Mainz, pp. 509-520

106. Lanteri, S., Regle, H., "Influence of Heating Rate on Recrystallization and Texture Formation in Ti-IF Steels" in Modern LC and ULC Sheet Steels for Cold Forming: Processing and Properties, 1998, Aachen, Germany, Verlag Mainz, pp. 521-532

107. Kong, B., Lu, J., "Comparison of Precipitate Behavior in Ti-IF Steels between Batch Annealing and Continuous Annealing" in Modern LC and ULC Sheet Steels for Cold Forming: Processing and Properties, 1998, Aachen, Germany, Verlag Mainz, pp. 545-552

108. Neutjens, J., Herman, J.C., Leroy, V., "Hot-band Toughness and Cold Work Embrittlement Behavior of Ultra Low Carbon Steels", in Modern LC and ULC Sheet Steels for Cold Forming: Processing and Properties, 1998, Aachen, Germany, Verlag Mainz, pp. 591-602

109. Shi.J., W.X., "Comparison of Precipitate Behaviors in Ultra-low Carbon, Titanium-stabilized Interstitial Free Steel Sheets under different Annealing Processes", Journal of Materials Engineering and Performance, 1999, 8(6), pp. 641-648.

110. Gupta, R.J., Martin, G, "Relationship between the Electronic Structure and the Precipitation of FeTiP in Interstitial-free ferritic Steels", Phil. Mag. A, 2000. 80(10), pp. 2393-2403.

111. Ramos, A.S., Sandim, H.R.Z., Hashimoto, T.M, "FeNbP in Ultra-low Carbon Nb-added Steel containing high P", Materials Characterization, 2000, 45, pp. 171-174.

112. McLean, D., in Grain Boundaries in Metals, 1957, Oxford, pp. 116-149.

113. Hondros, E.D., Seah, M.P., Hofmann, S., Lejcek, P, "Interfacial and Surface Microchemistry", in Physical Metallurgy, R.W. Cahn, Haasen, P, Editor. 1996, North Holland. pp. 1202-1289.

114. Flewitt, P.E.J., Wild, R.K, in Grain Boundaries: Their Microstructure and Chemistry, 2001, John Wiley and Sons. pp. 35-85.

115. Briant, C.L., Grabke, H.J., "Grain Boundary Segregation in Iron and its Alloys and its Effect on Intergranular Fracture", in Materials Science Forum, 1989, Trans Tech Publications, pp. 253-276.

116. Chalmers, C., Massalski, "Grain-boundary Segregation", Progress in Materials Science, 1972. 16, pp. 43-76.

117. Hondros, E.D., Seah, M.P., "Segregation to Interfaces", International Metals Review, 1977(222), pp. 262-301.

118. Grabke, H.J., "Surface and Grain Boundary Segregation on and in Iron and Steels", ISIJ International, 1989, 29 (7), pp. 529-538.

119. Briant, C.L., "On the Chemistry of Grain Boundary Segregation and Grain Boundary Fracture", Met Trans A, 1990, 21A, pp. 2339-2354.

120. Ramasubramanian, P.V., Stein, D.F, An Investigation of Grain-boundary Embrittlement in Fe-P, Fe-P-S, and Fe-Sb-S Alloys, Met Trans A, 1973, 4, pp. 1735-1742.

121. Miller, M.K., Smith, G.D.W, "Atom Probe Analysis of Interfacial Segregation", Applied Surface Science, 1995, 87/88, pp. 243-250.

122. Guttman, M., Surface Science, 1975, Vol. 53, pp. 213-227.

123. Misra, R.D.K., "Grain Boundary Segregation and Fracture Resistance of Engineering Steels", Surface and Interface Analysis, 2001, 31, pp. 509-521.

124. Mega, T., Shimomora, J., Yasuhara, E, " Boundary Segregation of Phosphorus and Boron in Extra-low Carbon Steels", Materials Transactions, JIM, 1995, 36(10), pp. 1206-1213.

125. Abe, T., Tsukada, K., Tagawa, H., Kozasu, I, "Grain Boundary Segregation Behavior of Phosphorus and Carbon under Equilibrium and Non-equilibrium Conditions in Austenitic Region of Steels", ISIJ International, 1990, 30(6), pp. 444-450.

126. Hua, M., Garcia, C.I., DeArdo, A.J., "The Grain Boundary Segregation of P,B, C and Nb in ULC Steels" in 40th MWSP Conference, 1998, Pittsburgh, PA, ISS, pp. 877-881

127. Cowan, J.R., Evans, H.E., Jones, R.B., Bowen, P, "The Grain Boundary Segregation of Phosphorus and Carbon in an Fe-P-C Alloy during Cooling", Acta Met, 1998, 18, pp. 6565-6574.

128. Misra, R.D.K., Weatherly, G., Embury, D, "Kinetics of Cold Work Embrittlement in Rephosphorised, Interstitial Free Steels", Materials Science and Technology, 2000, 16, pp. 9-12.

129. Inman, M.C., Tipler, H.R, "Grain-boundary Segregation of Phosphorus in an Iron-Phosphorus Alloy and the effect upon Mechanical Properties", Acta Met, 1958, 6, pp. 73-84.

130. Hashimoto, M., Ishida, Y., Yamamoto, R., Doyama, M, "Atomistic Studies of Grain Boundary Segregation in Fe-P and Fe-B Alloys-I", Acta Met, 1984, 32(1), pp. 1-11.

131. Hashimoto, M., Ishida, Y., Yamamoto, R., Doyama, M, "Atomistic Studies of Grain Boundary Segregation in Fe-P and Fe-B Alloys-II", Acta Met, 1984, 32(1), pp. 13-20.

132. Hashimoto, M., Ishida, Y., Yamamoto, R., Doyama, M, "Atomistic Studies of Grain Boundary Segregation in Fe-P and Fe-B Alloys-III", Acta Met, 1984, 32(1), pp. 21-27.

133. Dumoulin, P., Guttmann, M, "The Influence of Chemical Interactions between Metallic and Metalloid Solutes on their Segregation in alpha-Fe", Materials Science and Engineering, 1980, 42, pp. 249-263.

134. Erhart, H., Grabke, H.J, "Equilibrium Segregation of Phosphorus at Grain Boundaries of Fe-P, Fe-C-P, Fe-Cr-P, and Fe-Cr-C-P Alloys", Metal Science, 1981, 15, pp. 401-408.

135. Hanneman, R.E., "Effects of Excess Vacancies in Non-equilibrium Solute Segregation at Interfaces in Solids", Mass Transport in Metallic Solids, 1971, Stoke-on-Trent.

136. Lin, D., Zhang, Y, "A Theoretical Investigation on Non-equilibrium grain boundary segregation", Materials Science and Engineering, 1998, A256, pp. 39-50.

137. Song, S.H., Faulkner, R.G., Flewitt, P.E.J, "Combined Equilibrium and Non-equilibrium segregation treatment of Temper Embrittlement in Low Alloy Steels", Materials Science and Technology, 2001, 17, pp. 523-528.

138. Zhang, Z., Xu, T, Lin, Q., Yu, Z, "A New Interpretation of Temper Embrittlement Dynamics by Non-equilibrium Segregation of Phosphor in Steels", Journal of Materials Science, 2001, 36, pp. 2055-2059.

139. Bercovici, S.J., Hunt, C.E.L., Niessen, P, "A Model of Vacancy Flux Induced Segregation to Grain Boundaries during Cooling", Journal of Materials Science, 1970, 5, pp. 326-330.

140. Zhang, Z., Lin, Q., Yu, Z, "Grain Boundary Segregation in Ultra-low-carbon Steel", Materials Science and Engineering, 2000, A291, pp. 22-26.

141. Zhang, Z., Lin, Q., Yu, Z, "Non-equilibrium intergranular Segregation in Ultra low carbon Steel", Materials Science and Technology, 2000, 16, pp. 305-308.

142. Song, S., Xu, T, "Combined Equilibrium and Non-equilibrium Segregation Mechanism of Temper Embrittlement", Journal of Materials Science, 1994, 29, pp. 61-66.

143. Lejcek, P., "Role of Entropy in Anisotropy of Grain Boundary Segregation", Surface and Interface Analysis, 1998, 26, pp. 800-805.

144. Suzuki, S., Lejcek, P., Hofmann, S, "Effect of Metallurgical Factors on Grain Boundary Segregation of Solute Atoms in Iron", Materials Transactions, JIM, 1999, 40(6), pp. 463-473.

145. Suzuki, S., Abiko, K., Kimura, H, "Phosphorus Segregation related to the Grain Boundary Structure in an Fe-P Alloy", Scripta Met, 1981, 15, pp. 1139-1143.

146. Tatsumi, K., Okumura, N., Funaki, S., "Dependence of Grain Boundary Segregation of Phosphorus on Temperature and Grain Boundary Misorientation in alpha-iron", Grain Boundary Structure and Related Phenomena, 1986, pp. 427-434

147. Lehockey, E.M., Palumbo, G., Lin, P, "Grain Boundary Structure Effects on Cold Work Embrittlement of Microalloyed Steels", Scripta Met, 1998, 39(3), pp. 353-358.

148. Janovec, J., Grman, D., Perhacova, J., Lejcek, P., Sevc, P, "Thermodynamics of Phosphorus Grain Boundary Segregation in Polycrystalline Low-alloy Steels", Surface and Interface Analysis, 2000, 30, pp. 354-358.

149. Sevc, P., Janovec, J., Lejcek, P., Zahumensky, P., Blach, J, "Thermodynamics of Phosphorus Grain Boundary Segregation in 17Cr12Ni Austenitic Steel", Scripta Met, 2002, 46, pp. 7-12.

150. Lejcek, P., Hofmann, S, "Prediction of Enthalpy and Entropy of Grain Boundary Segregation", Surface and Interface Analysis, 2002, 33, pp. 203-210.

151. Boyle, K.P., Perovic, A., Embury, J.D., Thomson, J.G., Hood, J.E., Perovic, D.D., "A Metallographic Study of Phosphorus in Interstitial Free Sheet Steel", 39th MWSP Conference Proceedings, 1997, Indianapolis, IN, ISS, pp. 159-165

152. Aust, K.T et al., Trans AIME, 1959, Vol. 215, pp. 119.

153. Keast, V.J., and Williams, D.B., "Quantitative Compositional Mapping of Bi Segregation to Grain Boundaries in Cu" Acta Met., 1999, Vol. 47, pp. 3999-4008.

154. Wray, P.J., "Recent Advances in Grain Boundary Characterization and Some Implications for ULC Steel Research." 2000, BAMPRI, University of Pittsburgh.

155. Gupta, I. et al., "Development of Cold Rolled High Strength Sheet Steels", Mechanical Working and Steel Processing Conference, 1979, ISS-AIME.

156. Yamada, M.Y., Tokunaga, Y., and Yamamoto, M., "Effect of Nb and Ti on Resistance to Cold Work Embrittlement of Extra Low-Carbon High Strength Steel Sheet Containing Phosphorus", Tetsu-to-Hagane, 1987, Vol. 73, pp. 1049-1056.

157. Teshima, S., and Shimizy, M, "Recrystallization Behavior of Cold Rolled Mild Steel", Mechanical Working of Steel II, T.G. Bradbury, Editor, 1964, Gordon and Breach Science Publishers, pp. 279-320.

158. Eiko, Y., ISIJ International, 1984, 34(1), pp. 99-107.

159. McAdon et al., Phys. Rev Lett., 1986, Vol. 55, pp. 2563-2567.

160. McAdon, et al., J. Phys. Chem., 1987, Vol. 91, pp. 2607-2631.

161. Losch, W., Acta Met, 1979, Vol. 27, pp. 1885-1892.

162. Messmer, R.P., and Briant, C.L, "The Role of Chemical Bonding in Grain Boundary Embrittlement", Acta Met, 1982, Vol. 30, pp. 457-467.

163. Greenough, G.B., "Residual Stresses Associated with Lattice Strains", Residual Stresses in Metals and Metal Construction, W. Osgood, Editor, 1954, Reinhold Publishing Corporation, pp. 285-296.

164. Dieter, G., Mechanical Metallurgy, 1986, McGraw Hill, pp. 59.

165. Zhang, Z.T., and Lee, D.,"Effect of Processing Variables and Material Properties on Springback Behavior of 2D-Draw Bending Parts", Automotive Stamping Technology, SP-1067, SAE, 1995, pp. 11-18.

166. Zhang, Z.T., and Lee, D., "Springback Analysis and Control in Forming Two-Step Rail-Shaped Sheet Metal Parts", Sheet Metal Stamping for Automotive Applications, SP-1134, SAE, 1996, pp. 51-59.

167. Schmoeckel, D., and Beth, M., "Springback Reduction in Draw-Bending Process of Sheet Metals", CIRP Annals 1993, Manufacturing Technology, 1993, Vol. 42/1, pp. 339-342.

168. Changqing Du et al.,"Springback Prediction in Sheet Forming Simulation", Autobody Stamping Technology, SP-1021, SAE, 1994, pp. 113-123.

169. Sellors, J., and Patel, I., "Review of Springback and Side-Wall Curl", 1996, British Steel Internal Report.

170. Stein, J., "The Effect of Process Variables on Sheet Metal Springback.", SAE Paper No. 982299, 1998, pp. 65-73.

171. Stevenson, R., "Springback in Simple Axisymmetric Stampings", Met. Trans. A, 1993, Vol 24A, pp. 925-934.

172. Cahn, R.W., Haasen, P., Kramer, E.J, ed. Materials Science and Technology, Vol. 15, 1991, pp. 429-480.

173. Cahn, R.W., Haasen, P., Kramer, E.J, ed. Materials Science and Technology, Vol. 7, 1991, pp. 227.

174. Weiland, H., "Microtexture Determination and its Application to Materials Science", JOM, 1994, Vol. 46(No. 9), pp. 37-41.

175. E112-96, A.S., *Standard Test Methods for Determining Average Grain Size*, in *ASTM Standards for Testing of Materials*, 1966.

176. Hosford, W.F., "Analyses of Taylor and of Bishop and Hill", The Mechanics of Crystals and Textured Polycrystals, 1993, Oxford University Press, pp. 56-85.

177. Backofen, W.A., Deformation Processing, 1972, Addison-Wesley, pp. 57-87.

178. Douthwaite, R.M., Petch, N.J, A Microhardness Study Relating to the Flow Stress of Polycrystalline Mild Steel, Acta Met, 1970, 18, pp. 211-216.

179. Meric, C., Atik, Enver., Engez, Turgut, "Experimental Microhardness for AA 1030, Cu, CuSn7, CuZn30 and 6114 Alloys and a Correlation with the Hall-Petch Relation", Materials Research Bulletin, 1999, 34(12), pp. 2043-2052.

180. Miyahara, T., Matsuoka S., Hayashi, T, "Nanoindentation as a Strength Probe- a Study on the Hardness Dependence of Indent Size for a Fine-grained and Coarse-grained Ferritic Steel", Met Trans A, 2001, 32A, pp. 761-768.

181. Johnson, A., "A re-evaluation of the Hall-Petch analysis", Canadian Metallurgical Quarterly, 1974. **13**(1): p. 215-221.

182. Morcinek, P., Smid, V., Heczko, T., Prnka, T., "Structural Steels with Acicular Ferrite", Microalloying 75, 1975, Washington, D.C, pp. 272-278

183. Hook, R.E., "The Effect of Quench-Aging on Inhomogeneous Yielding of Steels with Very Low Interstitial Solute Content", Met Trans., 1970, 1, pp. 85-92.

184. Ainslie, N.G., Phillips, V.A., Turnbull, D, "Sulfur Segregation at alpha-Iron Grain Boundaries-II", Acta Met., 1960, 8, pp. 528-538.

185. Bleck, W., Bode, Ralph., Hahn, Franz-Josef, "Interstitial-free Steels, Processing, Properties and Application", in Metallurgy of Vacuum Degassed Steels, 1989, Indianapolis, TMS, Warrendale, PA, pp. 73-90